NASA Technical Memorandum 104566, Vol. 25

SeaWiFS Technical Report Series

Stanford B. Hooker, Editor
Goddard Space Flight Center
Greenbelt, Maryland

Elaine R. Firestone, Technical Editor
General Sciences Corporation
Laurel, Maryland

James G. Acker, Technical Editor
Hughes STX
Lanham, Maryland

Volume 25, Ocean Optics Protocols for SeaWiFS Validation, Revision 1

James L. Mueller
Roswell W. Austin
Center for Hydro-Optics and Remote Sensing
San Diego State University
San Diego, California

National Aeronautics and
Space Administration

Goddard Space Flight Center
Greenbelt, Maryland 20771

1995

This publication is available from the NASA Center for AeroSpace Information,
800 Elkridge Landing Road, Linthicum Heights, MD 21090-2934, (301) 621-0390.

PREFACE

This document stipulates protocols for measuring bio-optical and radiometric data for Sea-viewing Wide Field-of-view Sensor (SeaWiFS) algorithm development and system validation. The protocols begin in Chapter 2, with specifications of the measured variables which are to be included in data sets for validation of the SeaWiFS system's radiometric performance, algorithm development, and algorithm validation. The protocols in Chapter 3 specify the engineering performance characteristics required of radiometers, optical instruments, and other instrumentation used to measure these variables at sea. Chapter 4 details laboratory and field protocols for characterizing and calibrating each type of instrument. Procedures for actually measuring the validation variables are given in Chapter 5, and protocols for both data processing and methods of analysis are described in Chapter 6.

This volume, Revision 1, supersedes the earlier version (Mueller and Austin 1992) published as Volume 5 in the *SeaWiFS Technical Report Series*. Instrument performance specifications have been modified slightly from the previous version (e.g., radiometric saturation levels have been increased, and there are wavelength changes for some channels). Pigment protocols have been strengthened [R. Bidigare]† primarily to discriminate divinyl and monovinyl chlorophyll *a*. Spectrophotometric absorption protocols have also been expanded and reorganized [C. Trees, B. Mitchell, J. Cleveland, C. Roesler, C. Yentsch, and D. Phinney]. New protocols have been added for *in situ* measurements of spectral absorption and backscattering [R. Zaneveld], for above-water measurements of water-leaving radiance from ships and low-flying aircraft [R. Doerffer, K. Carder, and C. Davis], and for sampling in Case-2 water [R. Doerffer, K. Carder, C. Davis, and R. Arnone].

In general, the specifications and protocols set forth here simply describe and adapt instrument specifications and procedures that are common practice in the ocean optics community. In several areas, however, protocols call for significant improvements over today's instruments and practices; these very challenging protocols should, at least for the present, be regarded more as goals than as strict requirements. The motives for adopting these goals as protocols are that the improvements called for are necessary to meet the rigorous SeaWiFS uncertainty goals, and that the community feels these standards can be closely approached with a significant but affordable effort. Areas in which new research and development must be done to satisfy challenging protocols, and those areas in which there has been recent progress, are summarized below.

1. Model sensitivity studies and experimental verification are needed to develop methods for adjusting *in situ* radiometric measurements at a given wavelength to correspond to SeaWiFS measurements at a wavelength as much as 4 nm away, and with a different spectral response function (Sections 3.1.1 and 6.1.7).
2. Laboratory research is needed to improve absolute standards of irradiance and radiance, and associated absolute calibration procedures, to achieve or approach 1% internal consistency in the responsivity calibrations of radiometers to be used in SeaWiFS validation experiments (Section 4.2). The SeaWiFS Intercalibration Round-Robin Experiment (SIRREX) program has made significant progress in this area (Mueller 1993 and Mueller et al. 1994).
3. Radiometric linearity test procedures must be improved to extend linearity characterizations over the full operating dynamic ranges (Table 4) of the various irradiance and radiance sensors (Section 4.1.7). This is especially critical for downwelling irradiance measurements at the sea surface, where irradiances of laboratory irradiance standards are only 2–15% (depending on wavelength) of saturation irradiance.
4. Instrument self-shading effects are a significant, but probably correctable, source of error (Sections 3.1.8, 5.1.6, and 6.1.7). The diameter of a radiometer determines whether or not self-shading error can be corrected to within less than 5%. The maximum diameter which enables such a correction varies with the absorption coefficient, and is therefore a function of wavelength, water mass, and the solar zenith angle. For oligotrophic to moderately turbid coastal water masses, wavelengths less

† Names in brackets are the principal contributors to the revised protocols.

than 600 nm, and solar zenith angles greater than 30°, upwelled irradiance and radiance data from many of the currently popular radiometers having diameters of 20–40 cm can be adequately corrected. In more general conditions, however, new instruments must be developed to minimize self-shading effects, particularly for near-infrared wavelengths and in Case-2 waters. Self-shading corrections have been partially verified in recent experiments and a provisional protocol is included in this revision.

5. Measurements following the stringent protocols for avoiding ship shadows and reflections will require exclusive use of profiling radiometer configurations which are not widely used today (Section 5.1.1). Tethered free-fall systems appear to offer the most economical approach to meeting these requirements. More sophisticated and expensive approaches include optical systems on either remotely operated vehicles (ROVs), or on small surface platforms with self-contained winches.
6. Quantitative characterization of polarization sensitivity is critical for any airborne radiometer to be used for SeaWiFS radiometric validation, or algorithm development and validation. Protocols and procedures for polarization sensitivity characterization must be developed in more specific detail than was accomplished here because of time constraints (Sections 3.3 and 4.3).
7. The uncertainties specified here for cosine responses of irradiance collectors are significantly better than is typically realized in commercially available radiometers (Section 3.1.5). Moreover, the specified uncertainties may challenge the precision of the laboratory procedures used to characterize an instrument's cosine response (Section 4.1.5). Error in cosine response almost directly translates to an equivalent error in downwelling irradiance for the clear-skies case so critical to the SeaWiFS validation. Therefore, a significant effort to carefully characterize the effect, and to work with instrument manufacturers to approach or achieve the specific uncertainties, is an important factor in our strategy for reducing the overall error budget for water-leaving radiance measurements to less than 5%.
8. The use of a portable standard to trace a radiometer's performance stability during the course of a field deployment is called for in the present protocols (Section 4.2.5). Several manufacturers offer reasonably portable radiometric sources, which may be suitable for this purpose, but laboratory and field evaluations must be carried out to prove their suitability and to develop new and detailed procedures for their use in the field. The SeaWiFS Project Office (SPO) has sponsored work at the National Institute of Standards and Technology (NIST) to develop a prototype system.
9. The present protocols for deploying and analyzing data from moored and free-drifting optical systems are tentative, preliminary, and incomplete. Although moored and drifting optical systems have been used successfully in several oceanographic experiments, there are no previous examples of their use for ocean color remote sensing algorithm development, or for radiometric validation of airborne or satellite radiometers. New moored and drifting optical systems are currently being developed and tested in preparation for applications to SeaWiFS validation; significant progress has been made under the Marine Optical Buoy (MOBY) program (D. Clark). As results from this effort become available, new and detailed protocols for making these measurements will be developed and distributed with the next revision.

The protocols and recommendations in this document attempt to represent and consolidate the contributions of both the workshop participants and of many other individuals who participated in the review process. The final document, however, has by necessity been interpreted and rewritten by the authors, who accept full responsibility for any remaining mistakes and misrepresentations. As can be readily deduced from the above list of critically needed improvements, this document is an unfinished work in progress to establish protocols for ocean optical measurements. It will be appropriate to develop and issue a further revised set of protocols reflecting our collective experience in post-launch algorithm development and validation activities after the first year of operation of the SeaWiFS instrument.

San Diego, California
December 1994

—J. L. Mueller

Table of Contents

Table of Contents *cont.*

Table of Contents *cont.*

ABSTRACT

This report presents protocols for measuring optical properties, and other environmental variables, to validate the radiometric performance of the Sea-viewing Wide Field-of-view Sensor (SeaWiFS), and to develop and validate bio-optical algorithms for use with SeaWiFS data. The protocols are intended to establish foundations for a measurement strategy to verify the challenging SeaWiFS uncertainty goals of 5% in water-leaving radiances and 35% in chlorophyll *a* concentration. The protocols first specify the variables which must be measured, and briefly review the rationale for measuring each variable. Subsequent chapters cover detailed protocols for instrument performance specifications, characterizing and calibrating instruments, methods of making measurements in the field, and methods of data analysis. These protocols were developed at a workshop sponsored by the SeaWiFS Project Ofice (SPO) and held at the Naval Postgraduate School in Monterey, California (9–12 April 1991). This report began as the proceedings of the workshop, as interpreted and expanded by the authors and reviewed by workshop participants and other members of the bio-optical research community. The protocols are an evolving prescription to allow the research community to approach the unprecedented measurement uncertainties implied by the SeaWiFS goals; research and development are needed to improve the state-of-the-art in specific areas. These protocols should be periodically revised to reflect technical advances during the SeaWiFS Project cycle. The present edition (Revision 1) incorporates new protocols in several areas, including expanded protocol descriptions for Case-2 waters and other improvements, as contributed by several members of the SeaWiFS Science Team.

Prologue

The NIMBUS-7 Coastal Zone Color Scanner (CZCS) introduced ocean color remote sensing as a powerful new tool for observing ocean bio-optical properties. Through the early 1980s, CZCS data were exploited by a growing number of scientists studying marine phytoplankton, ocean productivity, and ocean optical properties. Practical applications to marine fisheries were also demonstrated. Unfortunately, a successor ocean color imaging system was not developed before the CZCS ceased operating in mid-1986. At present, therefore, research in these areas is limited to retrospective, albeit productive, investigations of the CZCS historical database. In mid-1995, the launch of the Sea-viewing Wide Field-of-view Sensor (SeaWiFS), the next generation ocean color sensor, will bring a welcomed and improved renewal of ocean color time-series observations to the ocean research community.

The National Aeronautics and Space Administration (NASA) SeaWiFS Prelaunch Science Working Group (SPSWG) has recommended baseline satellite ocean color products consisting of:

1) normalized water-leaving radiance (L_{WN}) at five wavelengths;
2) aerosol radiance at three wavelengths;
3) chlorophyll *a* concentration;
4) a chlorophyll-like pigment (chlorophyll *a* plus phaeopigment *a*) concentration;
5) the diffuse attenuation coefficient (K) at 490 nm, $K(490)$; and
6) calibrated radiances observed at the satellite.

The primary SPSWG goals for product uncertainty are derived water-leaving radiances to within 5% and chlorophyll *a* concentration to within 35% in Case-1 waters, both globally and throughout the projected five-year mission. These goals have been endorsed by the SeaWiFS Science Team and accepted by NASA. NASA has the responsibility to lead the product assurance, calibration, and validation program. NASA is also required to determine the degree to which the commercially procured ocean color data fulfills the contractually stated NASA requirements.

The CZCS mission was unquestionably a scientific success, but it also taught the participants that the satisfactory performance of a remote sensing satellite system cannot be taken for granted. Immediately after launch, and periodically throughout its five-year mission, the SeaWiFS system performance—including algorithms—must be independently verified using *in situ* optical measurements of the ocean and atmosphere. It is imperative that these supporting optical measurements meet a uniform standard of quality and accuracy if the primary SeaWiFS goals of 5% uncertainty in water-leaving radiance and 35% uncertainty in chlorophyll *a* concentration are to be met, or even closely approached. To that end, the NASA Goddard Space Flight Center (GSFC) SeaWiFS Project convened a workshop to draft protocols and define standards for optical measurements to be used in SeaWiFS radiometric validation, and algorithm development and validation. The original version of this document (Mueller and Austin 1992) reported the protocols agreed to by the participants, as expanded by the authors, made in consultation with both the workshop participants *and* other members of the ocean bio-optics community. The present revision incorporates the

expanded protocols and revisions contributed by several members of the SeaWiFS Science Team and other colleagues.

This report specifies the type and quality of supporting *in situ* optical measurements and analytical protocols that will be required to develop bio-optical algorithms and validate the SeaWiFS calibration. Economics dictate that these observations and data will accrue over several years from a variety of sources, using different instruments and approaches. These data must be internally consistent, of known and documented uncertainty, and in a form readily accessible for analysis by the SeaWiFS investigators.

Chapter 1

Overview of SeaWiFS Bio-Optical Requirements

INTRODUCTION

The *Ocean Optics Protocols for SeaWiFS Validation, Revision 1* are intended to provide standards, which if followed carefully and documented appropriately, will assure that any particular set of optical measurements will be acceptable for SeaWiFS validation and algorithm development. It is true that in the case of ship shadow avoidance, for example, there are some circumstances in which acceptable radiometric profiles may be acquired considerably closer to a ship than is specified here (Section 5.1.1). When the protocols are not followed in such cases, however, it is incumbent upon the investigator to explicitly demonstrate that the actual error levels are within tolerance. The most straightforward way for an investigator to establish a measurement that is both accurate enough to meet the SeaWiFS standards and uncontaminated by artifacts, such as ship shadow, will be to adhere closely to the protocols.

1.1 OBJECTIVES

Immediate concerns have focused this document on specific preparations for the SeaWiFS mission. A longer-term intention is the development of bio-optical databases that are relevant to future needs, and therefore, this document also recognizes the capabilities of other planned or potential ocean color sensors, including:

a) the Japanese Ocean Color Temperature Sensor (OCTS);

b) the Moderate Resolution Imaging Spectroradiometer (MODIS);

c) the Medium Resolution Imaging Spectrometer (MERIS); and

d) the German Reflecting Optics System Imaging Spectrometer (ROSIS).

The key objective of the working group was to recommend protocols and standards for supporting *in situ* optical measurements. These objectives addressed the following subject areas:

1. The required and useful optical parameters to be used for validation of SeaWiFS normalized water-leaving radiances and atmospheric correction algorithms, and for monitoring the satellite sensor's calibration and stability, will be defined.
2. The instrumentation requirements, and standards for measuring the parameters in item 1, including definitions of measured quantities, wavelengths, field-of-view (FOV) and band specifications, sensitivity, uncertainty and stability, will be delineated.
3. The optical instrument characterization, intercalibration standards, and related protocols will be defined. This objective includes the following subjects:
   a) laboratory calibration and characterization measurements, uncertainties, and procedures to be applied to instruments used in SeaWiFS validation and algorithm development activities;
   b) pre- and post-deployment measurements and procedures to be followed with moored instrumentation; and
   c) methods for instrument calibration and characterization, and the requirements for record keeping and traceability, including intercalibrations of radiometric and optical standards between participating laboratories.
4. The at-sea optical sampling strategy and protocols will be standardized. This objective includes such considerations as:
   a) the rationale and justifications for moored, underway, drifting, shipboard, and airborne measurements;
   b) ship shadow avoidance, depth resolution in optical profiles, and total sampling depths; and
   c) time of day, sky conditions, season, and geographic considerations.
5. The analysis approaches to be used shall be refined. This objective includes procedures and methodologies recommended for generating variables from *in situ* observations, e.g., $L_{WN}(z)$ from $L_u(z)$, $K(z)$, remote sensing reflectance, etc., as well as error analysis.

6. Protocols for ancillary measurements, data archiving, database population, and access to data will be standardized.
7. The required atmospheric measurements will be defined, and the degree to which standard methodologies are available will be evaluated.

The development and validation of bio-optical algorithms for SeaWiFS will be addressed by a separate working group, and thus, these topics are briefly examined in this report. Nonetheless, the SPSWG was charged with identifying data requirements and sampling strategies for bio-optical support measurements in the context of the optical and radiometric measurements. This topic includes the following subjects:

1. Discrete chlorophyll *a* and pigment concentrations will be measured using the US Joint Global Ocean Flux Study (JGOFS) program's protocols and standards for high performance liquid chromatography (HPLC) pigment sampling and analysis, which are adopted by reference to the *JGOFS Core Measurement Protocols* (JGOFS 1991), Chapter 9, "Pigments and Chlorophyll."
2. An assessment will be made of the roles of underway, moored, and discrete chlorophyll *a* fluorescence measurements, how such measurements are calibrated, and their usefulness for satellite data product validation.
3. The need for biogeochemical measurements of colored dissolved organic material (CDOM), coccoliths, suspended sediment, detritus, etc., will be examined on the basis of baseline product requirements. This subject will also the address the extent to which standards and protocols have been defined for such biogeochemical measurements.

This report is complementary to anticipated reports of US and International JGOFS working groups, which are concurrently evaluating bio-optical needs and sampling strategies for their respective science programs.

1.2 SENSOR CALIBRATION

The SPO must make every effort to track the sensor's performance throughout the duration of the mission. Since the instrument will be designed for a five-year mission, it is certain that the sensor calibration at each wavelength will change in some unpredictable manner as a function of time. Experience with CZCS has shown it is very difficult to determine a sensor's calibration once it has been launched (Viollier 1982, Gordon et al. 1983, Hovis et al. 1985, Mueller 1985, and Gordon 1987). Similar problems have been encountered with other Earth observing systems, such as the National Oceanic and Atmospheric Administration (NOAA) Advanced Very High Resolution Radiometer (AVHRR) (Brown and Evans 1985 and Weinreb et al. 1990). Because of the large atmospheric contribution to the total observed radiances (Gordon 1981) and the great sensitivity of the bio-optical algorithms to the estimated water-leaving radiances (Clark 1981), small errors in the calibration can induce sizable errors in derived geophysical products, rendering them useless for many applications.

By processing large quantities of so-called "clear water" imagery, i.e., water with pigment concentrations less than 0.25 mg m^{-3} (Gordon and Clark 1981), Evans and Gordon (1994) were able to develop a *vicarious* calibration that was used in the global processing of the entire CZCS data set (Esaias et al. 1986 and Feldman et al. 1989). The approach, however, requires assumptions that may limit the scientific utility of ocean color imagery. Specifically, the normalized clear water-leaving radiances, $L_{WN}(443)$, $L_{WN}(520)$, and $L_{WN}(550)$, were assumed to be 1.40, 0.48, and 0.30 mW cm^{-2} μm^{-1} sr^{-1}, respectively. The Ångström exponents were assumed to be zero and certain geographical regions such as the Sargasso Sea were assumed to be clear water sites at all times. Under these assumptions, analyses of the derived (L_{WN}) values were used to calculate calibration adjustment coefficients to bring CZCS derived (L_{WN}) values into agreement for these regions. The vicarious calibration of the 443 nm band is tenuous because of the great variability in $L_{WN}(443)$ even in clear water. Additionally, certain command and engineering data from the NIMBUS-7 platform were not archived, so that a detailed analysis of possible effects related to the spacecraft environment and the effects of spacecraft operation on the calibration could not be performed.

Unlike CZCS, SeaWiFS will routinely produce geophysical fields in a near-real time, operational mode for distribution to the science community. This aspect of the mission necessitates constant evaluation of the sensor performance and the derived products. Therefore, a multifaceted approach to address the problem of sensitivity degradation and sensor characterization is required during both the pre- and post-launch phases. The goal is to ensure that SeaWiFS level-1 radiances are accurately known and meet the specifications of the SPSWG.

The plan includes both onboard and vicarious calibration approaches. SeaWiFS will have a solar measuring diffuser plate to reference the response to the sun (Gordon 1981) and also will be capable of periodically imaging the moon by maneuvering the spacecraft. The vicarious calibration program will incorporate measurements of water-leaving radiances and other related quantities, from ships, drifting buoys, and fixed moorings, to develop time series and geographically diverse samples of oceanic and atmospheric data sets. Each approach has advantages and disadvantages, but when combined, they should provide a complementary and comprehensive data set that will be sufficient to monitor short-term changes and long-term trends in the sensor's performance.

1.3 BIO-OPTICAL ALGORITHMS

The SPO will be responsible for producing a standard set of derived products and will produce both *CZCS-type* products and *baseline* products. The CZCS-type products will consist of pigment concentration, $K(490)$, five normalized water-leaving radiances, and three aerosol radiances based on constant default wavelength dependence (epsilon) coefficients in aerosol corrections. The proposed baseline products will include five normalized water-leaving radiances, $K(490)$, chlorophyll a concentration, three aerosol radiances, and one or more error analysis products.

The basic quantities to be computed from the sensor radiances are the water-leaving radiances, from which all other derived products *except* the aerosol radiances are computed. Every effort must be made to ensure these radiances meet the specifications of the SPSWG, i.e., ±5% in Case-1 waters. This requires the atmospheric correction algorithms to be considerably more sophisticated than the current CZCS algorithms.

The baseline bio-optical products must meet the accuracy requirements established by the SPSWG over a variety of water masses. The current CZCS algorithms were based on a data set consisting of fewer than 50 data points (only 14 observations were available for the band-2-to-band-3 ratio algorithm) and performed poorly in regions of high chlorophyll a concentration, high suspended sediment concentration, high CDOM concentration, and coccolithophorid blooms (Groom and Holligan 1987). Accurate estimates of the baseline products are essential if SeaWiFS is to be useful in programs such as the Global Ocean Flux program [National Academy of Science (NAS) 1984].

SeaWiFS will have the capability, due to improvements in the signal-to-noise ratio (SNR), digitization, dynamic range, and wavelength selection, to increase the accuracy of these products and to flag areas where anomalies or low confidence conditions exist. Clearly, a much larger database will be needed for developing a broader variety of bio-optical algorithms, some of which will be region specific. The radiometric, optical, and chemical field observations used in deriving bio-optical algorithms and for vicarious calibration of the sensor must, therefore, conform to stringent requirements with respect to instrument calibration and characterization, and must also conform to the observation protocols which have been specified to take advantage of SeaWiFS capabilities.

The SPO will manage a program to compare the various atmospheric correction and bio-optical algorithms proposed by the science community. The purpose of this program is to independently evaluate suggested improvements or additions to the SeaWiFS products. This component of the calibration and algorithm development program will run in parallel with, but off-line from, operational processing and will provide an essential mechanism for incorporating data and analyses from the community at large.

1.4 COMMUNITY PARTICIPATION

The SPO will rely on the oceanographic community to perform field research for atmospheric and bio-optical algorithm development, and for all of the *in situ* data collection for the vicarious sensor calibration. A minimal subset of these observations will be sponsored by the SPO, but many projects sponsored by the NASA Research and Application Program and other government agencies are expected to make major contributions to the global five-year effort. This requires close coordination of the various programs involved and a clear definition of the observations, accuracies, and data collection protocols required for each type of activity. The purpose of this document is to clarify these requirements.

1.5 VICARIOUS CALIBRATION

For ocean observations, it is easy to show (Gordon 1987 and Gordon 1988) that satellite sensor calibration requirements based on the quality of the existing CZCS pigment algorithms exceed currently available capabilities. Furthermore, the sensor calibration is unlikely to remain unchanged through launch and five years of operation in orbit. The only foreseeable way of approaching the ocean calibration needs is through vicarious calibration, i.e., fine tuning the calibration in orbit.

The methodology used to achieve vicarious calibration for CZCS was described in detail by Gordon (1987). First, the calibration was initialized after launch by forcing agreement between the sensor-determined radiance and the expected radiance based on radiometric measurements made at the surface under clear atmospheric conditions. Next, since the CZCS responsivity was observed to be time dependent, the algorithms were applied to other scenes characterized by bio-optical surface measurements and more typical atmospheres, and the calibration was adjusted until the measured water-leaving radiances were reproduced. Finally, the surface measurements of pigments were combined with satellite pigment estimates for a wide variety of atmospheric conditions, and the radiance calibration was fine tuned until the best agreement was obtained between the retrieved and true pigments.

The CZCS vicarious calibration was not radiometric. It was a calibration of the entire system—sensor plus algorithms. To predict the radiance measured at the satellite, L_t, the water-leaving radiance, the aerosol optical thickness, and the aerosol phase function are all required. Also needed are ancillary data such as the surface pressure, wind speed, and ozone optical thickness. These data for vicarious calibration and validation will be obtained by measuring the upwelling radiance distribution just beneath the surface, along with the aerosol optical thickness and the sky radiance, at the time of the satellite overpass. The sky radiance will be used to deduce the required information about the aerosol phase function (Voss and Zibordi

1989). The data set will be used to deduce L_t, at the top of the atmosphere, coincident with a SeaWiFS overpass from which the calibration will be initialized.

It must be stressed that this exercise is absolutely essential for calibrating the SeaWiFS system, i.e., sensor plus algorithms, and that it cannot be effected without a high quality surface data set obtained simultaneously with the satellite imagery.

Chapter 2

Data Requirements

INTRODUCTION

The prime objective of in-water optical measurements for SeaWiFS is to derive accurate normalized water-leaving radiances that will be used both for direct validation comparisons with those derived from SeaWiFS data, and to develop and validate in-water bio-optical algorithms. Therefore, a comprehensive field program to measure optical and biogeochemical state variables will be required.

2.1 DEFINITIONS

The required and useful variables to be measured for SeaWiFS validation are listed in Table 1, classified into two discrete sets. The first set comprises variables that can be used for radiometric initialization and ongoing validation. The second set encompasses those variables that will be used for bio-optical algorithm development and validation.

Surface incident spectral irradiance, $E_d(0^-, \lambda)$; downwelled spectral irradiance, $E_d(z, \lambda)$; and upwelled spectral radiance, $L_u(z, \lambda)$, are the fundamental measurable quantities needed to derive normalized water-leaving radiances in most circumstances. Other ambient properties, like sky radiance, sea state, wind velocity, etc., are also useful initialization and calibration measurements and are discussed below.

Surface incident spectral irradiance, $E_d(0^-, \lambda)$, is usually derived from surface irradiance, $E_s(\lambda)$, measured on a ship well above the water, but the use of a radiometer floated just beneath the surface ($z = 0^-$) may provide a better approach (Sections 3.2.1 and 5.1.4). $E_d(0^-, \lambda)$ varies due to fluctuations in cloud cover and aerosols, and with time of day, i.e., solar zenith angle. Profiles of $E_d(z, \lambda)$ and $L_u(z, \lambda)$ must be normalized to account for such variabilities during a cast.

Downwelled spectral irradiance, $E_d(z, \lambda)$, is required to compute the diffuse attenuation coefficient, $K(z, \lambda)$, which in turn, is needed for diffuse attenuation coefficient algorithm development (Austin and Petzold 1981), and for optically weighting the pigment concentrations to be estimated from remotely sensed ocean color (Gordon and Clark 1981). $E_d(z, \lambda)$ is also required to compute the spectral (remote sensing) reflectance, $R_L(z, \lambda)$, which is used to normalize $L_u(z, \lambda)$ when developing and validating bio-optical algorithms. The need for this normalization arises because the spectrum of incident irradiance varies with changing solar zenith angle and atmospheric conditions. $E_d(0^-, \lambda)$ can then be used, through $R_L(z, \lambda)$, to convert $L_u(0^-, \lambda)$ measured under a given set of illumination conditions, e.g., overcast skies, to $L_{WN}(\lambda)$, which would be measured under the restricted illumination and viewing conditions associated with SeaWiFS measurements. As with $L_u(0^-, \lambda)$, $E_d(0^-, \lambda)$ must be determined by extrapolation from a profile of $E_d(z, \lambda)$ over the upper few optical depths and reconciled with the direct surface measurement of $E_s(\lambda)$. [Optical depth, $\tau(z, \lambda)$, in the context of this report is the integral of $K(z, \lambda)$, for either radiance or irradiance, depending on the context, from the surface to a given depth z.]

Upwelled spectral radiance, $L_u(0^-, \lambda)$, is the in-water variable which, when propagated upward through the sea surface, leads to the *measured* value of $L_W(\lambda)$. $L_W(\lambda)$ is, in turn, adjusted using $E_d(\lambda)$ to derive the normalized water-leaving radiance, $L_{WN}(\lambda)$, for a clear-sky zenith sun at the mean Earth-sun distance. Unfortunately, it is not practical to measure $L_u(0^-, \lambda)$ precisely at an infinitesimal depth below the surface. Therefore, the profile of $L_u(z, \lambda)$ must be measured over the upper few optical depths with sufficient accuracy to determine $K_L(z, \lambda)$ for $L_u(z, \lambda)$, and to propagate $L_u(z, \lambda)$ to the surface. At near-infrared (IR) wavelengths, the first optical depth is confined to the upper few tens of centimeters. Determination of $L_u(0^-, \lambda)$ in this situation is more challenging and will require special instruments and experiment designs to accommodate the effects of instrument self-shading, wave focusing, small-scale variability, possible fluorescence, Raman scattering, and extremely small working volumes. Careful measurements of inherent optical properties (IOPs), including $a(z, \lambda)$, $c(z, \lambda)$, and $b_b(z, \lambda)$, and spectral fluorescence, may be useful, in addition to $E_d(z, \lambda)$ and $L_u(z, \lambda)$ measurements made with specially designed radiometers.

Sky radiance is required to enable estimation of the aerosol phase function through inversion of the radiative transfer equation. It is also useful for estimating the mean cosine of the transmitted light field in the water. The sky radiance should be measured directly; for the latter application, however, it need only be estimated by occulting the

Table 1. Required observations for initialization and system calibration for satellite product verification and radiative transfer (also ongoing calibration and atmospheric algorithm validation studies) and bio-optical algorithm development and validation.

	Product Verification	Radiative Transfer	Bio-optical Algorithms
Primary Optical Measurements			
Incident Spectral Irradiance, $E_d(0^-, \lambda)$	×	×	×
Downwelled Spectral Irradiance, $E_d(z, \lambda)$	×	×	×
Upwelled Spectral Radiance, $L_u(z, \lambda)$	×	×	×
Spectral Solar Atmospheric Transmission, $\tau_s(\lambda)$	×	×	×
Submerged Upwelled Radiance Distribution, $L(z, \theta, \phi)$	×	×	×
Spectral Sky Radiance Distribution	×	×	×
Upwelled Spectral Irradiance, $E_u(z, \lambda)$		×	×
Calculated or Derived Variables			
Water-leaving Radiance, $L_W(0^-, \lambda)$	×	×	×
Attenuation Coefficient Downwelled Irradiance, $K_d(z, \lambda)$	×	×	×
Attenuation Coefficient Upwelled Radiance, $K_L(z, \lambda)$	×	×	×
Spectral Reflectance, $R_L(z, \lambda)$	×	×	×
Ambient Properties			
Sea and Sky State Photographs	×	×	×
Wind Velocity	×	×	×
In Situ Fluorescence Profiles		×	×
Aerosol Samples		×	×
Temperature and Salinity Profiles		×	×
Secchi Depth			×
Primary Biogeochemical Measurements			
Phytoplankton Pigments (HPLC Technique)		×	×
Phytoplankton Pigments (Fluorometric Technique)		×	×
Total Suspended Material (TSM) Concentration		×	×
Colored Dissolved Organic Material (CDOM)		×	×
Inherent Optical Properties			
Spectral Beam Attenuation Coefficient, $c(z, \lambda)$		×	×
Spectral Absorption Coefficient, $a(z, \lambda)$		×	×
Spectral Backscattering Coefficient, $b_b(z, \lambda)$		×	×
Spectral Volume Scattering Function, $\beta(z, \lambda, \theta)$		×	×
Red Beam Attenuation, $c(z, 660\ \text{nm})$		×	×
Algorithm Specific Research Measurements			
Airborne Fluorescence and Radiances		×	×
Coccolith Concentration			×
Detritus Absorption Coefficient		×	×
Humic and Fulvic Acids			×
Inorganic Suspended Material			×
Organic Suspended Material			×
Particle Absorption Coefficient		×	×
Particle Fluorescence			×
Particle Size Spectra		×	×
Particulate Organic Carbon (POC)			×
Particulate Organic Nitrogen (PON)			×
Phycobilipigments Concentration			×
Phytoplankton Species Counts			×
Primary Productivity (^{14}C)			×
Total Dissolved Organic Carbon (DOC)			×

× = Needed for the indicated effort.

sun's image on a deck cell measuring the incident spectral radiance from the sun and sky. The mean cosine at the surface can be used with profile measurements of $E_d(\lambda)$, $E_u(\lambda)$, and $c(\lambda)$ to estimate $b_b(\lambda)$ (Gordon 1991). An ability to exploit this and similar relationships will greatly enhance both development and verification of bio-optical algorithms. The spectral sky radiance distribution over zenith and azimuth angles is required to determine the aerosol scattering phase functions at radiometric comparison stations during the system initialization cruises and will be very useful if measured at all validation stations throughout the mission.

Upwelled radiance distribution measurements just beneath the sea surface will be required for quantifying the angular distribution of water-leaving radiance at stations used for system calibration initialization and long-term system characterization. These measurements will also be useful in relating radiance and irradiance reflectance, and K profiles, to IOPs and biogeochemical substances, e.g., chlorophyll *a* and CDOM, during bio-optical algorithm development and validation.

Atmospheric transmittance spectra should be measured using a sun photometer in order to determine aerosol optical depths at each station. These data are particularly needed to verify the atmospheric corrections in direct comparisons between SeaWiFS $L_W(\lambda)$ estimates and those determined from in-water $L_u(0^-,\lambda)$.

Sea state photographs are required to document surface wave conditions during radiometric measurements. This information is essential for identifying measurements made under questionable environmental conditions.

Wind velocity is required to generate, through models, estimates of the surface wave slope distribution, which will be used to calculate reflected skylight and sun glint in radiative transfer models (Cox and Munk 1954). Surface wave models driven by wind velocity may also be used to provide quantitative estimates of surface wave induced radiometric fluctuations. Qualitatively, wind velocity, and photographs or videotape recordings of sea state, will be useful for assessing station data quality.

Upwelled spectral irradiance, $E_u(z,\lambda)$, is a useful measurement, in addition to E_d and L_u, because there exist both empirical and theoretical relationships between IOPs, phytoplankton pigments, TSM, and irradiance reflectance. $L_u(0^-,\lambda)$ and $E_u(0^-,\lambda)$ are related by the factor $Q(\lambda)$, which is not well determined at present, and has been shown to vary with solar zenith angle (Morel and Gentili 1993). Combined measurements of $L_u(0^-,\lambda)$ and $E_u(0^-,\lambda)$ will be extremely useful in determining $Q(\lambda)$, which will, in turn, allow traceability of SeaWiFS measurements to previously derived irradiance reflectance relationships and algorithms.

IOPs must be measured for development and validation of the SeaWiFS semi-analytic Case-2 chlorophyll *a* algorithm. This algorithm is based on an explicit theoretical function of the ratio of backscattering to absorption, $b_b(\lambda)/a(\lambda)$. In the first implementation, however, $b_b(\lambda)/a(\lambda)$ is modeled statistically as a polynomial function of chlorophyll *a* concentration. This will introduce a strong, empirical component to the algorithm, suppressing the physical links between $R_L(\lambda)$ and $b_b(\lambda)/a(\lambda)$ and between $b_b(\lambda)/a(\lambda)$ and phytoplankton pigment concentration. A more robust algorithm would be based on direct measurements of absorption, scattering, pigments, and reflectance. Due to recent advances in instrumentation, it is now practical to routinely measure profiles of $a(z,\lambda)$ (Section 5.2.4) and backscattering variables (Section 5.2.5) from which $b_b(z,\lambda)$ may be approximated. Future development and validation experiments involving this algorithm must, therefore, include absorption, beam attenuation, and scattering measurements.

Red beam attenuation coefficient, $c(660)$, and *in situ* chlorophyll *a* fluorescence measurements are exceptionally useful in analyzing profiles of $E_d(z)$, $L_u(z)$, and $E_u(z)$ to derive profiles of $K_d(z)$, $K_L(z)$, and $K_u(z)$, respectively. If these profiles are viewed in real time, they are also useful guides for taking water samples at depths that allow the vertical structure of chlorophyll *a* and suspended particles to be accurately resolved in the top optical depth. Finally, the chlorophyll *a* fluorescence profile is used to interpolate HPLC and extracted fluorescence measurement of chlorophyll *a* concentrations from water samples at discrete depths. It is desirable to make these measurements simultaneously with irradiance and radiance profiles, if it can be done in a way to avoid self-shading of the instrument (Section 5.1.6).

Secchi depth measurements are required for real-time assessment of water transparency during a station and as a quality check during analysis of radiometric profiles.

Aerosol concentration samples using high volume techniques will be useful, in conjunction with aerosol optical depth spectra determined from sun photometer measurements, for chemical, size, and absorption characterization of aerosols, especially in studies of the effects of Saharan and Asian dust clouds on atmospheric corrections.

2.2 BIOGEOCHEMICAL DATA

Pigment concentrations will be determined using HPLC and fluorometric methods to develop and validate chlorophyll *a* algorithms, and to assess the effects of accessory pigment concentrations on water-leaving spectral radiances. These data will also be used to calibrate continuous profiles of chlorophyll *a* fluorescence (Section 2.1). Phytoplankton pigment concentration will also be determined using classical chlorophyll *a* and phaeopigment fluorescence techniques that were used for CZCS pigment validation and algorithm development. The HPLC technique provides more accurate and precise information for a greater number of pigments, but gives different values than does the fluorescence method for various species compositions and chlorophyll *a*-to-phaeopigment ratios. While the HPLC method is the primary pigment technique required

for SeaWiFS, the classical technique is still required to allow the CZCS and SeaWiFS data sets and algorithms to be compared.

Phycobilipigments, present in cyanobacteria and cryptophytes, are treated separately from the HPLC fat soluble pigments. Phycoerythrin and phycocyanin are the two major groups of phycobilipigments found in the marine environment. The concentration of these water soluble pigments is important due to the contribution of solar stimulated phycoerythrin fluorescence to the underwater light field, and also to characterize the phytoplankton population. At times, species which contain phycobilipigment can account for a large fraction of the primary productivity (especially in oligotrophic waters) and have been difficult to quantify due to their small size. These measurements are not required because SeaWiFS does not contain bands at their absorption or fluorescence peaks. The measurements are desirable, however, since several aircraft sensors, e.g., the Airborne Visible and Infrared Imaging Spectrometer (AVIRIS), Airborne Oceanographic Lidar (AOL), the Multispectral Airborne Radiometer System (MARS), and future satellite sensors, e.g., MODIS and MERIS, do possess bands at the absorption or fluorescence peaks of phycobilipigments. If such pigment information is required for a particular study, it is recommended that the glycerol-uncoupling technique described by Wyman (1992) be used to determine phycoerythrin concentrations.

TSM measurements are required to assess the effect of suspended sediment on the derived products. TSM is of primary importance in coastal waters, where simple radiance ratio algorithms for TSM have uncertainties equivalent to, or better than, those for estimating chlorophyll-like pigment concentration. Organic suspended matter and inorganic suspended matter concentrations are subfractions of TSM; this partitioning of TSM is particularly useful in process studies.

Particulates, both POC and PON, are required for process studies to help characterize the adaptive state of phytoplankton and to inventory critical biogeochemical elements.

DOC has been shown to be a major pool of carbon in the oceans. Quantification of the transformations of this pool is crucial to understanding the marine carbon cycle. The colored fraction, CDOM, of the DOC is highly absorbent in the blue range, thus decreasing blue water-leaving radiances, and it must be taken into consideration for pigment concentration algorithms. DOC measurements are needed to develop robust relationships between CDOM and DOC, which are needed to evaluate the usefulness of ocean color observations for estimating DOC concentrations.

CDOM concentrations are required to assess the effect of Gelbstoff on blue water-leaving radiances and chlorophyll concentration. This is of primary importance in Case-2 waters, but is also relevant to phytoplankton degradation products.

Humic and fulvic acids comprise the bulk of CDOM and have different specific spectral absorption coefficients. Their concentrations are useful for determining the correction used for phytoplankton pigment concentration algorithms in Case-2 waters and for estimating CDOM from ocean color observations.

Coccolith concentration, which is the number density of small plates (coccoliths) composed of calcium carbonate ($CaCO_3$), is very important to light scattering. Coccoliths are produced in copious amounts by marine phytoplankton called coccolithophores. Scattering of light by coccoliths is highly apparent in visible wavelength satellite imagery, because they perturb the usual relationships between water-leaving radiances and chlorophyll a concentration and adversely impact atmospheric corrections. Additionally, coccolith formation, sinking, and dissolution are significant factors in the ocean carbon flux budget. It is, therefore, necessary to measure coccolith concentration, both as number density and $CaCO_3$ concentration, to aid in 1) the correction of chlorophyll a concentration algorithms, 2) coccolith algorithm development, and 3) atmospheric correction development and validation.

The *particle absorption coefficient*, which is comprised of absorption by living, dead, and inorganic particles, is a useful variable for modeling the portion of solar energy that is absorbed by phytoplankton and bacteria.

Detritus (or *tripton*) *absorption coefficient*, i.e., absorption of light by detritus, represents a major loss of light which would otherwise be available to the phytoplankton component of the marine hydrosol. In many cases, absorption by detritus is a significant term in the marine radiative transfer processes, and its determination is useful for phytoplankton production models and for modeling the light field.

Particle size spectra are very useful for in-water radiative transfer calculations, particularly if measurements include particles smaller than 1 μm.

Particle fluorescence, measured using laser sources on single-cell flow systems, may be used to calculate particle scattering-to-fluorescence ratios for evaluating the population structure of the plankton (both phyto- and zooplankton).

Phytoplankton species counts are important because species-to-species variability in optical and physiological properties represents a major source of variability in bio-optical algorithms and primary productivity models. This has been recognized, but it is generally ignored in remote sensing algorithms due to the tedious nature of species enumeration, the small sizes of many species, and the large number of species involved. This information, however, at various levels of rigor, is useful in evaluating the population and pigment composition. This is especially important for some groups, such as coccolithophores.

Primary productivity, using the radioactive isotope ^{14}C estimation method, is not strictly required for validation of

water-leaving radiances or system initialization. Furthermore, primary productivity is not a standard derived SeaWiFS product, owing to the complexity of relating ocean color to production. It will, however, be extremely useful for process study applications of ocean color data if these measurements are made at the same time that the water column optical properties are determined. These data will aid in the development of models of primary production using satellite ocean color observations, a goal which is central to the overall SeaWiFS science mission. Of special importance are determinations of key photo-physiological parameters derived from production measurements as functions of irradiance. If ^{14}C productivity measurements are made, they should conform to the *JGOFS Core Measurements Protocols* (JGOFS 1991).

2.3 ABOVE-WATER TECHNIQUES

Above-water ocean color radiance measurements from aircraft and ships can augment in-water measurements of $L_u(z, \lambda)$ made to compare directly with SeaWiFS measurements for validation of its radiometric performance and algorithms. Above-water radiance measurements can, if they are accurately made, contribute an additional useful constraint in defining internally consistent sun-ocean-atmosphere-sensor models that will comprise the essence of SeaWiFS radiometric validation. For this application, above-water radiometers must meet the SeaWiFS specifications for radiometric uncertainty, SNR, and spectral resolution at a spatial resolution that will permit direct comparisons with in-water measurements, and with SeaWiFS measurements by means of spatial averaging. Conversely, above-water radiance measurements made with less accuracy than the SeaWiFS prelaunch specifications would introduce an unacceptable error source into the validation models and cannot be used for this purpose.

Airborne ocean color data may also be used to determine spatial variability in ocean optical properties during shipboard algorithm development and validation experiments. In this context, airborne ocean color measurements will be especially valuable in productive Case-1 and Case-2 waters, where variability in ocean optical properties can be large over mesoscale and smaller distances. Synoptic maps of ocean color distributions can be advantageously utilized to guide sampling by ships. It can also be used to place in-water data from an individual station in context with respect to nearby variability, and thus provide a basis for spatial interpolation and averaging when comparing in-water bio-optical measurements with SeaWiFS image data. This application can be accomplished using aircraft radiometers meeting somewhat less stringent performance specifications than is demanded for direct validation comparison between SeaWiFS and aircraft radiance measurements.

Airborne measurements of fluorescence by chlorophyll, CDOM, and phycoerythrin, both by laser and solar excitation, are useful to evaluate spatial and temporal variability near ship and mooring stations and to provide independent assessments of bio-optical algorithms.

2.4 ANCILLARY MEASUREMENTS

Hydrographic data, water temperature (T), and salinity (S), derived from conductivity, temperature, and depth (CTD) profiles, are useful for characterizing the physical water mass regime in which an optical profile is measured. A T-S characterization is especially important near ocean fronts and eddies where interleaving water masses of very different biogeochemical composition, and therefore fundamentally different bio-optical properties, can produce complex spatial and temporal patterns of near-surface optical properties. In these circumstances, T-S profiles can provide an indication of whether a station location is suitable for reliable remote sensing validation and algorithm development comparisons.

2.5 OPTICAL MOORINGS

Optical moorings will be maintained in one or more regions of low optical variability to provide long-term time series comparisons between *in situ* and SeaWiFS measurements of normalized water-leaving radiance. Moored optical systems will also be extremely useful in a variety of oceanographic studies. For example, global satellite observations of ocean pigment biomass and estimates of phytoplankton production are essential to achieve the objectives of the JGOFS program (NAS 1984); SeaWiFS will play a key role in this effort.

The oceans exhibit physical and biological variability over a wide range of space and time scales. This variability, and the need to synoptically measure distributions of physical and biological properties over large areas and long time periods, has motivated recent developments utilizing contemporaneous buoy, ship, aircraft, and satellite sampling strategies (Smith et al. 1987). In addition, long-term mooring data are required to provide continuous observations and permit an optimization of the accuracy of the derived satellite products (Booth and Smith 1988).

There are two sources of systematic error in estimates of phytoplankton pigment biomass derived from satellite ocean color data. First, errors in satellite estimation of pigment biomass arise because physical forcing, biological properties, and ocean optical properties all vary systematically with depth, and the upper layer optical signal observed by satellites may not adequately represent structure deeper in the water column. In many circumstances, subsurface changes may go undetected unless contemporaneous water column profile data from either shipboard or moored sensors is available. Second, visible wavelength sensor systems do not obtain data when the atmosphere is cloudy. Air-sea interactions giving rise to cloudiness are often closely linked to biological processes. For example, Michaelsen et al. (1988) showed that episodic wind events,

which give rise to coastal upwelling and subsequent phytoplankton production along the California coast, cause cloudiness that will bias the statistics of pigment concentrations derived from ocean color imagery. Similar biases of a factor of 3–4, due to wind mixing during cloudy periods, were observed by Muller-Karger et al. (1990). In circumstances of this nature, visible and infrared satellite observations of the ocean are not random samples. Moored optical sensors can measure systematic temporal variability in the vertical distribution of pigment biomass and, at the same time, provide the continuous time series that may be used to remove the sampling bias associated with cloudiness.

The detection and verification of intra- and interannual fluctuations in productivity and associated bio-optical variables are key goals of programs focused on studying global change. These goals place stringent requirements for long-term accuracy and precision on the measurement systems to be employed. The monitoring of bio-optical parameters to resolve variability at global and decadal scales, as proposed by the SeaWiFS and MODIS missions, will require that moored *in situ* optical instruments be maintained to supplement and support the satellite data sets. For example, the CZCS sensor degradation and the difficulties encountered in attempting to characterize that degradation, strongly point out how valuable in-water optical measurements would have been to that program.

2.6 DRIFTING OPTICAL BUOYS

Drifting optical buoys, which are expendable and analogous to the ARGOS sea surface temperature (SST) drifters, represent a viable, cost-effective way to obtain significant numbers of daily optical observations to validate global data sets of water-leaving radiance. Due to high cost, there will probably never be more than a few permanent optical moorings. Shipboard observations provide only a few measurements on any given day, due to both the cost of at-sea research and investigator availability. Optical data from drifting buoys, while less complete than measurements from ships and fixed optical moorings, can potentially surpass both in terms of global coverage and the number of near-real time comparisons with SeaWiFS observations. Judicious seeding of *inexpensive* drifters provides one means of sampling conditions and regions critical to SeaWiFS product verification. For example, chronically high levels of aerosols caused by desert dust storms constitute a regional condition that will affect atmospheric corrections. These instruments may also allow study of possible variations in SeaWiFS performance as a function of latitude, due to orbital variations in sensor performance and sun angle dependency of algorithms.

Optical drifter development activities occuring at Dalhousie University intend to develop instruments to measure seven and three upwelling spectral radiances, respectively, and a single downwelling irradiance. Along with temperature and barometric pressure, these data are transmitted over an ARGOS link. Storage procedures are designed to make maximum use of the limited ARGOS bandwidth. (An interrogating store and forward satellite system with greater bandwidth would be beneficial for this purpose.) The upwelling radiance data are obtained at a depth of approximately 0.5 m and must be propagated through the surface using $K_L(\lambda)$ estimated from the relative spectral shape. These water-leaving radiance estimates will, therefore, be inherently less accurate than surface reflectance observations made together with optical profiles and more complete ancillary observations.

Both of these systems are in the test and evaluation phases. High risk areas which are being examined include long-term stability, identification of bio-fouling effects, operating lifetime, and validation of the techniques used for calculating the water-leaving radiance from the simple drifting sensors. The accuracy of the ARGOS system for drifter location is sufficient for global area coverage (GAC), but experience needs to be gained in analysis of the data to demonstrate the feasibility of using ARGOS positioning (150 m to 1 km uncertainty) for system calibration and validation work in water mass regimes where mesoscale variability is significant.

The cost of optical drifters will limit the number deployed. Proponents envision 50 such buoys adrift at any one time throughout the world—a number sufficient to provide a large enough sample size to support viable global validation. In such a scenario, typically 60% of the drifters would be obscured by clouds during a SeaWiFS pass (those in some areas will have a much greater probability for clouds). Furthermore, current divergence areas will be systematically undersampled by drifters.

The uncertainty of calculated L_W derived from drifter data has been estimated to be of the order of 15%, even though at the time they are deployed, the calibrated uncertainty of the instruments will be less than 5%. This estimate may be pessimistic, based on:

1) the untestable possibility of drifts in radiometric responses during long-term deployment of an expendable instrument, and
2) errors associated with propagating $L_u(0.5\text{ m}, \lambda)$ through the water column and interface to estimate $L_W(\lambda)$ without benefit of measurements of $K(z, \lambda)$, surface roughness, and other ancillary measurements to be carried out at corresponding ship stations.

If L_{WN} from drifters is only good to 15%, then they cannot be used to verify SeaWiFS radiometry within 5%, no matter how many drifter comparisons are made. Uncertainties must be less than 5% if this technology is to be used for SeaWiFS radiometric validation. Uncertainties of 15% may, however, be useful for validating SeaWiFS and derived products, and for interpolating SeaWiFS data through periods of extensive cloud cover.

Chapter 3

Specifications

INTRODUCTION

This report describes measurements of optical properties, and other variables, necessary for validating data obtained with the SeaWiFS instrument, and for the development of in-water and atmospheric algorithms. The specifications herein are those required of instruments used on ships, or other platforms, to acquire that optical data. In some cases, the specifications have been selected to allow use of instruments that are affordable and that either currently exist, or that can be developed without major improvements in today's state-of-the-art technology. In a few cases, new or improved instruments must be developed to realize the specified performance characteristics. The data uncertainty requirements for this program are more severe than those for a general ocean survey. Here, various investigators will use a variety of instruments that will be calibrated independently at a number of facilities, and contribute data to a common database which will be used to validate SeaWiFS measurements. The resulting radiometric and bio-optical database will provide an essential means of detecting and quantifying on-orbit changes in the SeaWiFS instrument relative to its prelaunch calibration and characterization. This chapter specifies instrument characteristics and data uncertainties thought by the SPSWG to be necessary, as well as sufficient, for this task. The validation analysis would be significantly degraded should calibration errors or differences of even a few percent, or wavelength errors or differences of a few nanometers, occur in (between) the instruments used to acquire the SeaWiFS bio-optical database.

3.1 IN-WATER RADIOMETERS

This section specifies radiometric characteristics for instruments that are used to measure $E_d(z,\lambda)$, $E_u(z,\lambda)$, and $L_u(z,\lambda)$. The specifications are applicable to filter radiometers and to spectroradiometers based on monochromators. Minimum performance characteristics are specified for spectral resolution, radiometric responsivity and resolution, SNRs, radiometric saturation and minimum detectable values, angular response, temporal sampling resolution, linearity, and stability.

3.1.1 Spectral Characteristics

In-water radiometers shall be capable, as a minimum, of making measurements at the wavelengths shown in Table 2. The table presumes the use of properly blocked interference filters to provide the required spectral bandpass and out-of-band rejection (10^{-6} or better). Care must also be taken to avoid possible out-of-band leakage due to fluorescence by filter, or other optical component, materials. Filter radiometers should have channels with center wavelengths, as measured in the assembled instrument, matching those given in Table 2 to within ±1 nm for 410 and 443 nm, and within ±2 nm for all other spectral bands. Shifts of these magnitudes in center wavelengths will result in changes in measured radiometric values of approximately ±1% or less (Booth pers. comm.) and this specification should be met if possible.

Table 2. Recommended spectral bands for discrete wavelength filter radiometers using 10 nm full-width at half-maximum (FWHM) bandwidths. In addition, out-of-band blocking in the far tails of the instrument response functions should be at least 10^{-6}.

SeaWiFS Band	*Wavelengths* [nm]	E_d, E_u, L_u [nm]	E_s [nm]
1	402–422	412 [1]	412
2	433–453	443, 435 [2]	443
3	480–500	490	490
4	500–520	510	510
5	545–565	555	555
6	660–680	665, 683	665 [3]
7	745–785	[4]	780
8	845–885	[4]	875 [5]

[1] A preferred option is to replace two separate 10 nm FWHM bands centered at 406 and 416 nm, with a single 412 nm channel. The two channels would allow more accurate modeling of $L_{WN}(412)$ matching SeaWiFS characteristics.

[2] An optional extra band is used to improve modeling of $L_{WN}(\lambda)$ radiances to match the SeaWiFS 443 nm channel.

[3] E_s deck, only one channel in this band is necessary.

[4] Due to the specialized nature of infrared in-water measurements, specialized sensors will be needed.

[5] Optional for E_s.

It is recognized, however, that enforcing a ±1 nm hard-and-fast specification could be prohibitively expensive, and this tolerance should be regarded as a goal. With knowledge, to less than 0.2 nm, of the actual center wavelengths and complete spectral response functions, corrections probably can be made to infer effective radiometric quantities for the SeaWiFS channels, when the spectral characteristics of SeaWiFS channels have also been measured, shortly before launch. Bandwidths must be 10 nm ±2 nm FWHM. They are made narrower than the SeaWiFS channels to reduce the skewing of the parameters derived from underwater irradiance or radiance profiles in spectral regions where absorption by natural sea water may exhibit rapid variation with wavelength.

To maintain the above tolerances, it is anticipated that filters will be ordered to a center wavelength with a tolerance of $\lambda_0 \pm 1$ nm and a FWHM bandwidth of 8.5 ±1 nm. When the filter is installed in a radiometer with a 10° (half-angle) FOV, however, the spectral bandpass will broaden by 2–3 nm, and the center wavelength will shift. Furthermore, as a filter ages in use, its transmission curve may undergo changes to further broaden the FWHM bandpass and shift the peak. The tolerances specified above include an allowance for some degradation before expensive filter and detector changes must be done.

Table 3. High resolution spectroradiometric specifications.

Optical Sensors	
Spectral Range:	380 to 750/900 nm
Spectral Resolution:	5 nm (or less FWHM)
Wavelength Accuracy:	10% FWHM of resolution (0.5 nm)
Wavelength Stability:	5% FWHM of resolution (0.25 nm)
Signal-to-Noise Ratio:	1,000:1 (at minimum)
Stray Light Rejection:	10^{-6}
Radiometric Accuracy:	3%
Radiometric Stability:	1%
FOV Maximum:	10° (for radiance)
Temperature Stability:	Specified for 0–35° C
Linearity:	Correctable to 0.1%
Ancillary Sensors	
Temperature:	0.2° C
Pressure:	0.1% (full scale)
Horizontal Inclination	1° over 40° range

In a single instrument, all channels at a given nominal wavelength should match within 1 nm, if possible. It is desirable, therefore, to obtain all of the filters used by an investigator for measurements at any nominal wavelength (λ_n) from a single manufacturing lot when possible. If this is done, $E_s(\lambda_n)$, $E_d(\lambda_n)$, $E_u(\lambda_n)$, $L_u(\lambda_n)$, and any atmospheric radiometric quantities measured with that investigator's systems, would all have a greater likelihood of being measured over the same range of wavelengths, for each nominal wavelength (λ_n). In any event, the actual spectral response function of each instrument channel must be measured and known to be accurate to less than 0.2 nm.

High resolution monochromator-based spectroradiometers, with adequate sensitivity and stray light rejection characteristics, are also suitable instruments and are recommended for many algorithm development studies. Suitable specifications for such instruments are given in Table 3. (These instruments must also meet the specifications summarized in Tables 2 and 4.)

3.1.2 Responsivity, SNR, and Resolution

The expected operating limits for radiometric responsivities, SNR, and digital resolution are specified in Table 4, the limits for which were derived as follows:

1. An E_d saturation value of 300 μW cm^{-2} nm^{-1} is assumed at all wavelengths.
2. Implicit, but not stated, in Table 4 is that the minimum required $E_d(0)$ is 20 μW cm^{-2} nm^{-1}; it will not be appropriate to occupy validation stations when illumination is less than this minimum.
3. The minimum $E_d(0)$ implies a minimum detectable $E_d(z)$ value of 1 μW cm^{-2} nm^{-1} at 3 optical depths $(3/K)$.
4. Digital resolution must be less than or equal to 0.5% of the reading to maintain a 100:1 SNR. To permit a 1% uncertainty in absolute calibration, if that goal can be met in the calibration laboratory, the instrument must digitally resolve 0.1% of the irradiance (radiance) produced by the laboratory standards used; typical irradiance (radiance) values for calibration using 1,000 W FEL standard lamps traceable to the National Institute of Standards and Technology (NIST), and required digital resolutions at these signal levels, are given in Table 4 as "Calibration Irradiance" and "Digital Resolution (cal.)," respectively. A SNR of 100:1 requires a resolution in $E_d(z)$ at three optical depths to 0.005 μW cm^{-2} nm^{-1} per count, i.e., 2.5 digit resolution. At the surface, $E_d(0)$ should be resolved to 0.05 μW cm^{-2} nm^{-1} per count.
5. The Case-1 saturation values of $E_u(0)$ represent the *Instrument Specification Subgroup's* estimate of maximum reflectances to be expected in ordinary Case-1 waters: 12.5% at 410 nm, 7.5% at 488 nm and 0.5% at 670 nm. These saturation values will be too low for measurements in Case-2 waters or coccolithophore blooms. In these situations, a maximum expected reflectance of 40% for $\lambda < 660$ nm and 20% for $\lambda \geq 660$ nm is assumed. This implies that the expected maximum irradiance in $E_u(0)$ should be 80 μW cm^{-2} nm^{-1} for $\lambda < 660$ nm and 40 μW cm^{-2} nm^{-1} for $\lambda \geq 660$ nm.

Table 4. Required instrument sensitivities for SeaWiFS validation and algorithm development as a function of radiometric measured variable and wavelength.

Property	*Variable*	410 nm	488 nm	665 nm	*Comment*
$E_d(z,\lambda)$,	$E_d(0)_{\max}$	300	300	300	Saturation Irradiance
Downwelled	$E_d\left(\frac{3}{K_d}\right)$	1	1	1	Minimum Expected Irradiance
Irradiance	$\frac{dE}{dN}$	5×10^{-3}	5×10^{-3}	5×10^{-3}	Digital Resolution (profiles)
	$\frac{dE}{dN}$	5×10^{-2}	5×10^{-2}	5×10^{-2}	Digital Resolution (surface unit)
$E_u(z,\lambda)$,	$E_u(0)_{\max}$	120	120	60	Saturation Irradiance (Case-2/coccoliths)
Upwelled		37	22	1.5	Saturation Irradiance (Case-1)
Irradiance	$E_u\left(\frac{3}{K_d}\right)$	1×10^{-2}	2×10^{-2}	1.5×10^{-3}	Minimum Expected Irradiance
	$\frac{dE}{dN}$	5×10^{-4}	5×10^{-4}	5×10^{-5}	Digital Resolution (surface unit)
	$\frac{dE}{dN}$	5×10^{-5}	5×10^{-5}	5×10^{-6}	Digital Resolution (profiles)
$L_u(z,\lambda)$,	$L_u(0)_{\max}$	24	24	8	Saturation Radiance (Case-2/coccoliths)
Upwelled		7.5	4.5	0.3	Saturation Radiance (Case-1)
Radiance	$L_u\left(\frac{3}{K_d}\right)$	2×10^{-3}	4×10^{-3}	3×10^{-4}	Minimum Expected Radiance
	$\frac{dL}{dN}$	5×10^{-4}	5×10^{-4}	5×10^{-5}	Digital Resolution (surface unit)
	$\frac{dL}{dN}$	5×10^{-5}	5×10^{-5}	5×10^{-6}	Digital Resolution (profiles)
E_{cal}, Source	E_{cal}	2	5	15	Calibration Irradiance
Irradiance	$\frac{dE}{dN}$	2×10^{-3}	5×10^{-3}	1×10^{-2}	Digital Resolution (E_d, E_s, E_u cal.)
L_{cal}, Source	L_{cal}	0.6	1.5	4.5	Calibration Radiance
Radiance	$\frac{dL}{dN}$	6×10^{-4}	1×10^{-3}	4×10^{-3}	Digital Resolution (L_u cal.)

Notes: 1. E_u and E_d are in units of $\mu\text{W cm}^{-2}\ \text{nm}^{-1}$ and L_u is in units of $\mu\text{W cm}^{-2}\ \text{nm}^{-1}\ \text{sr}^{-1}$.
2. Responsivity resolution in radiometric units per digital count at the minimum required signal level.
3. Specified ranges should maintain a 100:1 SNR.

6. The minimum required irradiances at three optical depths (as given in Table 4) assumes minimum reflectances of 1% at 410 nm, 2% at 488 nm, and 0.15% at 670 nm.
7. The saturation and minimum radiances, and radiance responsivity resolutions, for $L_u(0)$ and $L_u(z)$ at three optical depths are 0.2 times the corresponding specification for $E_u(0)$ or $E_u(z)$. This assumes $E_u/L_u = Q = 5$ at all wavelengths and depths.

The specifications in Table 4 are meant as guidance to interpret the following required performance requirements:

a) The instrument must maintain a 100:1 SNR at every operating range encountered, during field measurements.

b) The data for measurements obtained in the field must be recorded with a digital resolution less than or equal to 0.5% of reading.

c) The dynamic range of the instrument's linear sensitivity must extend to include the signal levels encountered during laboratory calibrations, and the calibration signals must be recorded with a digital resolution of 0.1% of reading to permit 1% uncertainty in calibration.

In general, the above performance specifications do not pose exceptionally difficult engineering challenges, with the possible exception of the full dynamic range implied by Case-2 or coccolith saturation radiance $L_u(665)$ to minimum expected $L_u(665)$. In any event, this situation will require specially designed radiometers (Section 3.1.8). It is not necessary that every radiometer used for SeaWiFS validation operate over the full dynamic ranges given in Table 4. A radiometer is merely required to maintain the above performance specifications over the dynamic ranges of irradiance and radiance existing at locations and associated illumination conditions where it is used for SeaWiFS validation or algorithm development.

3.1.3 Linearity and Stability

Errors attributable to linearity or stability should be less than 0.5% of the instrumental readings over the dynamic ranges specified in Table 4. This is a challenging goal, but one which must be met if the equally challenging goal of achieving 1% uncertainty in absolute calibration is to be meaningful.

3.1.4 Sampling Resolution

Sampling frequency should be compatible with the profiling technique being used. For the preferred multispectral filter radiometers and spectroradiometric (dispersion) instruments using array sensors, the minimum sampling frequencies are determined by the profiling rate and the depth resolution required. In general, five or more samples per meter should be obtained at all wavelengths. All channels of $E_d(z,\lambda)$, $E_u(z,\lambda)$, and $L_u(z,\lambda)$ at all wavelengths should be sampled within 10^{-2} s at each given depth.

The time response of the instrument to a full-scale (saturation to dark) step change in irradiance should be less than one second to arrive at a value within 0.1%, or one digitizing step, whichever is greater, of steady state. In addition, the electronic e-folding time constant of the instrument must be be consistent with the rate at which the channels are sampled, i.e., if data are to be acquired at 10 Hz, the e-folding time constant should be 0.2 s to avoid aliasing. Individual data scans may be averaged to improve signal-to-noise performance, provided adequate depth resolution is maintained.

3.1.5 Angular Response Characteristics

The response of a cosine collector to a collimated light source incident at an angle θ from the normal must be such that:

1) for E_u measurements, the integrated response to a radiance distribution of the form $L(\theta) \propto 1+4\sin\theta$ should vary as $\cos\theta$ accurate to within 2%; and

2) for E_d measurement, the response to a collimated source should vary as $\cos\theta$ accurate to less than 2% for angles $0° < \theta \leq 65°$ and 10% for angles $65° < \theta \leq 85°$.

Departures from $\cos\theta$ will translate directly to approximately equal errors in E_d in the case of direct sunlight.

The in-water FOV for upwelled radiance bands should be approximately 10° (half-angle). The resulting solid angle FOV (approximately 0.1 sr) is large enough to provide reasonable levels of flux, using silicon detectors, yet small enough to resolve the slowly varying (with θ, for $\theta < 30°$) field of upwelled radiance. Smaller FOV sensors are appropriate, of course, if all of the other performance specifications are satisfied.

3.1.6 Operating Depth

The instruments shall be capable of operating to depths of 200 m. Depths should be measured with an uncertainty of 0.5 m and a repeatability of 0.2 m for profiles in bands 1–6.

3.1.7 Instrument Attitude

The orientations of the instrument with respect to the vertical shall be within ±10°, and the attitude shall be measured with orthogonally oriented sensors from 0–30° with an uncertainty of ±1° in a static mode; it is not intended that this uncertainty be maintained while an instrument is subject to large accelerations induced by surface waves. These data shall be recorded with the radiometric data stream for use as a data quality flag.

3.1.8 Red and Near-Infrared Wavelengths

The fact that the SeaWiFS red and near-IR channels—bands 6, 7, and 8 at wavelengths of 665, 780, and 865 nm, respectively—have such short attenuation lengths in water requires that special attention must be paid to these measurements. Problems due to instrument self-shading (Gordon and Ding 1992) and very rapid attenuation of $L_u(z,\lambda)$ must be considered at these wavelengths. Large instruments, such as the standard Marine Environmental Radiometer (MER) packages from Biospherical Instruments, Inc. (BSI), are not adaptable to these measurements.

Suggested procedures for making the measurements are to use either fiber optic probes carrying light back to a remote instrument, or very small single-wavelength discrete instruments. Each of these concepts is adaptable to deployment from a small floating platform. Care must be taken to avoid direct shading by the supporting platform, but at these wavelengths, the large attenuation coefficients of water makes shadowing by objects more than a few meters away irrelevant.

The minimum measurement scheme would be two discrete (10 nm FWHM) channels at 780 and 875 nm. Additional channels at 750 and 850 nm, or more elaborately, high resolution spectroradiometry, would be useful in determining the spectral distribution of the upwelling light field in these bands.

These measurements should be performed as part of the standard validation data acquisition, because of their importance in the atmospheric correction algorithms. It is anticipated that in the majority of cases, and particularly in most Case-1 waters, these measurements will show negligible upwelling light. In Case-2 waters, cases of extremely high productivity, or in coccolithophore blooms, $L_{WN}(\lambda)$ at these wavelengths may be significant, and these measurements will become very important.

When in-water measurements are performed at these wavelengths, the deck cell channels should be expanded to include bands at 750 and 875 nm (Table 2).

3.2 SURFACE IRRADIANCE

The spectral irradiance at the ocean surface shall be measured at wavelengths which correspond to the SeaWiFS spectral bands (Table 2), but with 10 nm FWHM bandwidth. A total radiation pyranometer may provide helpful ancillary information, but this is not a required instrument.

Instruments mounted aboard ships must be positioned to view the sky with minimum obstruction or reflections from the ship's superstructure, antennas, etc. Particular care must be taken to prevent sun shadows from antennas falling on the irradiance collecting surface. Gimbal mounting of the deck sensor may be helpful to keep the surface of the sensor horizontal. Improperly designed gimbal systems, however, can accentuate fluctuations caused by ship motion, and if there is obvious oscillation in the measured irradiance, the gimballing should be improved to eliminate the problem.

An intuitively attractive technique is to measure irradiance with a sensor floated a fraction of a meter below the sea surface, far enough away from the ship to avoid ship shadows. The flotation assembly should be designed to avoid shadowing the radiometric FOV and to damp wave-induced motions. This type of arrangement has an additional potential for supporting a small sensor to also measure upwelling radiance, $L_u(\lambda)$, just below the surface. Unfortunately, the oceanographic community has only had very limited experience with this approach for measuring $E_s(\lambda)$ (Waters et al. 1990) and its attendant difficulties with wave-induced fluctuations in near-surface E_d. Additional research should be performed to evaluate the use of a floating surface unit as the potentially preferred method for measuring $E_s(\lambda)$ in future revisions to these protocols.

3.2.1 Surface Radiometer Characteristics

The specified number of channels and spectral characteristics of deck cells are the same as those for subsurface irradiance measurements as shown in Table 2. Saturation irradiances are the same as for $E_d(\lambda)$ (Table 4). The dynamic operating range for these sensors needs to only be 25 db, with a SNR of 100:1 but must include the nominal calibration irradiance (Table 4). Linearity must be within $\pm 0.5\%$. Sampling frequency should match the frequency of the underwater radiometer, which should be 1 Hz or faster, and all wavelengths should be sampled within an interval less than or equal to 10^{-2} s. Cosine response characteristics should give relative responsivity to a collimated source (in air) which matches $\cos\theta$, accurate within 2% for $0° \leq \theta < 65°$, and within 10% for $65° \leq \theta \leq 90°$. If a floating surface radiometer is used, its cosine response and immersion characteristics must meet the same specifications as those for profiling irradiance meters.

For some oceanographic process studies, it may be acceptable to use a radiometer system measuring $E_s(\lambda)$ at only a single wavelength. If only a single channel deck radiometer is available, its spectral characteristic should closely match one of channels 2–5 with a 10 nm FWHM bandwidth. A broad-band, or photosynthetically available radiation (PAR), radiometer should never be used for this purpose.

3.3 ABOVE-WATER RADIOMETRY

The performance characteristics to be specified for an above-water ocean color radiometer will vary, depending on how a particular instrument is to be employed in SeaWiFS validation experiments. For radiometric comparisons with SeaWiFS and in-water measurements, the fundamental criterion to be met is that estimates of spectral normalized water-leaving radiance derived from shipboard or airborne measurements must have the same uncertainty specified for those derived from in-water measurements of $L_u(z, \lambda)$ (Table 4). A less accurate radiometer may be used to semi-quantitatively characterize spatial variability near ship stations.

In general, the spectral characteristics of above-water radiometers should match those specified for $L_u(\lambda)$ in Table 2. In some cases, however, it may be acceptable for a radiometer to match the SeaWiFS specifications, which specify center wavelength within 2 nm and 20 nm FWHM bandwidth. Recalling the sensitivity of solar radiometry to the exact center wavelength and detailed spectral response function (Sections 3.1.1 and 4.1.2), any use of airborne radiometers must quantitatively account for the different spectral responsivity functions between measurements of radiance by SeaWiFS, in-water radiometers, and above-water radiometers at each channel's nominal center wavelength.

A high-altitude imaging radiometer must have a radiometric uncertainty and SNR in all channels equal to those of the SeaWiFS instrument if its imagery is to be used for direct radiometric verification of SeaWiFS radiometric performance. In some cases, the requisite SNR may be realized through pixel averaging to a 1 km spatial resolution commensurate with that of SeaWiFS. Direct radiometric comparisons between aircraft and SeaWiFS radiances, however, also require that the different atmospheric path effects be carefully modeled, and that the uncertainty in those modeled adjustments be independently estimated. This can be done most effectively when the aircraft measurements are combined with the full suite of shipboard in-water, atmospheric, and ancillary measurements (Table 1). In this case, direct comparisons between aircraft and ship radiometry may require that both the SNR *and* the uncertainties realized in combined analyses of the two data sets will represent a smaller spatial resolution than the nominal 1 km instantaneous field-of-view (IFOV) for SeaWiFS.

Performance characteristic specifications are similar for ocean color radiometers used to measure water-leaving radiance from either the deck of a ship or an aircraft flown

at low altitude, i.e., 200 m altitude or lower. Radiometric characteristics should match the criterion set forth for in-water $L_u(\lambda)$ radiometers in Sections 3.1.1–3.1.4 and Tables 2–4. The instrument FOV should be between 5° and 10° (full angle), and all wavelengths must be coregistered within 10% of the IFOV. All channels must be scanned simultaneously, or within less than 10^{-2} s (depending on the digitizing design), to avoid aliasing due to varying wave reflectance in shipboard measurements, and to avoid time-space aliasing in airborne measurements. This constraint precludes use of filter wheel radiometers and others which scan channels sequentially over a time interval greater than 10^{-2} s. Sampling over longer periods of time may be done by either electronic integration of all channels simultaneously, or by averaging multiple scans.

A radiometer's sensitivity to the polarization of aperture radiance is critical for ocean color remote sensing applications. Polarization sensitivity is likely to be present in any radiometer having mirrors, prisms or gratings in its optical path. To measure accurate water-leaving radiances using instruments of these types, it is necessary to depolarize aperture radiance using either fiber-optics or a *pseudo-depolarizer*. Shipboard and airborne ocean color radiometers must have a polarization sensitivity of less than 2% in all channels. The sole exception to this rule will occur in the case of instruments designed to actually measure the polarization components of aperture radiance, e.g., the polarization channels of the French Polarization and Directionality of the Earth's Reflectances (POLDER) instrument.

Each application of a particular above-water radiometer system, if it is proposed for SeaWiFS validation, must be evaluated on its own merits. The instrument's responsivity, uncertainty, stability, FOV, and spectral characteristics must be evaluated in the context of the models to be used to compare its radiance measurements to in-water, or SeaWiFS, radiance measurements. The suitability of spatial averaging to improve SNRs must be evaluated in terms of the spatial variability prevailing in the experiment site, particularly when in-water and aircraft radiances are to be directly compared. Finer resolution aircraft imagery, or low-altitude trackline data, will often be essential for determining the validity of attempts to directly compare in-water and SeaWiFS radiances measured at a particular site.

In summary, airborne and shipboard above-water radiometry can obviously contribute extremely valuable data for validating the radiometric performance of the SeaWiFS instrument and the algorithms employed with SeaWiFS data. There is, however, a wide possible range of radiometer characteristics that can be applied to this program, and detailed specification of required characteristics can only be done in the context of each particular experiment's design. Only the guiding principals and desired end-to-end performance are specified here.

3.4 IOP INSTRUMENTS

The IOPs are:

1) the beam attenuation coefficient, $c(z,\lambda)$, in units of m^{-1};
2) the absorption coefficient, $a(z,\lambda)$, in units of m^{-1}; and
3) the volume scattering function, $b(z,\lambda_0,\theta)$, in units of m^{-1} sr^{-1}.

The integral of the volume scattering function over 4π steradians is the total scattering coefficient, $b(z,\lambda)$, with units of m^{-1}. The integral of the volume scattering function over the back hemisphere is the backscattering coefficient, $b_b(z,\lambda)$, with units of m^{-1}.

It will be possible to measure the spectral attenuation and absorption coefficients *in situ* at the time of SeaWiFS deployment. The instruments for the measurement of the spectral absorption and attenuation coefficients should, at a minimum, have the characteristics given in Table 5.

Spectral resolution at more than SeaWiFS wavelengths would be desirable to deduce pigment concentrations. In the case of beam attenuation coefficients, the requirements for uncertainty and precision correspond to changes in $c(\lambda)$ resulting from changes in concentration of approximately 5 and 2 $\mu g\, l^{-1}$ of suspended mass, respectively. Stability should be tested with instruments connected to the data acquisition system. Stability with time should be better than 0.005 m^{-1} between calibrations.

Table 5. Minimum instrument characteristics for the measurement of the spectral absorption and attenuation coefficients.

Instrument Characteristics	
Spectral Resolution:	410, 443, 490, 510, 555, and 670 nm
Bandwidth:	10 nm
Uncertainty:	0.005 m^{-1}
Precision for $\lambda < 650$ nm:	0.002 m^{-1}
Precision for $\lambda \geq 650$ nm:	0.005 m^{-1}
Stability with Temperature:	0.005 m^{-1} over 0–25° C
Sampling Interval:	$\geq$ 4 samples m^{-1}
Source Collimation Angle:	$\leq$ 5 mrad
Detector Acceptance Angle:	$\leq$ 20 mrad
Depth Capability:	200 m

The spectral total scattering coefficient cannot be measured directly. It can be obtained from $b(\lambda) = c(\lambda - a(\lambda)$, provided $c(\lambda)$ and $a(\lambda)$ are determined with the appropriate uncertainty. The spectral backscattering coefficient, $b_b(\lambda)$, has the same requirements for spectral resolution, bandwidth, and linearity as $a(\lambda)$ and $c(\lambda)$. Since $b_b(\lambda)$ is not a transmission-like measurement, however, the uncertainty of its determination will be approximately 10%.

The shape of the volume scattering function can, at present, be determined *in situ* only crudely with devices

like the ALPHA and Scattering Meter (ALSCAT) and the General Angle Scattering Meter (GASM), which were built more than a decade ago at the Visibility Laboratory of the Scripps Institution of Oceanography. These are single angle measurement devices, which must be scanned as a function of angle and wavelength. Because measuring scattering with these instruments is a slow process, they do not lend themselves readily to incorporation into other instrument platforms. Since it will be possible to independently determine $b(\lambda)$ and $b_b(\lambda)$ when SeaWiFS is deployed, the determination of the shape of the volume scattering coefficient could possibly be determined with acceptable uncertainty by means of measurement of a few moments of the scattering function. A new instrument development effort would have to be initiated to pursue this approach.

3.5 ATMOSPHERIC AEROSOLS

Sun photometers should be used to measure atmospheric aerosol optical thickness. These sun photometers should have specifications in agreement with the World Meteorological Organization (WMO) sun photometer specifications (Frohlich 1979). Specifically, the instruments should have a 2° FOV, temperature stabilization, and a precision of ±0.01%. The specific wavelengths of channels should correspond to the recommended WMO wavelengths of 380, 500, 675, 778, and 862 nm. For SeaWiFS validation, additional channels at 410, 440, 490, 510, and 555 nm should be added to the WMO set.

3.6 SPECTRAL SKY RADIANCE

Measurements of spectral sky radiance distribution should be made using a photoelectric all-sky camera. Spectral characteristics of the sky radiance camera channels are those specified for $E_s(\lambda)$ (Table 2). Data should be in a format such that absolute radiance values can be obtained with an uncertainty of 5% and sky irradiance can be determined from integrals of the data to within 10%. If the dynamic range of the camera is insufficient to capture both the sun and sky distribution, neutral density filters (or some other method) should be used so that radiance from both the sun and sky can be measured.

3.7 PHYTOPLANKTON PIGMENTS

HPLC equipment and associated standards must conform to protocols specified in Chapter 9 of the *JGOFS Core Measurement Protocols* (JGOFS 1991). *In situ* chlorophyll fluorometers should have a resolution of at least 0.001 mg of chlorophyll *a* per m^3.

3.8 HYDROGRAPHIC PROFILES

A calibrated CTD system should be used to make profiles to maximum depths between 200 and 500 m. The instrument should meet the minimum specifications given in Table 6.

Table 6. The minimum instrument characteristics for the measurement of hydrographic profiles are listed.

Parameter	*Range*	*Uncertainty*	*Resolution*
Pressure [dbars]	0–500	0.3%	0.005%
Temperature [°C]	−2–35	0.015° C	0.001° C
Salinity [PSU]	1–45	0.03 PSU	0.001 PSU

Chapter 4

Sensor Characterization

INTRODUCTION

This chapter details procedures to characterize the sensor performance specifications prescribed in Chapter 3. Procedures for characterizing environmental radiometers are presented in Section 4.1, including special characteristics of underwater radiometers. Section 4.2 describes radiometric standards used as a basis for absolute responsivity characterization of radiometers. Special consideration for radiometers measuring $L_W(\lambda)$ above water, either from a ship or aircraft, are discussed in Section 4.3. The remaining Sections, 4.4–4.8, address calibrations of IOP instruments, sun photometers, radiance distribution cameras, HPLC and fluorometric systems, and CTD profiles.

4.1 RADIOMETRY

The characterization of radiometric instruments used for the acquisition of field data for SeaWiFS validation and algorithm development shall include the determination of those instrument characteristics that affect its calibration as used in the field environment. In addition to the obvious radiometric calibration, it is therefore necessary to determine:

a) the spectral sensitivities of the various measurement channels;

b) the angular sensitivities of an irradiance or radiance sensor in the medium, i.e., air or water, in which it is to be used;

c) the temporal response of the system;

d) the effects on responsivity caused by water immersion; and

e) the effects of temperature and pressure on the above characteristics.

The elements of radiometer characterization and calibration are outlined schematically in Fig. 1.

For any instrument to provide suitable data for SPO use, the investigator must be certain that the instrument characterization has not changed beyond accepted limits and that the time history of the calibration is traceable. Certain attributes, e.g., angular response characteristics, are sufficiently constant that they only need to be determined once, unless the instrument is modified. The exact nature of instrument modifications during maintenance will determine which characterization procedures must be repeated. On the other hand, radiometric calibrations and the assessment of system spectral characteristics of filter radiometers, must be repeated before and after each major field deployment.

4.1.1 Absolute Radiometric Calibration

Determination of the absolute radiometric responses of the irradiance and radiance sensors requires the availability of a properly manned and equipped radiometric calibration facility. Such a facility must be equipped with suitable stable sources and sensors, e.g., lamp standards of spectral irradiance and flat response radiometers, respectively. Either the sources or the sensors must have defined spectral radiometric characteristics that are traceable to NIST (Section 4.2). The calibration facility must also have a variety of specialized radiometric and electronic equipment, including: reflectance plaques, spectral filters, integrating spheres, and highly regulated power supplies for the operation of the lamps. Precision electronic measurement capabilities are also required, both for setting and monitoring lamp current and voltage and for measuring the output of the radiometer.

It is not expected that every investigator will be able to perform his own radiometric calibrations; because of this, a few centrally located facilities will be equipped and staffed to perform these calibrations as a routine service for the community. The facilities will perform frequent intercomparisons to assure the maintenance of the radiometric traceability to the NIST standard of spectral irradiance. The goal shall be to provide reproducible calibrations from 400–850 nm to within better than $\pm 1\%$; the minimum requirement for radiometric data to be used in SeaWiFS validation is for repeatable calibrations within less than 5%.

Radiometric calibrations of irradiance sensors will be performed after it has been ascertained that: the conformity of the sensor angular response to the required cosine function is satisfactory, the sensor linearity is satisfactory, and the spectral sensitivity, including out-of-band blocking, is known and satisfactory.

Radiometers shall be calibrated using a 1,000 W FEL standard of spectral irradiance, with calibration traceable

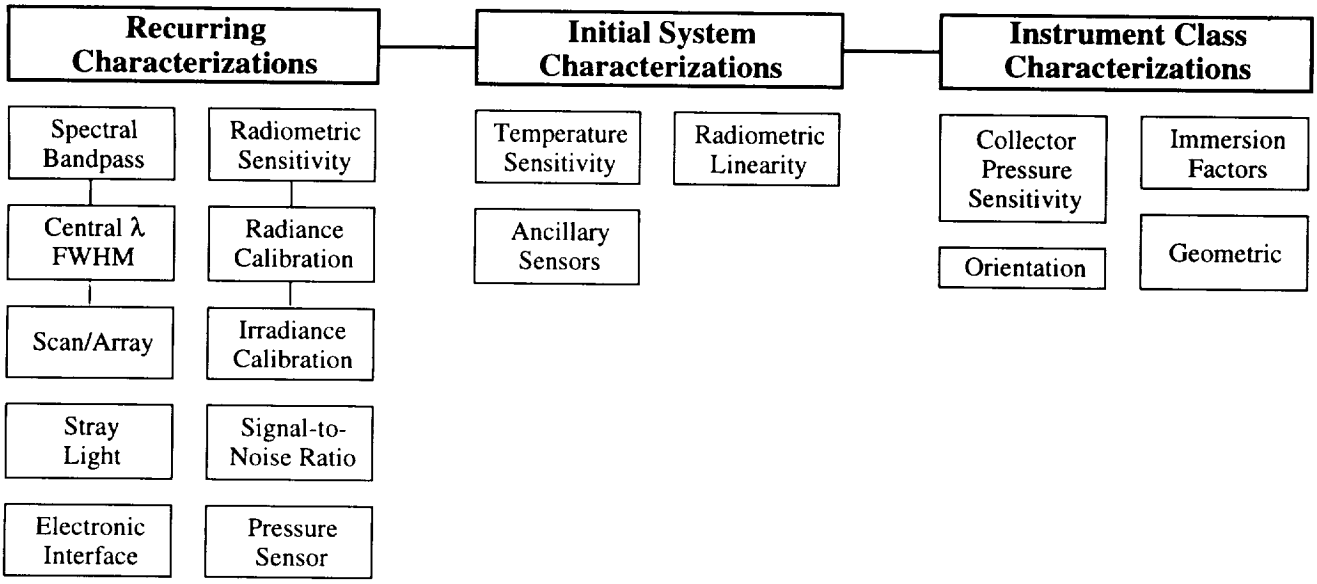

Fig. 1. Elements of radiometer characterization and calibration.

to NIST and lamp operation in accordance with Walker et al. (1987). The irradiance collector is placed normal to, and at the prescribed distance from, a working standard lamp of spectral irradiance. The lamp should be of appropriate size to provide an irradiance at the sensor that will be at least 30%, and preferably above 50%, of full-scale for the sensor channel being calibrated, although this is not always achievable in practice (Table 4). The lamp-sensor space shall be appropriately baffled and draped so that occulting the direct path between lamp and sensor will result in a response of less then 0.1% of the response to the lamp flux.

For multispectral instruments, all channels may be calibrated simultaneously if sufficient flux is available at all wavelengths. The instrument response is recorded for all channels together with associated dark responses. Ambient and photosensor temperatures are recorded, where available. For characterization, the radiometric calibration should be performed at temperature extremes of $-2°$ C and 40° C for in-water sensors, and at $-10°$ C and 45° C for irradiance sensors used above the surface. If responses differ significantly at temperature extremes, responses should also be determined at intermediate temperatures.

The portable irradiance and radiance reference standard to be used to trace instrument stability during field deployments (Section 4.2.5) should be placed in position on the sensor immediately following the calibration to establish the instrument response to this reference unit.

Radiance calibration activities require a uniform source of known radiance that will fill the angular field of view of the radiance sensor. The two procedures that may be used are given below.

Calibration Methods

1. A working lamp standard of spectral irradiance is placed at the prescribed distance from a plaque of known Lambertian reflectance. The plaque is normal to, and centered on, the lamp calibration axis. The radiance sensor is positioned to view the plaque at an angle of 45° from the plaque normal (any other angle at which the diffuse reflectance of the plaque is known is acceptable also). It must be established that the plaque fills the sensor's FOV and that the presence of the sensor case has not perturbed the irradiance on the plaque. The instrument response and dark signal is recorded. It must be verified that the plaque fills the FOV with uniform radiance for each channel of a multichannel radiance sensor. Separate calibration setups may be required for different channels and the lamps may have to be moved as much as 3 m away from the plaque to assure uniform illumination. This procedure is difficult to apply to sensors with a large FOV.
2. An integrating sphere with an exit port of sufficient size to fill the FOV of the radiance sensor may be used if the radiance of the exit port, at the channel wavelengths, can be determined with sufficient uncertainty.

These methods are discussed more fully in Section 4.2.2.

4.1.2 Spectral Bandpass Characterization

These instruments should be characterized to define the nominal wavelengths and bandwidths, defined as the full width of the passband as measured to the FWHM intensity points. The nominal, or center wavelength, will usually be defined as the wavelength halfway between wavelengths at which the normalized response is 0.5, and the channel is characterized by this wavelength and the FWHM bandwidth. The determination of the spectral response function, i.e., the passband, will be made for each channel with

a scanning monochromatic source, with a bandwidth less than 0.2 nm; the source output must be normalized to a detector of known spectral sensitivity. The response function thus measured is then normalized to the maximum (peak).

Although the results of this characterization are usually represented by only the nominal wavelength and FWHM bandpass, the full normalized response function should be recorded for use in detailed wavelength adjustments and comparisons with the SeaWiFS channel response functions, which will not be known until shortly before launch. It is further recommended that the internal instrument temperature be monitored during these tests, and that the test be repeated at two temperatures at least 15° C apart, e.g., 10°and 25° C. If a significant shift, greater than 1.0 nm, with temperature of either the center wavelength or bandwidth is detected, then additional temperature calibration points are recommended. Dark offsets must be recorded during each test.

For spectral characterizations of irradiance diffusers, the entire surface of the diffuser should be illuminated by the monochromator's output. In the case of radiance detectors, a diffuser should be used to diffuse the monochromator slit image and uniformly fill the instrument's FOV.

The wavelength response of a monochromator-based radiometer is calibrated by scanning over line sources, with sharp peaks at well known wavelengths. Suitable spectral calibration sources, such as, mercury, cadmium, and neon lamps, are provided by several vendors, together with tabulations of the wavelengths of the emission lines generated by each source.

The width of the slit function of a monochromator may be estimated by scanning over a laser line, e.g., helium-neon, at a very small wavelength interval. The instrument FOV must be filled during the test.

It is anticipated that the monochromator-based spectral characterization will not be able to adequately measure leakage of broadly distributed out-of-band radiation; therefore, blocking of blue light in channels longer than 540 nm must be routinely tested. Where continuous wave (CW) argon lasers are available, out-of-band response should be measured at 488 nm. One recommended test that can be performed during the absolute calibrations at $\lambda \leq 640$ nm is the sequenced measurement of three Schott BG-18 filters, each 1 mm thick, using an FEL-type light source. The procedure is to measure the channel signal using each filter separately, then in combination, and comparing the computed and measured transmissions. If a significantly higher combined transmission of the three filters, when they are used in combination, is measured relative to the calculated transmittance, then spectral leakage is present. At wavelengths greater than 640 nm, other filters that attenuate the wavelength of interest, with a transmission value of less than or equal to 0.1 and which pass shorter wavelength light with significantly greater transmission, should be substituted for the BG-18.

Consideration must also be given to unblocked fluorescence by the filters, or other optical elements, as a possible source of light leaks. Methods to test for fluorescence contamination specifically, are not well established at this time.

While leakage of blue light into red channels is the most significant oceanographic optical problem, the leakage of red and IR light into blue channels can cause significant errors when the instrument is calibrated using a red-rich source. A convenient way to measure this leakage is to place a long wavelength-pass, sharp-cut, absorbing glass filter that does not exhibit fluorescence between a broad band (e.g., incandescent) source and the sensor. A non-zero response indicates unwanted out-of-band red response and the need for improved red blocking.

4.1.3 Temporal Response

The temporal response of a spectrometer may be examined by introducing a step function of near full-scale flux to the system using an electrically operated shutter and measuring the system's transient response at 0.1 s, or shorter, intervals. The response should be stable within one digitizing step, or 0.1%, whichever is greater, of the steady state value in one second or less.

4.1.4 Radiance Field-of-View

It is required that the radiance FOV of the instrument be known. The FOV should not normally enter into the absolute calibration, however, if the FOV is fully filled by a calibration source of uniform radiance.

In this test, the instrument is placed on a rotational stage with the entrance aperture of the radiometer over the rotation axis. A stable light source with a small filament is placed several meters in front of the instrument, which is then scanned from $-30°$ to $+30°$ in 2° increments. The angle positioning should be within $\pm 0.1°$. The on axis, 0°, mechanical alignment is made using the window surface as reference, by adjusting to get the reflection of the lamp filament to return on axis. The error in this alignment is approximately $\pm 0.1°$. The in-air measurement angles, θ_a, are converted to corresponding angles in seawater, θ_w, using the relation $\theta_w = \theta_a / n_w$, where n_w is the index of refraction of seawater at the particular wavelength of each channel.

4.1.5 Collector Cosine Response

The directional response of cosine collectors must be characterized. The directional response of the deck cell is determined in air, and the in-water instruments are measured immersed in water. Full spectral determinations are required. For instruments measuring upwelling irradiance $E_u(z, \lambda)$, it is recommended that the cosine response of each instrument be measured individually. For downwelling irradiance $E_d(z, \lambda)$ instruments, checking a production

run may be satisfactory if the vendor's material and design are demonstrated to be uniform throughout the duration of the run.

Absolute responsivity calibration of an irradiance meter is done in air, using light incident normal to the collector. To properly measure irradiance incident on the plane at all angles θ (relative to the normal), the instrument's response should follow a cosine function. In other words, for an instrument response $V(0)$ to a given collimated irradiance incident at $\theta = 0$, if the instrument is rotated to the angle θ away from the original normal axis, the response should be $V(\theta) = V(0)\cos\theta$. If this requirement is met, then the on-axis calibration is sufficient and the device will correctly measure irradiance arriving at the plane of the collector, regardless of the directional distribution at which the light arrives.

The preferred irradiance collector design has an improved cosine response over that of a simple flat plate diffuse collector (Boyd 1955 and Tyler and Smith 1979). This improvement is mostly for near-grazing angles (θ approaching 90° to the normal) and is particularly important when measurements of the upwelling underwater irradiance are made, i.e., with the collector facing downward. In that case, most of the light is from the sides, in the region of these near-grazing angles.

Since $E_d(z,\lambda)$ measurements are to be made underwater, the testing to determine the fidelity of the instrument to the cosine function must be made with the instrument submerged. A description of the suitable experimental procedure follows Petzold and Austin (1988).

The instrument is suspended in a tank of water while supported by a fixture designed to allow rotation about an axis through the surface and center of the collector. A tungsten-halogen lamp with a small filament is enclosed in a housing with a small exit aperture and placed approximately 1 m from a large window in the tank. The collector is placed approximately 25 cm behind this window; an equivalent lamp distance of 1.25 m or more is required. A circular baffle should be placed immediately in front of the window to reduce stray light. The water should be highly filtered to the extent that the effects of scattered light are indiscernible.

The equivalent air path lamp distance should be approximately 1.25 m or greater. At this distance, the fall-off at the outer edge of a 6 cm diameter diffuse collector would be 0.9994, or −0.06%, when the diffuser is at $\theta = 0°$ with the normal. The net effect over the entire area of the diffuser would be 0.9997 or −0.03%. When $\theta = 90°$, with the diffuser edge-on to the lamp, the distance to the lamp varies for different points on the surface. The net error over the entire surface for this condition is 0.99997 or −0.003%. All other angles fall between these limiting cases.

The signals from the instrument are recorded for $\theta = 0°$ and at 5° intervals to $\theta = \pm 75°$ and 2.5° intervals over $75° < \theta < 90°$. The readings at $\theta = 0°$ are recorded at the beginning, the middle, and the end of each run and examined as a measure of lamp and instrument stability over the time involved. At least two runs should be made about different axes through the surface of the diffuser. All readings are normalized to 1.000 at $\theta = 0°$ and then compared with the value of the cosine of each angle. If $V(\theta)$ is the normalized measured value, relative local error at angle θ is given as $(V(\theta)/\cos\theta) - 1$.

Assuming the average response to the four measurements made at each θ (four separate azimuth angles ϕ) adequately represent the overall mean cosine response of the collector, then the error, ϵ, in measuring irradiance over the interval $\theta_n < \theta < \theta_N$ for a uniform radiance distribution is approximately

$$\epsilon = \frac{\sum_{i=n}^{N} \overline{V}(\theta_i)\sin\theta_i\,\Delta\theta}{\sum_{i=n}^{N} \cos\theta_i\sin\theta_i\,\Delta\theta} - 1, \qquad (1)$$

using a simple trapezoidal quadrature. Similarly, for a radiance distribution of the form $1 + 4\sin\theta$, to simulate upwelled irradiance

$$\epsilon = \frac{\sum_{i=0}^{N} \overline{V}(\theta_i)(1+4\sin\theta_i)\sin\theta_i\,\Delta\theta}{\sum_{i=0}^{N} \cos\theta_i(1+4\sin\theta_i)\sin\theta_i\,\Delta\theta} - 1, \qquad (2)$$

where $\theta_0 = 0$, $\theta_N = \frac{\pi}{2}$ and $\Delta\theta = \frac{\pi}{2N}$.

The asymmetry of the cosine response, δ, is equivalent to an effective tilt of an ideal cosine collector with respect to the instrument's mechanical axis, which can be quantified as

$$\delta = \frac{\int_{\theta_1}^{\theta_2} \cos(\theta+\theta_t)\sin\theta\,d\theta}{\int_{\theta_1}^{\theta_2} \cos(\theta-\theta_t)\sin\theta\,d\theta}, \qquad (3)$$

where θ_t is the tilt angle.

The measured asymmetry is computed as the ratio of sums of measurements at opposite ϕ ($\theta \geq 0$) and $-\pi$ ($\theta < 0$) in the same plane, that is,

$$\delta = \frac{\sum_{i=0}^{\theta_N=\pi/2} \overline{V}(\theta_i,0)\sin\theta_i\,\Delta\theta}{\sum_{i=0}^{\theta_N=-\pi/2} \overline{V}(\theta_i)\sin\theta_i\,\Delta\theta} - 1, \qquad (4)$$

for $\Delta\theta = \pm\frac{\pi}{2N}$.

Variations in asymmetry from channel to channel may be due to the placement of the individual detectors behind the diffuser. Any offset of the average asymmetry with the

mechanical axis could be due to any one of a variety of causes:

1) the alignment on the rotating test fixture not being correct,
2) tilt of the diffuser,
3) the detector array not being centered,
4) nonuniformity of the reflectance of the internal surfaces of the instrument between the diffuser and the sensor array, or
5) nonuniformity of the diffuser.

4.1.6 Immersion Factors

When a plastic, opal-glass, or Teflon diffuser is immersed in water, its light transmissivity is less than it was in air. Since an instrument's irradiance responsivity is calibrated in air, a correction for this change in collector transmissivity must be applied to obtain irradiance responsivity coefficients for underwater measurements.

The change in a collector's immersed transmissivity is the net effect of two separate processes: a change in the reflection of light at the upper surface of the collector, and internal scattering and reflections from the collector's lower surface. A small part of the light flux falling on the collector is reflected at the air-plastic, or water-plastic, interface, and the majority of the flux passes into the collector body. The relative size of this reflectance, called *Fresnel reflectance*, depends on the relative difference in refractive indices between the diffuser material and the surrounding medium.

The refractive index of the collector material is always larger than that of either water or air, and because the refractive index of water is larger than that of air, Fresnel reflectance is smaller at a diffuser-water interface than at a diffuser-air interface. Thus, the initial transmission of light through the upper surface of an irradiance collector is larger in water than in air. The immersed upper surface is, on the other hand, also less effective at reflecting the upward flux of light backscattered within the diffuser body and light reflected at the lower diffuser-air interface in the instrument's interior, processes that are not affected by immersion. Therefore, a larger fraction of the internally scattered and upwardly reflected light passes back into the water column than would be lost into air. Because the increased upward loss of internally reflected flux exceeds the gain in downward flux through the diffuser-water interface, the net effect of these competing processes is a decrease in the collector's immersed transmissivity.

To measure this effect, a suggested and acceptable procedure is as follows: The instrument is placed in a tank of water with the irradiance collector level and facing upward. A tungsten-halogen lamp with a small filament, powered by a stable power supply, is placed at some distance above the water surface. The depth of the water is lowered in steps and readings are recorded for all wavelengths from each carefully measured depth. A final reading is taken with the water level below the collector, i.e., with the collector in the air. The amount of energy arriving at the collector varies with the water depth and is a function of several factors:

a) the attenuation at the air-water interface, which varies with wavelength;
b) the attenuation over the water pathlength, which is a function of depth and wavelength; and
c) the change in solid angle of the light leaving the source and arriving at the collector, caused by the light rays changing direction at the air-water interface, which varies with wavelength and water depth.

Using Fresnel reflectance equations, the transmittance through the surface is

$$T_s(\lambda) = \frac{4n_w(\lambda)}{\left(1+n_w(\lambda)\right)^2}, \tag{5}$$

where $n_w(\lambda)$ is the index of refraction of the water at wavelength λ.

The transmittance through the water path, $T_w(\lambda)$, will be

$$T_w(\lambda) = e^{-K(\lambda)\,z}, \tag{6}$$

where $K(\lambda)$ is an attenuation coefficient of the water and z is the path length in corresponding units.

The change in solid angle with water depth z is given by the factor

$$G(z,\lambda) = \left[1 - \frac{z}{d}\left(1 - \frac{1}{n_w(\lambda)}\right)\right]^{-2}, \tag{7}$$

where d is the distance of the lamp source from the collector surface.

The immersion correction factor $F_i(\lambda)$ for irradiance is then calculated for each depth z as

$$F_i(\lambda) = \frac{E_a(\lambda)}{E_w(z,\lambda)}\,T_s(\lambda)\,T_w(z,\lambda)\,G(z,\lambda), \tag{8}$$

where $E_a(\lambda)$ and $E_w(z,\lambda)$ are the irradiance in air and the irradiance underwater at depth z, respectively.

There are two unknowns in (5)–(8): the attenuation coefficient of the water $K(\lambda)$ and the immersion factor $F_i(\lambda)$. A minimum of three measurements must be made to solve for $F_i(\lambda)$: one in air to get $E_a(\lambda)$, and two at different water depths for $E_w(z,\lambda)$. The recommended method is to take readings of $E_w(z,\lambda)$ at many depths. Then, using the exact form of (8), a least-squares regression is solved for the $F_i(\lambda)$ and $K(\lambda)$ terms giving the best fit. The complete derivation of (5)–(8) is given in Petzold and Austin (1988).

The absolute calibration for the spectral radiance channels is found by viewing a surface of known radiance in air in the laboratory. When the instrument is submerged in water, a change in responsivity occurs and a correction must be applied. This change in responsivity is caused by the change in the indices of refraction of the different media in which the instrument is immersed—in this case air and water. Two optical changes occur, both of which are caused by the change in refractive index. The two effects to be corrected are:

1) the change in transmission through the interface between the air and the window during calibration, and the same effect through the water-window interface during data measurement, and
2) the change in the solid angle included in the underwater FOV relative to that in air.

Since the refractive index of seawater, $n_w(\lambda)$, is a function of wavelength λ, the correction factor $F_i(\lambda)$ will also be a function of wavelength.

If the refractive index of air is assumed to be 1.000 at all wavelengths, and if $n_g(\lambda)$ is the index of refraction for the (glass) window and $n_w(\lambda)$ is the index of refraction for water, then, as shown in Austin (1976), the correction for the change in transmission through the window, $T_g(\lambda)$, is

$$T_g(\lambda) = \frac{\left(n_w(\lambda) + n_g(\lambda)\right)^2}{n_w(\lambda)\left(1 + n_g(\lambda)\right)^2}, \quad (9)$$

and the correction for the change in the FOV, F_v, is

$$F_v(\lambda) = \left(n_w(\lambda)\right)^2 \quad (10)$$

The index of refraction of a Plexiglas™ window, $n_g(\lambda)$, may be computed using an empirical fit to the Hartmann formula, that is,

$$n_g(\lambda) = 1.47384 + \frac{7.5}{\lambda - 174.71}, \quad (11)$$

where λ is the wavelength in nanometers (Austin 1976). The index of refraction for seawater $n_w(\lambda)$ may be similarly computed using an empirical fit of the data from Austin and Halikas (1976),

$$n_w(\lambda) = 1.325147 + \frac{6.6096}{\lambda - 137.1924}. \quad (12)$$

The immersion factor $F_i(\lambda)$ is then obtained as

$$F_i(\lambda) = T_g(\lambda)\, F_v(\lambda) = \frac{n_w(\lambda)\left(n_w(\lambda) + n_g(\lambda)\right)^2}{\left(1 + n_g(\lambda)\right)^2}. \quad (13)$$

4.1.7 Linearity and Electronic Uncertainty

The linearity of the radiometric channels must be determined over their expected range of use. The above-surface (deck cell) and underwater irradiance sensors intended for the measurement of downwelling irradiance have full-scale (saturation) values that are not readily obtained with the usual incandescent blackbody sources, such as 1,000 W 3,200 K tungsten-halogen projection lamps. The linearity at the high end of the calibrated range may be determined by using 900–2,000 W high pressure xenon arc lamps, which provide a small, stable source of high intensity (approximately 6,000 K) radiation. With such lamps, irradiance levels approximating full sunlight can be attained. Using such sources for the high end, and the more easily managed tungsten-halogen lamps over the range below 20–30% of full scale, the linearity of the response characteristic of the radiometric channels can be assessed. The flux should be changed in 5 db (0.5 log), or less, steps using a proven and accepted procedure for controlling irradiance such as inverse square law, or calibrated apertures. These suggested procedures for testing linearity at the higher levels are not well established in practice, and research is needed to determine the precision which can be attained.

If departures from linearity are found, they must be incorporated into the calibration function for the instrument and be properly applied to the raw level-1 data to obtain calibrated level-2 irradiance and radiance data. Level-1 and level-2 data are defined in Section 6.1.

It is recommended that all instruments utilizing inputs from ancillary sensors, e.g., transmissometers, be characterized for the linearity and uncertainty of the voltage measurement covering the full output range of the ancillary sensor. For instruments with range dependent gain changing, either manual or automatic, the scale offset and linearity for each range should, at a minimum, be tested annually. Uncertainties exceeding 0.1% of any reading within the normal working range must be investigated and corrected.

Other characteristics of electronic sensor systems may adversely affect measurement uncertainty. During the design and engineering prototype development of a radiometer, the design and implementation must be analyzed to characterize, and correct as needed, possible effects of hysteresis, overload, recovery times, cross talk between either optical transducers or electronic channels, and sensitivity to orientation in the Earth's magnetic field, which is particularly likely with photomultiplier tubes.

4.1.8 Temperature Characterization

Two major types of temperature-induced variation may be seen in an optical radiometric instrument: 1) offset or *dark* changes, and 2) scale *responsivity* changes. Each underwater instrument must be individually characterized over the range of −2–40° C. In the case of deck cells, the

temperature range for testing should be extended to −10–45° C. Sensors exhibiting temperature coefficients greater than 0.01% per °C over this temperature range, should be fully characterized over their respective ranges to establish the means and precision with which post-acquisition processing can be used to correct for temperature dependency. Although knowledge of the zero, or dark current, drift is essential for working at the lowest radiances or irradiances, it should be emphasized that more significant near-surface errors may be induced by temperature variations in responsivity. These possible responsivity changes must be individually determined across the spectrum.

In the above discussion, the temperatures cited are *environmental* temperatures, but it should be emphasized that any correction must use the temperature of the affected element, which is normally in the interior of the instrument. This is best accomplished by routinely using temperature sensors placed at critical locations within the instrument. For highest precision, dynamic temperature testing involving temporal transients, as well as possible temperature gradients within an instrument, may be appropriate.

4.1.9 Pressure Effects

Pressure can cause radiometric measurement errors by deforming irradiance collectors. Pressure coefficients associated with polytetrafluoroethylene (PTFE) based irradiance diffusers are known to exist, but they are not uniform and there may be hysteresis effects. It is recommended that each type of irradiance detector be examined for variations in responsivity with pressure. If a significant effect is observed, then pressure-dependent responsivity coefficients should be determined separately for each instrument and collector. The pressure characterization should also test for, and quantify, hysteresis and temporal transients in responsivity under a time varying pressure load. The characterization of pressure effects has not previously been common practice, and the requisite procedures are therefore poorly defined; new protocols must be developed.

4.1.10 Pressure Transducer Calibration

The radiometer's pressure transducer, which is used to measure instrument depth during profiles, should be tested and calibrated before and after each major cruise.

4.2 RADIOMETRIC STANDARDS

This section describes sources and methods by which the NIST scale of spectral irradiance is transferred to calibrate irradiance and radiance sensors. The principal working standards used for spectral irradiance responsivity calibration are FEL lamp working standards (Section 4.2.1). The spectral irradiance scales of the FEL lamps are in turn transferred to spectral radiance scales using plaques of known bidirectional reflectance, or integrating spheres, or both (Section 4.2.2). An ongoing series of SeaWiFS Intercalibration Round-Robin Experiments (SIRREXs) has been initiated by the SPO to assure internal consistency between the laboratories which calibrate radiometers for SeaWiFS validation (Mueller 1993 and Mueller et al. 1994).

4.2.1 Lamp Irradiance Standards

The options available for radiometric calibration standards are limited to standard sources or standard detectors. Lamp standards of spectral radiance and irradiance are provided by NIST and various commercial standardizing laboratories and manufacturers who furnish NIST traceable secondary standards. The uncertainty cited for these standards by NIST is, at best, 1% in the visible and 3% is a more realistic estimate of absolute uncertainty attainable using lamp standards alone. Over the calibration range from 250–2,500 nm, the uncertainty is approximately 6% at the endpoints.

The lamp standard of spectral irradiance is traditionally used for radiometric calibration, mainly because of its ease of use compared to the spectral radiance lamp. NIST publishes guidelines for the setup, alignment, and use of these standards. The vendors that manufacture and calibrate these lamps also issue guidelines for their use.

4.2.2 Radiance

Spectral radiance may be obtained by using an irradiance standard lamp and a Lambertian reflecting plaque. The standard lamp is positioned on axis and normal to the center of the plaque at the calibrated distance. The instrument or detector package to be calibrated is nominally positioned to view the plaque at 45° measured from the axis. The radiance, then, is given by

$$L(\lambda) = \frac{1}{\pi}\rho(\lambda)E(\lambda), \tag{14}$$

where $\rho(\lambda)$ is the bidirectional reflectance of the plaque for 0° incidence and 45° viewing, $E(\lambda)$ is the known spectral irradiance from the lamp during calibration and the total FOV of the instrument being calibrated is filled by the illuminated plaque.

The known radiance of the plaque provides an uncertainty comparable with that of the irradiance standard lamp, i.e., less than or equal to 3%, for calibrating a radiance detector with a very narrow FOV (≈1°). Large plaques, e.g., 40 cm^2, have been successfully used to calibrate radiance sensors having up to 25° full-angle FOVs. Intercomparisons of calibrations on underwater radiance sensors (possessing in-air full-angle FOVs ranging from 20–24°), made using this technique at different laboratories, have generally agreed within approximately 5%.

A better approach to calibrating multispectral radiance sensors is to view an integrating sphere that is uniformly illuminated by stable, appropriately baffled lamps, and that

also has an exit port large enough to completely fill the sensor's FOV. The sphere and exit port must be large enough to place the radiance sensor far enough away to prevent significant secondary illumination of the sphere walls due to retro-reflection off the sensor's entrance optics; if the sensor is too close, the retro-reflected light will both increase and distort the uniformity of the radiance distribution within the sphere. Traditionally, the calibration of an integrating sphere radiance source has been accomplished by appropriately transferring the known output from a standard lamp irradiance source.

Sphere Calibration Methods

1. The approach used at NASA/GSFC is to view the irradiance output of the lamp, initially, and then the sphere, with a spectroradiometer equipped with integrating input optics (McLean and Guenther 1989 and Walker et al. 1991). The spectral irradiance responsivity of the radiometer is calibrated using the lamp data, and the (assumed) Lambertian radiance of the sphere is determined by dividing the measured spectral irradiance output of the sphere by π.
2. An alternative method is to calibrate a stable, narrow FOV radiometer by viewing the standard lamp output reflected from a plaque, as described above. The output from the sphere's exit port is then viewed within this radiometer. The radiometer should also be used, at this point, to map the angular distribution of radiance in the sphere as viewed through the exit port. This important verification of a uniform radiance distribution is not possible when Method 1 is used to calibrate sphere radiance. A promising variant of Method 2 is to calibrate the sphere using a self-calibrating radiometer (Palmer 1988).

4.2.3 Radiance Standardization

Detectors of the type embodied in the United Detector Technology QED-200 (where QED stands for Quantum Efficient Device) radiometer are 99.99% quantum efficient. Palmer (1988) shows how such a detector may be combined with precision apertures and well-characterized filters to measure self-calibrated spectral radiance with an absolute uncertainty less than 1%. A calibration approach based on such radiometer standards is essential to achieve 1% internal consistency in the radiometric *uncertainty* of measurements made for SeaWiFS radiometric validation.

It is worth emphasizing here that the essential objective is to achieve internal consistency in the SeaWiFS optical database through uniform application of calibration techniques based on a common radiometric standard with precision approaching 1%, or less if possible. An important, but not essential, goal is to establish NIST traceable absolute uncertainty of less than 1% with this standard.

A self-calibrating radiometer may be used directly to calibrate and map the radiance distribution of integrating sphere sources (Method 2 in Section 4.2.2 above). The self-calibrating radiometer standard of radiance may be transferred to a stable lamp source of irradiance through the reversal of the reflectance plaque technique, described above, for calibrating radiance sensors with a standard lamp irradiance source.

These ideas have not yet been incorporated into a practical and widely accepted set of procedures for the calibration of oceanographic or airborne radiometers using self-calibrating radiometric standards. A significant level of laboratory work must be done to establish the repeatability of results attainable through these techniques under a variety of conditions, and to codify that experience into calibration protocols. The spectral responsivity of the QED-200 type detector is known, for example, to vary systematically with temperature (Kohler et al. 1990), and the spectral transmission functions of the filters in a self-calibrating radiometer must be re-characterized at a frequency that will guarantee the uncertainty of the calculated radiance. This frequency must be established through experience, but a reasonable first approximation is that filter transmission functions should be remeasured every few months.

One goal of the SeaWiFS mission is to base radiometric validation on shipboard, moored, and airborne radiometry with 1% uncertainty. If that goal is to be substantially achieved, then the work described above to establish *new* calibration standards and protocols must be pursued vigorously over the next two years.

4.2.4 Traceability and Comparisons

The variety of instruments available for validation measurements makes it imperative that some common calibration traceability exists. Recognizing that it would be impractical to characterize and calibrate all oceanographic and airborne radiometers at GSFC, several remote calibration facilities should be established, and working standards and protocols used at these facilities should all be traced directly to those at the GSFC calibration facility. This organizational structure is shown schematically in Fig. 2. Methods of standards intercomparison may include use of NIST calibrated filter radiometers to track and document the operation of each facility (radiometer wavelengths for this intercomparison will be determined). Round-robin *blind* calibration comparisons of a *standard* instrument would also be implemented to benchmark the internal consistency of calibrations performed at the various facilities involved.

4.2.5 Portable Standards

Between radiometric calibration activities, stable lamp sources in rugged, fixed geometric configurations should be

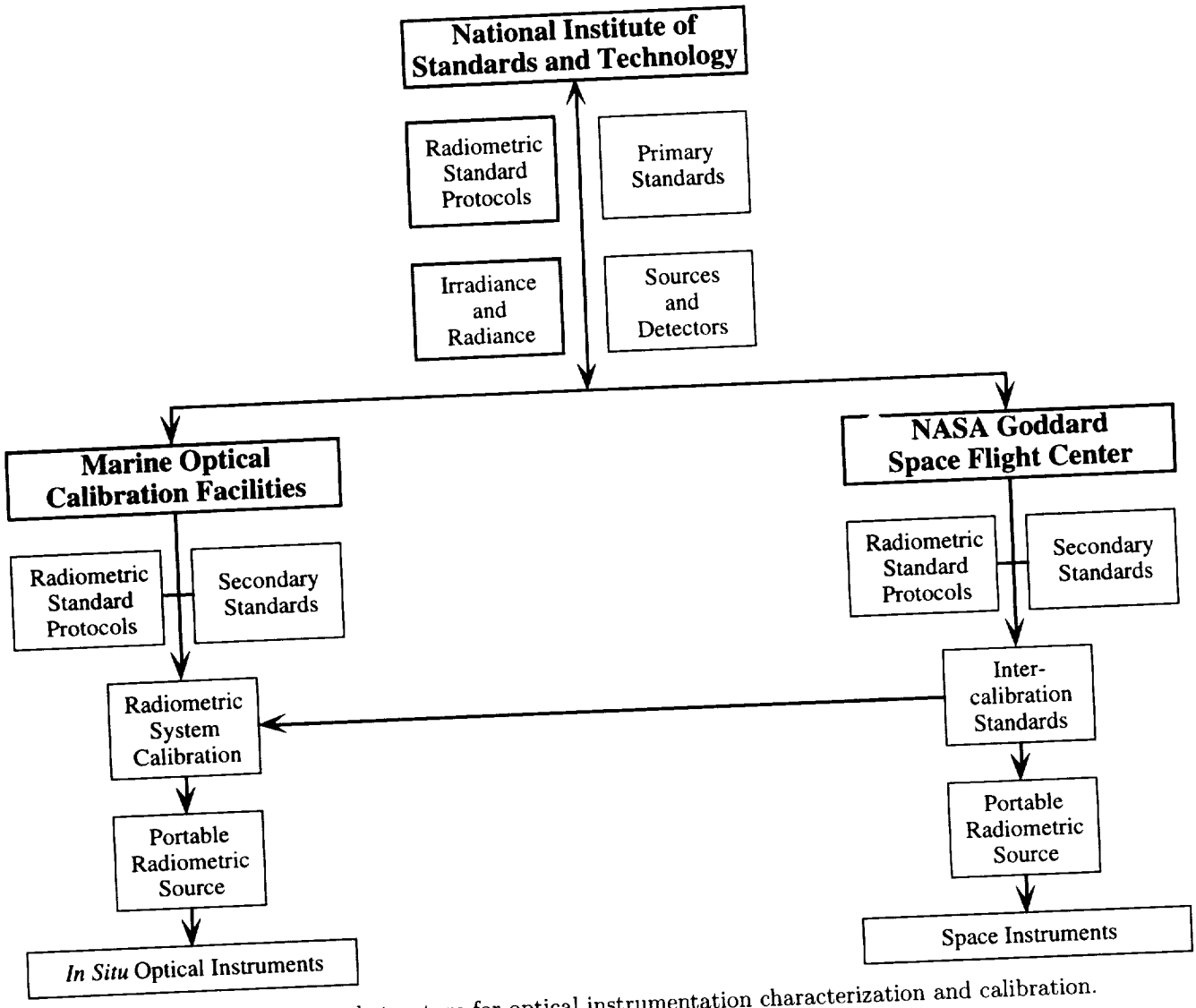

Fig. 2. Organizational structure for optical instrumentation characterization and calibration.

used to track instrument performance. Irradiance channels can be monitored with irradiance sources at fixed distances from the collectors, while radiance sources can be monitored by filling the FOV with diffuser plates placed in front of the irradiance sources, or by using integrating cavity sources. In each case, careful attention must be given to fixing specific geometries of source and detector in each use. The stability of the lamp output and the repeatability of measurement must be sufficient to detect 2% variations in an instrument's performance. An instrument should be connected to the portable standard and its response recorded daily, keeping a record of instrument responsivity throughout an experiment. Furthermore, these sources would provide an essential warning of problems if they appear.

The portable field reference source must be available when the complete radiometric calibrations are performed so that a baseline may be established and maintained for each sensor channel (Section 4.1.1). These sources are not a substitute for complete calibrations. The temporal record they provide will, however, be invaluable in cases where the pre- and post-cruise calibrations disagree or if the instrument is disturbed, e.g., opened between calibrations or if the data quality are otherwise suspect. These portable standards are an important part of the recommended instrument package.

Although several manufacturers offer somewhat portable irradiance and radiance sources, there has been very little previous work to validate and use portable radiometric standards to test oceanographic radiometers in the field. Therefore, detailed hardware specifications and procedural protocols must be developed through a series of laboratory and field tests using candidate equipment and standards.

4.3 ABOVE-WATER RADIOMETRY

In general, the protocols specified in Section 4.1 for in-water oceanographic radiance sensors are applicable for

characterizing and calibrating shipboard and airborne radiometers used to measure water-leaving radiance. Obvious exceptions are that immersion and underwater FOV characterizations are not appropriate for above-water sensors.

Polarization sensitivity is more critical in above-water radiometry than underwater radiometry. If a radiometer measures polarization components of radiance, then its responsivity and rejection of cross-polarization radiance must be characterized for each component channel. For above-water scalar radiance instruments, as with the SeaWiFS radiometer, sensitivity to linear polarization must be less than 2%, and the actual degree of polarization sensitivity must be characterized for each channel.

A generalized protocol for characterizing the polarization sensitivity of a radiometer is given here. The instrument should view a source of linearly polarized radiance, and its apparent radiance response $L_1(\lambda)$ should be recorded. The instrument should then be rotated 90° about its FOV axis, still viewing the linearly polarized radiance source, and the apparent radiance response $L_2(\lambda)$ should be recorded. The polarization sensitivity of the instrument will be calculated as

$$P(\lambda) = \left| \frac{2\big(L_1(\lambda) - L_2(\lambda)\big)}{L_1(\lambda) + L_2(\lambda)} \right|. \qquad (15)$$

As required for the SeaWiFS radiometer, airborne and shipboard radiometers must satisfy $P(\lambda) < 0.02$.

A very simple, semi-quantitative test of a radiometer's polarization sensitivity can be performed outdoors on a cloud- and haze-free day. The instrument should be pointed at the sky in the zenith-sun plane at an angle of approximately 90° from the sun, and its response $L_1(\lambda)$ recorded. Since singly-scattered Rayleigh radiance is 100% polarized at a scattering angle of 90°, if aerosol scattering is small, the sky radiance viewed at this angle will be strongly polarized. If the instrument is then rotated 90° about its FOV axis to measure $L_2(\lambda)$, an approximate estimate of $P(\lambda)$ may be computed, as above.

Specification of detailed protocols for laboratory characterization of a radiometer's polarization sensitivity will require more attention than is available here. In particular, protocols should be developed which describe in detail:

1) laboratory setups for producing a stable, uniform, extended source of linearly polarized radiance; and
2) laboratory procedures for measuring the actual degree of polarization of the polarized radiance source and for determining the uncertainty of the polarization sensitivity estimate achieved using a particular experimental setup.

Temperature dependence of an airborne radiometer's polarization sensitivity should initially be characterized at 5°and 30° C. If significant differences in $P(\lambda)$ exist at these extremes of instrument operating temperatures, then polarization sensitivity measurements should be made at several additional temperatures in that range.

4.4 CALIBRATION OF IOP METERS

Calibration of beam transmissometers has traditionally been carried out by means of in-air measurements, with a subsequent adjustment for changes in the Fresnel reflections by the windows upon submergence into water. The 660 nm transmissometers produced by Sea Tech, Inc. are independently calibrated at the factory after which calibration is maintained via frequent air calibrations (Sections 5.4.1 and 6.7). This approach is adequate for this generation of 660 nm transmissometers.

The newer generation of combined spectral absorption and beam transmission meters require a more accurate calibration procedure. This class of instruments must be calibrated with optically pure water, which has been freshly prepared using multiple-pass reverse osmosis filtration and analyzed with special optical techniques to verify optical purity. Ordinary laboratory grade *pure water*, prepared using distillation, deionization, or ordinary reverse osmosis filtration, will not ordinarily be optically pure enough to serve as a calibration standard. In general, it will not be practical to perform this calibration procedure either at sea or in the average oceanographic laboratory. Annual recalibration, either by the manufacturer, or another qualified laboratory, together with air calibrations every three days during deployments, are recommended (Section 5.2.4). The air calibration procedure for this class of instruments is also more elaborate than for the red (660 nm) transmissiometers (Section 5.2.4).

Procedures for calibrating a scattering meter depend on the detailed design of the instrument. For example, backscattering meters are calibrated with Spectralon plaques of known reflectance. Detailed protocols for calibrating scattering meters remain to be developed in a future revision to this document.

4.5 SUN PHOTOMETERS

Sun photometer calibrations should be performed at least annually, when used consistently, through a Langley calibration procedure. In this procedure, the solar signal transmitted through the atmosphere is measured over different air masses, i.e., at different solar zenith angles, throughout the course of the day. The validity of using these measurements as *calibration* of a sun photometer hinges strongly on the assumption that aerosols are uniformly distributed and do not vary throughout the day. These Langley calibrations, therefore, should be performed in areas of atmospheric stability with low aerosol loading. Suitable locations include the astronomical observatories at Mauna Loa, Hawaii, and Kitt Peak, Arizona. In between these calibrations, radiance calibrations with standard lamps may be used as a stability check (Shaw 1976).

Temperature stability should be characterized for each instrument. Linearity and spectral calibrations should be performed with the same frequency as the absolute calibration; these characterizations must be performed in the laboratory.

4.6 SKY RADIANCE CAMERAS

Absolute and spectral calibrations should be performed on the radiance distribution camera before and after each cruise. A full characterization of the instrument should be performed initially, including camera lens roll-off characteristics for each camera (Voss and Zibordi 1989). If attenuation devices are used to prevent solar saturation, these should be calibrated frequently to track drift. Linearity calibrations should also be performed with the same frequency as the absolute and spectral calibration. Procedures for characterizing this class of instruments are essentially the same as for other radiance detector systems. Each individual detector element in the detector array is essentially regarded as an independent radiometer.

4.7 PIGMENT CALIBRATIONS

HPLC equipment used to measure phytoplankton pigment concentrations is to be calibrated using standards distributed under the auspices of the SeaWiFS Program.† Concentrations of the pigment standards should be determined using a monochromator-based spectrophotometer and the extinction coefficients summarized in Bidigare (1991). The use of a diode array spectrophotometer can result in the underestimation of chlorophyll *a* concentration because of errors associated with fluorescence contamination (Latasa et al. 1994). Bench fluorometers used to measure concentrations of *extracted* chlorophyll *a* and phaeopigments should be calibrated using authenticated *standard* chlorophyll *a* adopted for HPLC. *In situ* fluorometers should be calibrated against extracted chlorophyll *a* from concurrent bottle samples.

4.8 CTD CALIBRATIONS

The conductivity probe, temperature probe, and pressure transducer of the CTD should be recalibrated before and after each major cruise by a properly equipped physical oceanographic laboratory, including those maintained by many CTD manufacturers. In addition, the conductivity probe should be independently calibrated during the course of each cruise by obtaining salinity water samples (Section 5.2.3) simultaneous with CTD readings. These salinity samples are to be analyzed, either at sea or ashore, with a laboratory salinometer calibrated with International Association for the Physical Sciences of the Ocean (IAPSO) Standard Seawater.

If simultaneous deployment of the CTD with optical instruments having independent pressure transducers is practical, the two depths measured by the different instruments should be compared over the range of the cast. If depth measurements disagree significantly, these comparisons may be used to correct whichever transducer is found to be in error through analysis of pre- and post-cruise pressure transducer calibrations.

† The HPLC pigment standards are available from Robert R. Bidigare, Department of Oceanography, University of Hawaii, Honolulu, HI 96822.

Chapter 5

Measurement Protocols

INTRODUCTION

This chapter describes the methods and procedures by which measurements are to be made during oceanographic deployments for SeaWiFS algorithm development and validation. Section 5.1 gives protocols for obtaining radiance and irradiance measurements from ships and aircraft. Section 5.2 gives protocols for measuring IOP, chlorophyll *a* fluorescence, and CTD profiles. Section 5.3 gives protocols for sun photometry and sky radiance distribution measurements. Section 5.4 covers protocols for obtaining and processing water samples for phytoplankton pigment concentration measurements and spectrophotometric determination of absorption by particles and dissolved matter. Sections 5.5–5.7 describe ancillary observations to be recorded at each station, radiometric measurements from moorings, and radiometry on drifting buoys. Finally, Section 5.8 gives protocols addressing sampling strategy, station location, and coordination of ship and aircraft measurements in Case-1 and Case-2 water masses.

5.1 IRRADIANCE AND RADIANCE

Determinations of in-water spectral E_d, E_u, and L_u, both near the surface and as vertical profiles, are required for calibration and validation of the water-leaving radiance as retrieved from the SeaWiFS satellite sensor. Near-surface measurements should profile through at least the top three optical depths to reliably extrapolate to $z = 0$; it is essential to obtain a profile through at least the top optical depth. To better characterize the water column for remote sensing applications, e.g., primary productivity estimation, deeper vertical profiles should be made to 200 m, or seven optical depths whenever possible. Sea bed reflection influences on L_u and E_u should be avoided for SeaWiFS validation and algorithm development by collecting data only from water deeper than six optical depths for $E_d(490)$; remote sensing applications for optically shallow situations where bottom reflectance is present are not within the scope of these protocols.

There are two primary sources of error in the determination of these optical parameters: the perturbation of the in-water radiant energy field by the ship (Gordon 1985, Smith and Baker 1986, Voss et al. 1986, and Helliwell et al. 1990), and atmospherically induced variability in radiant energy incident on the sea surface during in-water measurements (Smith and Baker 1984). The influence of ship shadow on the vertical profiles of E_d, E_u, and L_u is dependent upon the following variables: solar zenith angle, the spectral attenuation properties of the water column, cloud cover, ship size (length, beam, draft, and freeboard) and color, and the geometry of instrument deployment. Atmospheric variability is primarily dependent upon sun elevation and variations in cloud cover. The near surface in-water data also show variability caused by wave focusing, which can be minimized at a fixed depth by averaging over several wave periods, but which can pose severe problems in vertical profiles during which the instrument descends at speeds of 0.5–1 m s^{-1}. Raman scattering and fluorescence result in second-order errors near 490 nm (CDOM fluorescence), and at longer wavelengths, contributions from phycoerythrin and chlorophyll *a* fluorescence and water Raman scattering are significant.

5.1.1 Ship Shadow Avoidance

The complete avoidance of ship shadow, or reflectance, perturbations is a mandatory requirement for all radiometric measurements to be incorporated into the SeaWiFS validation and algorithm database. The influence of ship shadow is best characterized in terms of attenuation length $1/K_d(\lambda)$ (Gordon 1985). Because L_W is required with an uncertainty of 5% or better, the protocol requires that vertical profiles be measured outside the effects of ship perturbation to the radiant energy field. To accomplish this, the instrument must be deployed from the stern, with the sun's relative bearing aft of the beam.

Estimates of the minimum distance away from the ship, under conditions of clear sunny skies, are given below. The distances are expressed in attenuation lengths to minimize error. For $E_d(\lambda)$ measurements, the general equation for distance away, ξ, in meters is given as

$$\xi = \frac{\sin(48.4^\circ)}{K_d(\lambda)}. \tag{16}$$

The distance from the ship is required to be $3/K_u(\lambda)$ m for $E_u(\lambda)$ and $1.5/K_L(\lambda)$ m for $L_u(\lambda)$ measurements. These

distances should be increased if the instrument is deployed off the beam of a large vessel.

A variety of methods have been used to deploy optical instruments beyond the influence of the ship. During CZCS algorithm development, floating plastic frames were equipped with small winches and instruments to obtain near surface optical profiles at some distance away from the ship. An umbilical cable provided power and data transfer. These platforms, while being somewhat difficult to deploy, worked well at avoiding ship shadow. Alternatively, extended booms can be used to deploy the instrument away from the ship and have the advantages of allowing relatively rapid deployment and simultaneous rosette bottle sampling. As a point of caution, however, very long booms may accentuate unwanted vertical motions due to ship pitch and roll.

Waters et al. (1990) used an optical free-fall instrument (OFFI) that allows optical data to be obtained outside the influence of ship perturbation. In addition, the OFFI approach allows optical data to be obtained independently from violent ship motion, which may be transmitted to the instrument via the hydrowire, especially on a long boom. Yet another method for the deployment of optical sensors is via an ROV. Some groups, e.g., Smith (pers. comm.), have deployed a spectrometer on an ROV and obtained data completely free of ship influences.

The above criteria for ship shadow avoidance are admittedly very conservative. Unfortunately, the above cited models and observations provide only approximate guidance on minimum distances at which ship reflectance and shadow effects become insignificant under all circumstances. Therefore, the SPSWG has adopted relatively extreme distance criteria, recognizing that in many specific combinations of lighting conditions, ships and optical properties, ship shadow, and reflection effects may become unimportant much closer to the ship.

The essential requirement is that each investigator establish that any measurements of E_d, E_u, and L_u, submitted for SeaWiFS validation and algorithm development, are free from ship-induced errors. The simplest way to do this is to adhere to the above distance criterion, which is not difficult when using either a tethered free-fall system or instruments mounted on an ROV. In other cases, it is incumbent on the investigator to otherwise demonstrate the absence of ship effects, e.g., through analysis of a series of profiles at increasing distance.

At wavelengths where attenuation lengths are the same order of magnitude as, or less than, the size of the instrument package, e.g., in the ultraviolet-B (UVB) or red and near infrared spectral regions, care must be taken to consider possible perturbation of the radiant energy field by the instrument package itself. Methods of accounting for self-shadowing by the instrument are not well established and new measurement approaches must be developed (Section 5.1.6).

5.1.2 Depth Resolution in Profiles

The instrument sampling rate and the speed at which the instrument is lowered or raised through the water column should yield at least two, and preferably six to eight, samples per meter.

5.1.3 Instrument Dark Readings

The dark current of optical sensors is frequently temperature dependent. As a consequence, accurate radiometric measurements require that careful attention be given to dark current variability. It is recommended that each optical measurement be accompanied by a measurement of the instrument dark current. When there is a large temperature difference between the instrument on the deck and the water temperature, the instrument should be allowed to equilibrate with ambient water temperature at the beginning of each cast.

Deep casts, e.g., 500 m, may permit the determination of the dark current in each optical channel at the bottom of each cast. Many instruments, however, are not designed to be safely lowered to 500 m, and this approach is usually not feasible. Furthermore, there is some intrinsic uncertainty over possible contamination by bioluminescence when dark readings are obtained in this way. If the instrument is equipped with a shutter, dark currents can be measured at any depth in the cast. If the dark current is not determined during the cast, it should be determined as soon as possible after the instrument is returned to the deck.

Temperature effects on sensor responsivity can be significant and should not be ignored. Therefore, sensors should be equipped with thermistors on detector mounting surfaces to monitor temperatures for data correction. Otherwise, deck storage should be under thermally protected conditions prior to deployment and on-deck determination of dark voltages.

5.1.4 Surface Incident Irradiance

Atmospheric variability, especially under cloud cover, leads directly to variability of the in-water light field and must be corrected to obtain accurate estimations of optical properties from irradiance or radiance profiles. First order corrections for this variability can be made using above water (on deck) measurements of downwelling spectral irradiance, $E_s(\lambda) = E_d(0^+, \lambda)$. Smith and Baker (1984) and Baker and Smith (1990) theoretically computed the irradiance just below the air-water interface, $E_d(0^-, \lambda)$, from deck measurements to correct in-water profile data.

The deck sensor must be properly gimballed to avoid large errors in $E_s(\lambda)$ due to ship motion in a seaway. Improper gimballing can actually accentuate sensor motion under some circumstances, however, and this aspect of a shipboard radiometer system must be engineered with some care.

Recently, Waters et al. (1990) have demonstrated a method to more directly determine $E_d(0^-, \lambda)$ by deploying an optical surface floating instrument (OSFI) to obtain continuous optical data just below the air-water interface. These $E_d(0^-, \lambda)$ are used as a normalization factor to correct for variations in irradiance during a vertical profile, or over the period of a day for a sequence of profiles. Research and development is needed to determine whether this should be the preferred approach for SeaWiFS validation measurements.

5.1.5 Instrument Attitude

An instrument's attitude with respect to the vertical is a critical factor in measurements of $E_d(z, \lambda)$ and $E_u(z, \lambda)$, and is only slightly less critical for $L_u(z, \lambda)$. Roll and pitch sensors must, therefore, be installed in the underwater radiometers used for the SeaWiFS program. The data from these attitude sensors are to be recorded concurrently with the data from the radiometric channels and are to be used as a data quality indicator. It is not deemed necessary to determine or control attitude determination errors resulting from surface wave-induced accelerations at very shallow depths.

5.1.6 Instrument Self-Shading

Gordon and Ding (1992) recently modeled the errors introduced by an instrument's own shadow in direct measurements of $L_u(\lambda)$ and $E_u(\lambda)$. For this source of error to be less than 5%, without modeled corrections, the instrument radius r must satisfy $r \leq \left[40a(\lambda)\right]^{-1}$ for $E_u(\lambda)$ and $r \leq \left[100a(\lambda)\right]^{-1}$ for $L_u(\lambda)$. They calculate for $\lambda = 865\,nm$ in pure water, as an example, that the instrument radius must be approximately 0.3 cm to measure $E_u(865)$ with a maximum of 5% error; the instrument radius must be significantly smaller for direct measurement error in $L_u(865)$ to be 5% or less.

Gordon and Ding (1992) also propose a simple model for correcting $L_u(\lambda)$ and $E_u(\lambda)$ for the self-shadowing effect. They write

$$\widehat{L}_u(\lambda) = \frac{\widetilde{L}_u(\lambda)}{1 - \varepsilon(\lambda)} \tag{17}$$

and

$$\varepsilon(\lambda) = 1 - e^{-k' a(\lambda) r}, \tag{18}$$

where $\widehat{\ }$ is the true value, $\widetilde{\ }$ is the measured value, $k' = y/\tan\theta_{0w}$, θ_{0w} is the refracted solar zenith angle and y is an empirical factor for which they give values determined by fitting their model results ($y \approx 2$). A similar correction, with a different table of values for y applies to $E_u(\lambda)$.

When the above geometric corrections are applied, Gordon and Ding (1992) estimate that errors less than or equal to 5% in $L_u(\lambda)$ could be determined from measurements with instruments having maximum diameters of 24 cm for $\lambda \leq 650$ nm, and with instruments of maximum diameter 10 cm for $650 < \lambda \leq 700$ nm at solar zenith angles (θ_0) greater than or equal to 20°, and maximum chlorophyll concentrations of 10 mg m^{-3}. To measure $L_u(\lambda)$ correctable to less than 5% error at $\theta_0 = 10°$ (with chlorophyll concentrations less than or equal to 10 mg m^{-3}), maximum instrument diameters are 12 cm for $\lambda \leq 650$ nm and 5 cm for $650 < \lambda \leq 700$ nm. Even with these corrections, however, instrument diameters of 1 cm or less must be used to assure self-shading $L_u(\lambda)$ errors are 5% or less at 780 and 875 nm.

The Gordon and Ding (1992) model predictions have recently been compared to experimental measurements of $L_u(\lambda)$ just beneath the sea surface, using a fiber-optic radiometric probe (Zibordi and Ferrari 1994). The experiment was performed in a lake, with solar zenith angles ranging between 25° and 50°, on several days with cloud-free skies. Spectrophotometric methods (similar to those in Sections 5.4.2 and 6.8.2) were used to measure absorption by particles and Gelbstoff. At wavelengths of 500, 600, and 640 nm, a series of discs was employed to vary instrument self-shading geometry in several steps over the range $0.001 < a(\lambda)r \leq 0.1$. The Gordon and Ding (1992) model predicted self-shading radiance and irradiance effects that may be applied as corrections, and which agreed with measured values within 5% and 3% respectively. The model corrections were all biased high relative to the measured values. Zibordi and Ferrari (1994) chose to compare their measurements to the Gordon and Ding (1992) *point sensor* model, and use of their *finite-sensor* model results may have improved the comparisons.

This initial confirmation of the Gordon and Ding (1992) instrument self-shading model is confined to clear-sky conditions, solar zenith angles greater than 25°, near-surface $L_u(0^-, \lambda)$ and $E_u(0^-, \lambda)$, and $a(\lambda)r$ less than or equal to 0.1. Additional theoretical and experimental research will be necessary to generalize this correction for cloudy sky conditions and for variations with depth in $L_u(z, \lambda)$ and $E_u(z, \lambda)$ profiles. The above restrictions notwithstanding, the excellent agreement shown so far covers a very important range of conditions for SeaWiFS algorithm development and validation. Therefore, a provisional protocol for applying self-shading corrections to $L_u(0^-, \lambda)$ and $E_u(0^-, \lambda)$ is given in Section 6.1.7.

5.1.7 Airborne Ocean Color Radiometry

Ocean color may be measured from aircraft using either imaging radiometers (usually flown at high altitude), or single FOV spectral radiometers (usually flown at low altitude to measure profiles of ocean color beneath an aircraft's trackline). For SeaWiFS validation, either of these types of data can be an extremely valuable addition to shipboard measurements.

Aircraft measurements observe the horizontal variability in ocean color radiance spectra on spatial scales which

are much smaller than SeaWiFS pixels; therefore, these data are more comparable to shipboard measurements. At a qualitative level, this information can indicate how well shipboard radiometric and bio-optical measurements can be compared to SeaWiFS data at greater than 1 km pixel resolution. For more quantitative work, if an airborne radiometer's characteristics conform to specifications of Section 3.3, and if accurate corrections are applied for atmospheric and surface reflection effects, the high resolution airborne data may be spatially integrated to quantitatively extrapolate shipboard bio-optical measurements to SeaWiFS pixel scales. (Note that the original data must be corrected for sun and sky glitter, as well as atmospheric transmission and path radiance, before spatial integration to SeaWiFS resolution.) Finally, in cases when airborne normalized water-leaving radiances estimated from aircraft measurements are independently validated as being in conformity with SeaWiFS uncertainty goals, they may be used for direct radiometric validation of SeaWiFS radiometric performance.

Methods for atmospheric correction and estimation of normalized water-leaving radiances from high altitude airborne ocean color imagery are nearly identical to, and as challenging as, those methods which must be applied to SeaWiFS data itself (Carder et al. 1992 and Hamilton et al. 1992). These problems and their solutions lie beyond the scope of the ocean optical protocols per se, at least in this revision. The elements of ocean color radiometry from low flying aircraft are more closely associated with shipboard ocean optical measurements and will be addressed here.

Under clear skies, or partial cloud cover, the radiometer should be pointed approximately 15–20° from nadir in the azimuth direction opposite from the sun, to avoid specular sun glint from wave facets. If seas are rough and the solar zenith angle is small, an even larger nadir angle may be necessary. Under completely uniform overcast conditions, the instrument should point to the nadir. If an imaging radiometer is fixed in the nadir plane, sampling should be scheduled to provide a solar zenith angle between 35° and 45°, and all flight lines should be flown toward or away from the sun.

For quantitative low altitude ocean color radiometry, solar downwelling spectral irradiance must be measured using a sensor mounted on top of the aircraft. Incident solar irradiance spectra are modified significantly by transmission through the atmosphere above the aircraft, and direct spectral irradiance measurements are absolutely essential for computing normalized water-leaving radiances from flight level radiances. The measured flight-level downwelled irradiances should be used to model atmospheric transmission and path radiance corrections, which must be applied at altitudes of 100 m and higher. Reflected skylight must also be removed from the measured radiances. Finally, for use in algorithms related to SeaWiFS, the water-leaving radiances must be normalized by the ratio $\overline{F}_0(\lambda)/E_s(\lambda)$, where $\overline{F}_0(\lambda)$ is the mean extraterrestrial solar flux, and $E_s(\lambda)$ is the measured incident spectral irradiance propagated to the sea surface. This normalization is also critical for ratios of water-leaving radiance, because the spectral quality of incident irradiance is modified significantly, in a generally unpredictable way, by atmospheric transmittance.

Under either clear skies or a completely uniform cloud cover, i.e., overcast skies, the downwelling irradiance measurements may be used directly to model corrections for low altitude atmospheric transmission and path radiance, and for reflected sky radiance. On the other hand, ocean color radiance data measured under variable cloud conditions are very difficult to correct and interpret. Under these conditions, the area on the sea surface viewed by the radiometer is often illuminated differently than is the incident irradiance sensor at the aircraft, and sky radiance incident on the surface also varies unpredictably.

The requirement to directly measure incident spectral irradiance may sometimes be relaxed when the experimental objective is simply to characterize spatial variability of bio-optical properties qualitatively. Under cloud-free conditions, moreover, it may often be possible to model surface incident irradiance accurately enough for semi-quantitative analyses of chlorophyll concentrations from low altitude airborne spectral upwelled radiance measurements alone.

For atmospheric correction and analyses of aircraft radiance data, the following ancillary parameters must be recorded: date and time [Greenwich Mean Time (GMT)], azimuth and nadir angle of the radiometer, heading of the aircraft (and all other aircraft attitude angles, if available), the flight altitude, and air pressure at that altitude. The height of the inversion should also be recorded, as most of the aerosols will normally be concentrated under this height. Furthermore, a precise navigation recording is required for identification of the aircraft track within the satellite image and for comparisons to shipboard measurements. In addition to the radiometer, a video camera is very helpful to check for the effects of cloud shadows, foam, and ocean fronts—effects which are difficult to identify in the horizontal radiance profile alone.

5.1.8 Shipboard Radiance Measurements

Water-leaving radiances can, of course, be measured from the deck of a ship using methods directly analogous to those of low-altitude airborne radiometry (Section 5.1.7). Given a very close proximity to the sea surface, no corrections are needed for atmospheric transmission and path radiance. Shipboard water-leaving spectral radiances must, however, be corrected for light reflected at the sea surface, and must also be normalized using direct measurements of $E_s(\lambda)$. Performance characteristics for radiometers used to measure $E_s(\lambda)$ and $L_u(\lambda)$ are specified in Sections 3.2–3.3.

The best position for measuring the water-leaving radiance is usually near the bow of the ship. At this position, the ship will have the least influence with respect to shading or reflection. It is also easy to point in a direction away from the sun to reduce specular reflection of sunlight. While underway, ocean color radiance measurements should always be made from the bow, because this is the only position where the water is normally undisturbed by the ship's wake and without foam.

To measure $L_W(\lambda)$, the radiometer should point to the sea surface with an angle of about 20° from nadir and away from the sun's azimuth by at least 90°. (A viewing angle that is 180° away from the sun's azimuth may be contaminated by the *glory* phenomenon.) This is the point with the minimum in specularly reflected sun and sky radiance. Under overcast conditions, the instrument should point closer to nadir, but not so close that ship shadow or hull reflections affect the water-leaving radiance. (Indeed, some larger ships have a long bulbous bow nose, which must be avoided.) Under a high sun elevation (such as in tropical regions) and a rough sea, it may be very difficult, or even impossible, to avoid large amounts of specularly reflected sunlight, since large nadir angles cause severe problems due to variations in reflected skylight. In addition, foam and floating material must be avoided during measurements.

Because of temporal variability due to waves, it is important to record a number of spectra within a period of a few seconds, e.g., 30 spectra within 15 s. Before calculating final mean and standard deviation spectra, outliers should be removed by computing initial estimates of these statistics and rejecting radiance spectra containing values falling more than 1.5 standard deviations from the estimated mean.

Incident spectral irradiance $E_s(\lambda)$ should be measured at a location free from shadows of, and reflections by, the ship's superstructure. As in low-altitude aircraft radiometry, $E_s(\lambda)$ must be used both to normalize measured water-leaving radiance and to calculate spectral reflectance. Some investigators (Carder and Steward 1985 and Doerffer pers. comm.) advocate calculating spectral reflectance using relative $E_s(\lambda)$ estimated by viewing a reference diffuse reflectance plate. Spectralon plates are used most often, but Kodak gray cards and plates painted with Nextel™ coating have good Lambertian reflectance characteristics (Doerffer pers. comm.).

The contribution by specularly reflected sky light to a water-leaving radiance measurement can be calculated from measurements of the sky radiance, made either by looking at a horizontal *first surface* mirror (a mirror with no layers other than the reflective surface) at the same nadir and azimuth angles, or by pointing the radiometer into the sky with a zenith angle equal to the nadir angle and with the same azimuth angle. The specular reflectance of the water surface can be calculated using the Fresnel equation (reflectance is approximately 0.02 within 20° of nadir).

The sequence of water-leaving radiance, diffuser plate, and sky radiance $[L_{sky}(\lambda)]$ measurements can usually only be completed under clear sky or uniform overcast conditions. When coupled with concurrent direct measurements of $E_s(\lambda)$, however, $L_W(\lambda)$ and $L_{sky}(\lambda)$ can probably be measured under variable cloud conditions, provided a sequence of several $[L_W(\lambda), E_s(\lambda)]$ and $[L_{sky}(\lambda), E_s(\lambda)]$, sets of spectra can be measured in rapid succession without significant variations.

5.2 ANCILLARY PROFILES

Beam transmittance, CTD profiles, and chlorophyll *a* fluorescence should be measured at the same stations as the irradiance and radiance measurements. Preferably, these auxiliary profiles should be measured simultaneously with, or otherwise immediately before or after, the radiometer profiles. If possible, these profiles should be made in conjunction with bottle samples. For the verification of the satellite sensor, these data will be used as a guide to the uniformity of the first optical depth and to determine water bottle sampling depths.

The IOP, fluorescence, and CTD profiles will also be used as a guide for, and constraints on, the smoothing of $K(z, \lambda)$ from the radiometric profiles. The location of maxima and other features in the structure of these profiles identify inflection points for segmenting the optical profiles into finite depth elements (layers) for the analytical methods described by Mueller (1991) or Petzold (1988). Both of these techniques use multiple segments for the statistical fit of analytic functions to the measured profiles. These data will also be used to develop and validate pigment and primary productivity algorithms.

5.2.1 Beam Transmittance

The windows on the beam transmissometer must be cleaned with lens cleaner or a mild detergent solution and a soft cloth or tissue, rinsed with distilled water, then rinsed with isopropyl alcohol and wiped dry. An approximate *air calibration* reading should be made before every cast to verify that the windows are clean. A transmissometer *dark voltage* should also be measured at this time. These *on-deck air calibrations* are not, however, very reliable measures of temporal drift or degradation in the instrument's source or detector. In the humid, or even wet, environment on the deck of a ship, the windows are often quickly obscured by condensation, and the glass also tends to absorb enough water to affect transmission slightly (Zaneveld pers. comm.). A very careful air calibration should be performed before and after each cruise under dry laboratory conditions. During an extended cruise, it is also recommended to remove the instrument to a dry location in a shipboard laboratory, and after allowing several hours for the windows to dehydrate, a careful air calibration should be performed. Only the laboratory air calibrations should

be used in the final processing of beam transmissometer data.

Both the laboratory condition air calibration and dark voltages, and the factory calibration voltages, assume the data acquisition system measures instrument response as true volts. It is imperative, therefore, to calibrate the end-to-end analog-to-digital (A/D) data acquisition system and characterize its response to known input voltages. Corrections are in the form of a linear function:

$$\widehat{V} = g(T)\widetilde{V} + f(T), \quad (19)$$

where T is temperature, must usually be applied to external voltage inputs recorded with the A/D circuits of CTDs or profiling radiometer systems. The range dependent A/D bias coefficients should be determined at approximately 5° C intervals, over the range from 0–25° C, to characterize the temperature sensitivity of the data acquisition system.

For the development of bio-optical algorithms describing the inherent and apparent optical properties of the water, and for algorithms estimating primary productivity, more stringent requirements are recommended for transmissometer calibration and characteristics. Spectral measurements of beam transmittance should be made with absolute uncertainties of 0.1% transmittance per meter, or 0.001 m^{-1} beam attenuation coefficient $c(\lambda)$.

Different and more stringent calibration protocols are specified in Section 5.2.4 for the new combined spectral absorption and beam attenuation meters. Laboratory calibrations of these instruments are based on measurements using optically pure water, produced using extraordinarily careful reverse osmosis procedures. It is ordinarily impractical to produce and verify optically pure water either at sea or in the average oceanographic laboratory. As with the older red-wavelength beam transmissometers, air calibrations are prescribed as a basis for correcting instrumental drift between calibrations at a qualified laboratory. The increased sensitivity required for the new instruments makes it essential to carry out more frequent air calibrations at sea. As discussed above, accurate air calibrations must be carried out in a dry laboratory environment with controlled relative humidity—conditions which may be difficult to implement on some ships.

5.2.2 Chlorophyll *a* Fluorescence

An *in situ* fluorometer should be employed to measure a continuous profile of chlorophyll *a* fluorescence. The fluorometer should be mounted on the same underwater package as the transmissometer, CTD, and water sampler, if one is employed. If possible, the radiometer should also be on this package.

The A/D channel used to acquire and record signal voltages from the *in situ* fluorometer must be calibrated, and its temperature-dependent response to known voltage inputs characterized. During processing, a correction of the form given in (19) must usually be applied to values recorded with the A/D circuits of CTDs and profiling radiometer systems. As in beam transmittance, the range dependent A/D bias coefficients should be determined at approximately 5° C intervals over the range from 0–25° C to characterize the temperature sensitivity of the data acquisition system.

Zero fluorescence offsets should be measured on deck before and after each cast; the optical windows should be shaded to avoid contamination of the zero offset value by ambient light. Before each cast, the fluorometer windows should be cleaned following the manufacturer's instructions.

For chlorophyll *a* determinations, the fluorescence measurements should be compared to HPLC and extracted pigment measurements from discrete water samples, to permit comparison with JGOFS standard measurements and historical databases. The *in situ* fluorescence measurements will be used to provide continuous vertical profiles of interpolated pigment concentration using the bottle samples as tie points.

5.2.3 CTD Profiles

Vertical profiles of CTD should be measured to at least the depth of the deepest bio-optical profile. If the station schedule will permit it, sections of CTD casts extending to 500 m, or deeper, will be useful for computing relative quasi-geostrophic currents and shear, which may affect the advection and mixing of bio-optical properties during a cruise. A real-time analysis and display of the CTD profile, together with displays of $c(660)$ and *in situ* fluorescence profiles, should be available as a guide in choosing the depths at which water sampling bottles will be closed.

If possible, a few deep (1,500 m depth or greater) CTD and bottle sample profiles should be made during each cruise to obtain data for calibrating the CTD's conductivity probe. During these *CTD calibration casts*, water samples should be taken at depths where the vertical gradient of salinity is very small. This practice will minimize errors in the conductivity calibration resulting from the spatial separation of the water bottle and CTD profile. The bottled salinity samples may be stored for post-cruise analyses ashore at a laboratory equipped with an accurate salinometer and IAPSO Standard Seawater, if suitable equipment and standard water are not available aboard the ship.

5.2.4 Spectral Absorption Profiles

Currently, there are two methods for measuring spectral absorption coefficients which use commercially available equipment. The first is conventional benchtop spectrophotometer measurements of spectral absorption by particles extracted from water samples and concentrated on filters, followed by measurements of the spectral absorption

by the dissolved component in the filtrate (Section 5.4.2). More recently, *in situ* profile measurements of spectral absorption have been made using instruments which capture most scattered light using a reflecting tube. A combination of these two methods allows one to measure profiles of total absorption and absorption by the dissolved component with the reflecting tube instrument, and to independently partition the absorption spectrum at discrete depths into its components due to particulate and dissolved substances using filters and spectrophotometry.

In situ spectral absorption coefficient profiles can also be measured with spectral radiometers conforming to the performance specifications listed in Section 3 above, if the radiometric package is extended to measure $E_d(\lambda)$ and $E_u(\lambda)$, as well as scalar irradiances $E_{0d}(\lambda)$ and $E_{0u}(\lambda)$. This combination may be approached either using hemispherical collectors to measure upwelling and downwelling hemispherical irradiances, or by using cosine collectors on one radiometer in tandem with spherical collectors on another radiometer. Given these irradiance components, spectral absorption is then computed using Gershun's equation as

$$a(\lambda) \;=\; K(\lambda)\frac{E(\lambda)}{E_0(\lambda)}, \qquad (20)$$

where $E(\lambda) = E_d(\lambda) - E_u(\lambda)$ is vector irradiance, and $K(\lambda)$ is the vertical attenuation coefficient for vector irradiance.

In a recent experiment, comparisons between absorption profiles measured using Gershun's equation with $E(\lambda)$ and $E_0(\lambda)$ (scalar irradiance) data, and absorption profiles measured with a reflecting tube instrument, agreed within 8% (Pegau et al. 1994). This level of agreement is well within the calibration uncertainties of the particular prototype instruments used for that experiment, which were approximately 10% uncertainties in both the scalar irradiance radiometer and in the reflecting tube instrument. Less than 5% uncertainty in absorption is expected in future experiments. In very clear oligotrophic water, however, uncertainty in water absorption values may make it impossible to realize this level of relative agreement. Unfortunately, an adequate commercially available scalar, or hemispherical, irradiance radiometer does not exist today, and development and characterization of suitable spherical or hemispherical collectors is a prerequisite to application of this method. The present version of the protocols will, therefore, emphasize the combination of filter spectrophotometry (Section 5.4.2) and *in situ* reflecting tube total absorption measurements. The present section covers field calibration and sampling procedures for using the reflective tube absorption and beam transmission meter. Recommended methods of data analysis to derive vertical profiles of $a(z,\lambda)$ and $c(z,\lambda)$ are presented in Section 6.8.1.

It is always best to determine optical properties *in situ*, if possible. Sampling variability, changes of light intensities, filtration procedures, and sample degradation over time all affect the particulate matter and distort its true optical properties as they existed in the ocean, and as they determine the remote sensing reflectance viewed by SeaWiFS. The reflecting tube method has been used to measure spectral absorption in the laboratory for many decades (James and Birge 1938). In recent years, this method has been adapted for use in the ocean (Zaneveld 1992). Suitable instruments are now commercially available and are coming into general use within the oceanographic community.

The reflecting tube does not perfectly gather all scattered light and transmit it to the detector, and as a result, there is a scattering error on the order of 13% of the scattering coefficient. This error can be largely corrected if the beam attenuation coefficient is measured simultaneously. In that case, the scattering coefficient is obtained as $b(\lambda) = c(\lambda) - a(\lambda)$. By assuming that the measured absorption is due to water and scattering error at a wavelength in the infrared, and by subsequent correction at other wavelengths using a provisional $b(\lambda)$, it is possible to correct the spectral absorption to within a few percent of the scattering coefficient. Only in waters with very high scattering and very low absorption would this error pose a serious absorption error. This correction method is described in more detail in Section 5.4.5 below.

The *in situ* reflecting tube is normally used to measure profiles of total spectral absorption, but it has been recently demonstrated that if the unit's intake is fitted with a large area 0.2 μm filter, the spectral absorption of the dissolved component can be measured (Zaneveld pers. comm.). A pair of reflecting tube absorption meters can thus be used to determine the separate constituents of absorption due to particulate and dissolved substances—a distinction of fundamental importance in relating absorption to remote sensing reflectance. More traditionally, the filtration and spectrophotometry techniques developed over the last decade also lend themselves well to this task. Using the methods described in Section 5.4.2, the spectral absorption coefficient is partitioned into components associated with Gelbstoff, pigments, and non-pigmented particles (the latter sometimes referred to misleadingly as *detritus*).

There are two primary weaknesses of the filtration spectroscopic method:

1. Uncertainties associated with correcting the filter absorption values for scatter within the filter are not well characterized. The correction factor for this phenomenon, called the β factor, does not currently have a unanimous consensus value.
2. The instrumental uncertainty in absorption due to the dissolved component, which attenuates weakly over the 10 cm path of a typical spectrophotometer, is also not well characterized.

Note that some longer path spectrophotometers are in use experimentally, and may reduce this source of uncertainty following a suitable validation procedure. In any event, when the filter spectroscopy absorption values are combined with total absorption values measured with the reflecting tube, the absolute values may be largely corrected to remove these uncertainties, if two reflecting tube meters are not available. Conversely, these comparisons serve to validate and control the quality of the $a(\lambda)$ profiles measured *in situ*.

5.2.5 Backscattering Profiles

While the spectral absorption can now be measured with sufficient accuracy for the purpose of SeaWiFS, backscattering is not routinely measured, yet it has a large influence on the reflectance. The now generally accepted dependence of the remote sensing reflectance on the ratio of the backscattering coefficient and the absorption coefficient has never led to a systematic investigation of the dependence of $b_b(\lambda)$ on the various particulate parameters. Gordon (1989a) showed that the irradiance reflectance depends on the shape of the scattering function in the backward direction. Zaneveld (1994) derived the functional dependence of the remote sensing reflectance on backscattering.

There is little historic data on the variation of the shape of the volume scattering function, $\beta(\theta, \lambda)$, in the backward direction. Petzold (1972) described $\beta(\lambda)$ measured with the GASM. This reference is the one most widely used to describe shapes of $\beta(\theta, \lambda)$. Since that time, only Balch et al. (1994) have published new data regarding the shape of $\beta(\theta, \lambda)$. Several single wavelength integrated backscattering $b_b(\theta, \lambda)$ meters have been constructed (Maffione et al. 1991 and Smart 1992), all of which measure a weighted integral of the scattering function. Maffione's meter has the centroid angle near 150°, whereas Smart's meter has the centroid angle near 170°. The 150° centroid angle is more appropriate for SeaWiFS. This observation also points out a problem in the reporting of results from scattering meters, in that results are commonly reported as simple $b_b(\lambda)$. In the future, more detail should be provided to allow intercomparisons between results reported by different investigators.

All scattering sensors measure a parameter that is a weighted integral of the volume scattering function. The weighting function $W(\theta)$ depends on the geometry of the device. Knowledge of the weighting function is critical in comparing scattering meters. For each scattering meter, documentation should be available describing this weighting function and how it was derived. The weighting function can generally best be derived by moving a Spectralon target through the scattering volume space.

The scattering meter measurement may be defined as

$$\overline{\beta}_b(\overline{\theta}, \Delta\theta, \lambda, \Delta\lambda) = 2\pi \int_0^\pi \beta(\theta, \lambda) W(\theta) \sin\theta \, d\theta, \qquad (21)$$

where θ is the centroid angle computed as

$$\overline{\theta} = \frac{\int_0^\pi \theta W(\theta) \sin\theta \, d\theta}{\int_0^\pi W(\theta) \sin\theta \, d\theta}, \qquad (22)$$

and $\Delta\theta$ is the FWHM bandwidth of the weighting function multiplied by $\sin(\theta)$, λ is the central wavelength of the color filter, and $\Delta\lambda$ is the FWHM bandpass of the filter. While the parameters do not give a complete description of the weighting function, they allow an informed comparison of scattering meter results. Investigators making backscattering measurements are encouraged to report backscattering meter results in the format $\overline{\beta}_b(\overline{\theta}, \Delta\theta, \lambda, \Delta\lambda)$.

Backscattering measurement should be made in close proximity to absorption meters, if both are used, to avoid space-time aliasing.

5.3 ATMOSPHERIC RADIOMETRY

This section is concerned with two types of atmospheric radiometric measurements that are distinct from those described earlier in Section 5.1. The first of these is the photometric measurement of the direct solar beam to determine the optical thickness of the atmosphere (Section 5.3.1). The second is a measurement of the sky radiance distribution using a radiance distribution camera (Section 5.3.2).

5.3.1 Sun Photometry

Measurements of the direct solar beam, using the sun photometer, should be performed during the optical stations. If sky radiance distribution measurements are performed, it is important that these measurements are performed concurrently. While the preferred method of determining the optical thickness of the atmosphere is by measuring the solar transmission as a function of solar zenith angle, the atmospheric conditions are rarely stable enough at sea for this method to work. Thus, a stable, well calibrated photometer can be used with measurements at a single zenith angle to obtain the solar transmission, and thus, the aerosol optical depth.

Atmospheric measurements should be performed only when clouds, including high cirrus, do not obstruct the solar disc. Careful documentation of sky conditions is important, as are accurate recordings of the time of day and the geographic location of the station. The latter data are important in determining the true solar zenith angle and, hence, the air mass in the solar path. It should also be obvious that care should be taken to avoid ship perturbations (e.g., stack gas) from interfering with the measurements. Ancillary measurements, such as barometric pressure, are important in separating Rayleigh scattering from the aerosol scattering.

5.3.2 Sky Radiance Distribution

Complete sky radiance distributions should be measured with a radiance distribution camera during the SeaWiFS radiometric initialization and validation optical stations. For this purpose, it is critically important that these measurements be obtained whenever totally clear sky conditions persist. Coincident with these measurements, sun photometer measurements should be obtained. When locating the camera system for these measurements, it is important that the FOV be as unobstructed as possible. While it would be optimum to have a completely unobstructed FOV, this is often not practical. During measurements, therefore, at least one hemisphere (defined by the sun-zenith plane) should be unobstructed; through symmetry, this should yield a complete radiance distribution.

Ship perturbations, e.g., stack gas, must be avoided completely. It is important to document where the instrument is located and what possible perturbations might exist, even though these effects may be obvious in the data.

It would also be highly desirable to add sky radiance measurements to every SeaWiFS algorithm development and validation cruise. Gordon (1989b) rigorously demonstrated the importance of determining $\overline{\mu}_d$, the mean cosine for downwelling radiance (Morel and Smith 1982), for the bio-optical interpretation of $K_d(z,\lambda)$. Gordon (1989b) also showed, for cloud-free skies, how to obtain a reasonable estimate of $\overline{\mu}_d(0^+)$ from spectral irradiance deck cell measurements with, and without, the sun blocked from the view of the irradiance collector. This procedure should be done routinely whenever it is practical to do so. Unfortunately, the collective scientific experience is that cloud-free skies rarely occur at ocean optical stations.

If a calibrated spectral radiance distribution camera is available, then $L_{\text{sky}}(\lambda,\theta,\phi)$ should be measured several times during each spectral radiometer cast and used to compute $\overline{\mu}_d(0^+,\lambda)$. Radiance distribution cameras are expensive to build, however, and one is not likely to be available aboard every SeaWiFS validation vessel. A recommended alternative approach is to acquire:

1) all-sky photographs taken either with a conventional camera or, preferably, a digitally recorded camera system (some research must be done to develop procedures for attenuating, or blocking, the sun's image and for using filters);
2) measurements, with a narrow FOV spectral radiometer of $L_{\text{sky}}(\lambda,\theta_i,\phi_i)$ at several discrete angles θ_i and ϕ_i; and
3) $E_s(\lambda)$ measurements of $E_{\text{sun}}(\lambda)+E_{\text{sky}}(\lambda)$ with the sun's image blocked by shadowing the deck cell irradiance collector (Gordon 1989b).

During the prelaunch experiments, $\overline{\mu}_d(0^+,\lambda)$ values estimated from measurements of these types should be compared with $\overline{\mu}_d(0^+,\lambda)$ values determined from direct measurements of sky radiance using a spectral radiance distribution camera system.

5.4 WATER SAMPLES

Duplicate samples should be taken at each of 12 depths, including at least three depths within the first attenuation length, $1/K(490)$; however, in coastal areas with short attenuation lengths, this may not be possible. Samples should also be taken in the *in vivo* fluorescence and beam attenuation maxima. The remaining samples should be spaced throughout the water column using beam attenuation, *in situ* fluorescence, and CTD profiles as a guide.

5.4.1 Pigment Analysis

Water samples should be taken at the site of, and simultaneously with, the surface in-water upwelled radiance and reflectance measurements, and at depth increments sufficient to resolve variability within the top optical depth. The $K(z,\lambda)$ profiles over this layer will be used to compute optically weighted, near-surface pigment concentration for bio-optical algorithm development (Gordon and Clark 1980).

When possible, samples should be acquired at several depths distributed throughout the upper 200 m of the water column [or in turbid water, up to seven optical depths, $\ln((E(0)/E(z)) = 7]$, to provide a basis for relating chlorophyll *a* fluorescence signals to pigment mass concentration.

For low uncertainty determinations of chlorophylls *a*, *b*, and *c*, as well as carotenoid pigments, HPLC techniques are recommended. It should be noted, however, that the reverse-phase C18 HPLC method recommended by the Scientific Committee on Oceanographic Research (SCOR) (Wright et al. 1991) is not capable of separating monovinyl chlorophyll *a* from divinyl chlorophyll *a* nor monovinyl chlorophyll *b* from divinyl chlorophyll *b*. This method, therefore, *only* provides estimates of total chlorophyll *a* and total chlorophyll *b* concentrations, respectively.

Divinyl chlorophyll *a*, the major photosynthetic pigment found in prochlorophytes, accounts for 10–60% of the total chlorophyll *a* in subtropical and tropical oceanic waters (Goericke and Repeta 1993, Letelier et al. 1993, Bidigare et al. 1994, and Bidigare and Ondrusek 1994). Divinyl chlorophyll *a* is spectrally different from *normal* (monovinyl) chlorophyll *a*, and its presence results in a significant overestimation of *total* chlorophyll *a* concentration as determined by the conventional HPLC methods (Goericke and Repeta 1993, Letelier et al. 1993, and Latasa et al. 1994). To avoid these errors, it is recommended that monovinyl and divinyl chlorophyll *a* be spectrally resolved or chromatographically separated in order to obtain an unbiased determination of total chlorophyll *a* (that is, total chlorophyll *a* equals divinyl chlorophyll *a* plus monovinyl chlorophyll *a*) for the purpose of ground-truthing SeaWiFS imagery. These co-eluting chlorophyll species can be resolved spectrally following C18 HPLC chromatography (Wright et al. 1991) and quantified using dichromatic equations at 436 and 450 nm (Goericke and Repeta 1993 and

Latasa et al. 1994). Alternatively, these two chlorophyll species can be separated chromatographically and individually quantified using the C8 HPLC technique described by Goericke and Repeta (1993). (C18 and C8 designate column packing materials used in HPLC.)

These protocols, to be employed in the SeaWiFS validation program for HPLC pigment analyses, are prescribed in the *JGOFS Core Measurement Protocols* (JGOFS 1991). These protocols include:

a) use of Whatman GF/F glass fiber filters, approximately 0.7 μm pore size,

b) extraction in 90% acetone, and

c) calibration with authenticated standards.

It is recommended that seawater samples not be prefiltered to remove large zooplankton and particles as this might result in the exclusion of pigment-containing colonial and chain-forming phytoplankton, e.g., diatoms and *Trichodesmium sp.* Large zooplankton can be removed following filtration using forceps.

When it is appropriate to measure phycoerythrin concentration, it is important to discriminate between *Trichodesmium* and *Synechococcus* phycoerythrins, as they have different spectral absorption characteristics. The concentration of *Trichodesmium* phycoerythrin may be determined using the glycerol uncoupling method described by Wyman (1992). Separating *Trichodesmium* from *Synechococcus* may require pre-filtering.

In addition to HPLC analyses, it is recommended that the standard fluorometric methodology used for measuring chlorophylls and phaeopigments (Yentsch and Menzel 1963, Holm-Hansen et al. 1965, and Strickland and Parson 1972) also be applied to the same extracted pigment samples used for HPLC analysis (Section 6.6.1). This additional analysis will enable a direct link to the historical bio-optical algorithms and database development during the CZCS validation experiments.

5.4.2 Spectrophotometric Absorption

This section describes laboratory protocols for separating the total spectral absorption coefficient, $a(z, \lambda)$, into its components due to absorption by pure water, *in vivo* phytoplankton pigments [$a_\phi(\lambda)$], dissolved material [$a_g(\lambda)$, Gelbstoff], and other particulate material [$a_t(\lambda)$, tripton] by spectrophotometric measurements of filtered discrete water samples. Associated data analysis protocols are presented in Section 6.8.2.

All equipment utilized in water sample processing for Gelbstoff samples should minimize contamination by organic or colored material and should protect samples from photodegradation. Glass provides the best material for filtration units and sample storage containers. Glass filtration units should have stainless steel filter supports and not ground glass frits, since these tend to clog over time and change particle retention efficiencies of the units. Amber-colored borosilicate glass bottles are preferred for samples and filtrate collection because they protect the dissolved samples from ambient light. Caps lined with PTFE are preferred to minimize contamination. Prior to each experiment, all filtration and storage bottles should be thoroughly cleaned with detergent and rinsed several times with distilled water (DIW).

For measurement of absorption by dissolved organic matter (DOM), samples should be filtered through 0.2 μm membrane filters, e.g., Nuclepore™ polyester 0.2 μm filters. Membrane filters minimize the contamination of the filtrate by filter fibers. It is recommended that separate water samples be filtered for DOM, particulate matter, and pigment analyses. Combining several analyses in one filtration can introduce errors, because each analysis has a specific filtering protocol.

The procedure for preparing a sample for DOM measurements is as follows:

1. Before filtering a sample for the measurement, filter at least 100 ml of DIW through the filter to remove wetting agents or other organic material.
2. Swirl and rinse the filter trap.
3. Filter 30–50 ml of the available volume, and capture in a trap.
4. Rinse the filter and flask a second time with a second aliquot of sample, or, if sample is scarce, refilter the first-pass filtrate.
5. Swirl and rinse the trap after the second filtration, and discard the filtrate.
6. Filter the remaining volume, capture in the trap, and refilter the sample.
7. Rinse a clean, amber glass, storage bottle three times with filtrate, then fill, cap and store upright.

If it is necessary to delay the measurement of the Gelbstoff sample for more than a few hours, freeze each filtrate sample in an amber bottle, and store upright and in the dark.

An alternate simple and rapid filtration method for measuring absorption spectra of dissolved organic matter in water samples has been proposed by Yentsch and Phinney (pers. comm.). A high-volume 0.22 μm Sterivex™ filter cartridge† is used to perform a one-step filtration with the sample introduced directly into the cuvette from the filter cartridge. The sample is pushed through the cartridge using a 50 cc sterile plastic syringe attached by a Luer lock connection. Sample handling is minimized and preparation time, including rinses, is only a few minutes per sample. The cartridges cost approximately $2.00 each, which makes them expensive to use for only one sample. Yentsch and Phinney found, however, that rinsing between samples with distilled water permits the use of one cartridge per station with no measurable contamination effects. They verified non-contamination by measuring the

† A membrane filter made by Millipore Corporation.

absorption spectrum of a final distilled water rinse after all samples for a station were filtered, and then comparing the absorption spectrum of this sample to the baseline spectrum measured prior to the sample analysis.

A potential disadvantage of the Yentsch and Phinney method results from the need to detach and reattach the cartridge to the syringe between sample and rinses. Back pressure applied while removing the syringe plunger with the cartridge attached can rupture the membrane. This problem can be avoided by using a peristaltic pump to introduce the sample and rinse water directly from separate bottles.

The samples should be allowed to equilabrate to room temperature before spectrophotometer measurements are made, and they should be protected from ambient light. If the Yentsch and Phinney suggestion to inject the sample directly into a cuvette is followed, this implies use of several cuvettes per station and some type of dark storage arrangement. Otherwise, the samples should be injected into amber bottles which have been prerinsed in the sample filtrate. It may be possible to wait approximately 20 minutes before filtering, to allow the samples to warm to room temperature, provided an investigator demonstrates that this delay does not allow modification of the sample filtrate.

To summarize, the following method can be employed on samples collected and stored using any currently established technique:

1. Prerinse a Sterivex cartridge using 100 ml of Nanopure or similarly polished DIW.
2. For spectrophotometric baseline determination, rinse the reference and sample cuvettes 2 or 3 times with filtered DIW and fill the cuvette, measure the absorption spectrum, and store it as the baseline.
3. For each successive sample, evacuate the cartridge, and rinse it with 50 ml DIW. Then, evacuate the cartridge and rinse it with a 50 ml sample. Refill the syringe with a sample, rinse the sample cuvette, and inject the sample from the syringe through the filter cartridge into the cuvette. Measure the absorption spectrum in a spectrophotometer (see below).
4. After all samples have been analyzed, rinse the cartridge with 50 ml DIW, refill the syringe with DIW, rinse the sample cuvette and fill it with filtered DIW, and measure the absorption spectrum. Compare this absorption spectrum to the baseline.

To measure the absorption of the dissolved fraction, minimize the distance between the detector and the cuvettes in the spectrophotometer, and use 10 cm quartz cuvettes to maximize the absorption signal. Warm the filtrate samples to room temperature while protecting them from direct light. Filter reverse osmosis or *Milli Q* purified water (ROW) through a rinsed GF/F filter for reference as a blank, discarding the first 100 ml. Begin the analyses when the sample and reference material are both at room temperature. Perform a new baseline measurement range using a ROW blank each time the instrument has been powered up or the configuration changes.

Using a dual beam spectrophotometer, scan the instrument's baseline optical density spectrum $OD_b(\lambda)$ from approximately 300–700 nm, beginning at the lowest ultraviolet (UV) wavelength the instrument will measure without cuvettes in the light path. Place the reference blank ROW, filtered as described above, in both sample and reference cuvettes and scan the reference optical density spectrum $OD_r(\lambda)$. Rinse the sample cuvette with approximately 5 ml of the sample three times. Rinse and fill the sample cuvette with the DOM sample filtrate and scan $OD_g(\lambda)$. Replace reference water blanks every few samples to prevent bubble formation in the reference cuvette. Between samples, block the reference light and open the sample compartment door to minimize temperature changes in the ROW reference.

The GF/F filter (which is binder-free and combustible, with a nominal pore size of 0.7 μm) is the best choice for particle absorption sampling. This filter has a large scattering coefficient at visible wavelengths, which increases the optical path length of the photons and improves the accuracy of particulate absorption measurements. This type of filter is also recommended by (JGOFS 1991) for carbon, hydrogen, and nitrogen (CHN); pigment; and primary productivity analyses. The optical transparency of the GF/F filter decreases significantly below 380 nm.

Some authors have reported that particulate material less than 0.7 μm in size will not be retained by the GF/F filter, and that this fraction may contain up to 10–15% of the phytoplankton biomass as measured by chlorophyll concentration. Chavez et al. (1995), however, found no statistical difference between GF/F and 0.2 μm filters for chlorophyll and productivity measurements.

The goals for filtration of particulate samples are to minimize contamination and particle degradation, maximize retention, and concentrate an adequate amount of particles on the filters to permit accurate spectrophotometric measurements. Vacuum pressures below 5 inches of mercury, i.e., 117 mm Hg, are recommended to reduce the chances of particle breakage. It is currently recommended to set the filtration volume for each sample to approximate an optical density value of 0.25 at 400 nm (Roesler and Perry 1992). Small area (13 mm^2) filtration units may be used to reduce water sample volumes.

Optical density spectra of the filters should be measured as soon as possible, because pigment decomposition may occur (Stramski 1990). If necessary to store filters, place the unfolded filters into polypropylene tissue capsule containers and store in liquid nitrogen. Freezing in conventional freezers causes ice crystals to form on the particles and leads to cell breakage and pigment degradation.

A new instrument baseline scan should be measured each time the spectrophotometer is powered up or anytime its configuration has been changed. To measure the particulate absorption spectrum, first prepare a blank filter by soaking it in 50 ml DIW for 20 minutes (remembering to select it from the same box as the sample filters). An alternative approach is to use prefiltered seawater (prefiltered using a 0.2 μm Millipore GS filter) to wet the GF/F filter blank (Cleveland pers. comm.), for the reason that the sample filters are also wetted with seawater. If using a single beam spectrophotometer, scan the instrumental baseline $OD_b(\lambda)$ without the filter. Then insert the wetted filter blank to obtain the reference spectrum $OD_r(\lambda)$. With a dual beam spectrophotometer, two wetted reference filter blanks must be used to measure the reference spectrum, and one is left in the reference beam during sample measurements. Some investigators recommend aligning the filter fibers in a fixed orientation each time a filter is inserted.

If the samples were frozen, remove the sample filter from the liquid nitrogen. Place a few drops of DIW or filtered seawater on a glass (or Plexiglas) slide and then place the sample filter, bottom side down, on the water. This moistens the filter and hastens thawing. Place the filter in the sample compartment with the filtered material facing the source. Scan the $OD_p(\lambda)$. Place the sample filter back in the filter cup. Gently pour 30–50 ml of hot spectrophotometric- or HPLC-grade methanol over the filter, taking care not to lift any particulates off the filter (Kishino et al. 1985). Let the filter sit 10–15 minutes under the methanol, filter through, and repeat the process. Rinse with 10–20 ml of 0.2 μm DIW. Seawater is not used here, because methanol may cause precipitates to form on the filter. Position the filter in the spectrophotometer and scan $OD_t(\lambda)$. This spectrum is associated with raw, non-pigmented particulates, often referred to as *detritus* or *tripton*. The absorption spectrum should decrease exponentially with wavelength. If there is a residual chlorophyll *a* absorption peak at 676 nm, repeat the extraction process until the peak disappears.

Recommended methods for analysis to convert the measured optical density spectra to absorption spectra are discussed in Section 6.8.2.

5.4.3 Total Suspended Matter

All suspended particulate material (SPM) dry weight ($mg\,l^{-1}$) will be determined gravimetrically as outlined in Strickland and Parsons (1972) and as specified in JGOFS (1991). In general, samples are filtered through 0.4 μm preweighed polycarbonate filters. The filters are washed with three 2.5–5.0 ml aliquots of DIW and immediately dried, either in an oven at 75° C, or in a dessicator. The filters are then reweighed in a laboratory back on shore using an electrobalance with at least seven digits of precision.

5.5 ANCILLARY OBSERVATIONS

Ancillary observations are often of key importance in flagging and interpreting apparently aberrant data. The minimal set of ancillary supporting observations must include:

1) date and time (both GMT and local);
2) geographic location, using the Global Positioning System (GPS) if possible, before and after each cast and at times of satellite and aircraft overpasses;
3) solar azimuth and zenith angles, as calculated from position, date, and time;
4) position of the optical cast in relation to the ship orientation and position of the ship relative to the sun (a sketch in the field notes is recommended);
5) sea state (photographed if possible) with approximate swell height, direction, and notes on presence and density of whitecaps;
6) quantitative measurements of surface wire angles during deployments of the instrument package;
7) time of cast (begin and end), as well as time and depth of water samples collected;
8) percent cloud cover and cloud type, and solar occlusion conditions; and
9) wind direction and velocity.

Desirable additional ancillary measurements include:

a) an all-sky photograph plus a photographed time history of sea surface is advised for radiometric stations; and
b) Secchi depth.

5.6 PROTOTYPE OPTICAL BUOY

A prototype optical measurement system designed for long-term buoy deployment with a satellite data telemetry capability is presently under development and is focused on satisfying the SeaWiFS optical data requirements. The concept is constrained by the requirement that the instrument be capable of maintaining measurement integrity while being unattended for long periods of time. This constraint has lead to a design that minimizes the number of moving parts to one, and has resulted in the spectrographic application of concave holographic diffraction gratings. These holographic gratings provide an approximate flat focal field to the degree that planar silicon photodiode arrays may be used as detectors. Inherent within this technology are the features of simplicity, compactness, durability, and stability.

The optical system utilizes two spectrographs, in tandem with a dichroic mirror specifically designed to avoid measurements in the water absorption region, in order to

measure radiometric properties with high spectral resolution and stray light rejection. The dichroic mirror is designed to transmit the red (630–900 nm) and reflect the blue portions (380–600 nm) of the spectrum, making the transition from reflectance to transmittance between 600 and 640 nm. The potential for stray light is greatly reduced by splitting the visible spectrum at the beginning of the water absorption region, since most of the short wavelength energy is diverted from the entrance slit of the long wavelength spectrograph. The splitting also allows the spectrographs, i.e., gratings and sampling periods, to be optimized for the two distinctive spectral domains. A further reduction of stray light for the long wave spectrograph will be achieved by utilizing a minus blue filter.

The optical system will be deployed on a slack-line moored wave rider buoy that has a 10–20 m *optical bench* attached. Apparent optical properties will be measured by a series of remote collectors that are coupled to the instrument with fiber optics. Data will be compressed, stored, and forwarded through a NOAA Geostationary Operational Environmental Satellite (GOES) and an ARGOS telemetry link.

This type of optical mooring represents a new and challenging technology. Detailed protocols for deploying and maintaining this type of mooring, and for evaluating its data quality, must be developed in light of the experience to be gained over the next 2–3 years.

The current practice is to apply marine antifouling compounds (such as OMP-8) to prevent the growth of marine organisms on the windows of moored radiometer systems. This approach is less satisfactory for IOP instruments, because for collimated light, transmission characteristics of the optical windows can be adversely affected by the layer of the anti-fouling material.

5.7 DRIFTING OPTICAL BUOYS

Drifting optical instruments are a recent development and there is almost no history of their quantitative application to problems in ocean color algorithm development and remote sensing radiometric validation. It is probable that significant experience in the uses and limitations of such instruments will be gained in SeaWiFS related experiments during the prelaunch period. The critical questions about these instruments, which should be answered during prelaunch work, include:

1. How accurately can $L_W(\lambda)$ be estimated from $L_u(z,\lambda)$ at a single near surface depth, using only an estimate of $K_L(\lambda)$ obtained from ocean color ratios? Is 5% uncertainty feasible?
2. How accurately can a normalized water-leaving radiance ratio $L_{WN}(\lambda_1)/L_{WN}(\lambda_2)$ be estimated with these instruments using only a single channel $E_d(\lambda)$ measurement for normalization, which is contemplated for instruments currently being developed (Section 2.6)? Are the normalized water-leaving radiance ratios from clear sky and overcast conditions comparable enough that the drifter data can provide a basis for interpolating SeaWiFS data through cloudy periods?

When answers to these fundamental questions are in hand, it will be possible to draft and implement more detailed protocols for the use of optical drifters in SeaWiFS radiometric validation and algorithm development.

Many potential applications of optical drifters in oceanographic research using SeaWiFS data are more obvious, but from a radiometric standpoint are less stringently demanding. Protocols for those applications are, however, beyond the scope of this report.

5.8 SAMPLING AND VALIDATION

The following discussion of bio-optical sampling protocols is organized into three subtopics: sampling for the initial and ongoing validation of the SeaWiFS radiometric system performance (Section 5.8.1), algorithm development and validation in Case-1 waters (Section 5.8.2), and algorithm development and validation in Case-2 waters (Section 5.8.3). The distinction between the first subtopic and the second two is clear-cut, but what precisely is meant by *Case-1* and *Case-2* water masses?

In its literature and reports, the ocean color research community has formally adopted definitions originally due to Morel and Prieur (1977), who stated:

> "Case-1 is that of a concentration of phytoplankton [which is] high compared to that of other particles. The pigments (chlorophyll, [and] carotenoids) play a major role in actual absorption. In contrast, the inorganic particles are dominant in Case-2, and pigment absorption is of comparatively minor importance. In both cases, [the] dissolved yellow substance is present in variable amounts and also contributes to total absorption."

In practice, however, only those water masses where the CZCS-type blue-green ratio algorithms for phytoplankton pigment concentration (chlorophyll *a* + phaeopigment *a*) work reasonably well have been treated as *Case-1*. All other water masses have often been loosely lumped into the *Case-2* definition, albeit with considerable confusion over how to categorize coccolithophorid blooms, and similar phenomona normally classified as *Case-1* waters, in which strong concentrations of Gelbstoff vary independently from chlorophyll *a* concentration.

In the present discussion of sampling protocols, Case-1 will be considered to refer to what might be called *ordinary open ocean Case-1* waters, wherein scattering and absorption are dominated by phytoplankton, pigments, and Gelbstoff concentrations, and where *global* blue-green color ratio algorithms for chlorophyll *a* concentration and $K(490)$ work well. Most areas in the deep ocean belong to this case. Water masses which do not satisfy this criteria will

be grouped under the heading Case-2. Within Case-2, by this definition, water masses with a wide diversity of bio-optical characteristics will be found. Prominent subcategories include:

1) coccolithophorid blooms, wherein the detached coccoliths dominate light scattering and remote sensing reflectance independently from pigment concentration;
2) coastal areas, wherein DOM of terrestrial origin contributes a strong absorption component which does not co-vary with pigment concentration;
3) phytoplankton blooms with unusual accessory pigment concentrations, e.g., *red tides*, which require the use of special regional or local ocean color algorithms; and
4) classical extreme Morel and Prieur (1977) Case-2 waters where optical properties are dominated by inorganic particles, with many possible variations in chemical and geometric characteristics.

It is important to recognize that some aspects of the water mass distinctions given above are dependent on the spectral regions in which measurements are to be made. Strong absorption at UV, red, and near-IR wavelengths requires the use of radiometric techniques similar to those required for Case-2 waters.

In addition to determining the bio-optical category and characteristics of a particular water mass, the validation sampling strategy must be concerned with spatial and temporal variability. Spatial and temporal variability in bio-optical properties will profoundly affect the validity of comparisons between SeaWiFS and in-water optical measurements. A single SeaWiFS instantaneous FOV measurement will integrate $L_W(\lambda)$ over approximately a square kilometer, or a larger area at viewing angles away from nadir. Furthermore, the location uncertainty for a single pixel may be several kilometers, except in near-shore areas where image navigation can be improved by using land-navigated anchor points.

Bio-optical profiles measured at a single station are representative of a spatial scale that is only a small fraction of a kilometer. Data from a grid of several station locations may be required to estimate the spatial averages of optical properties represented by a SeaWiFS pixel, or a block of pixels. Because the ship measurements over the grid are not instantaneous, temporal variability in bio-optical properties can add additional uncertainty to the comparisons. Aircraft radiometric observations can, conceptually, be used both to locate comparison sites away from areas of strong spatial variability and to document changes in the pattern of spatial variability over the period required for a ship to occupy all stations in a comparison grid.

Vertical stratification of water temperature, salinity, and density often affect the vertical structure of variability in bio-optical properties. This variability, in turn, affects the remote sensing reflectance. Vertical stratification of the water column becomes especially important in many Case-2 waters, where the top attenuation depth may be as shallow as 1–2 m and the entire euphotic zone may be confined to less than 10 m depth. It is important, therefore, to minimize ship-induced disruption of vertical stratification in the water column. Whenever possible, the ship should be maneuvered as little as possible while on station with its propellers and bow thruster, and the practice of backing down hard to stop quickly when on station should be strongly discouraged. If wind and sea conditions permit, the preferred method of approaching a station is to take enough speed off the ship to coast to a stop over approximately the last 0.5 km of approach to the station. The approach should be planned to allow the ship to be turned, preferably using only the rudder, to place the sun abaft the beam or off the stern, depending on where the radiometers will be deployed. It must be realized, however, that depending on wind and sea conditions, and a particular ship's hull and superstructure configuration, it may not be possible to maintain an acceptable orientation, with respect to the sun, while the ship is adrift. In these situations, some use of the engines to maintain an acceptable ship's heading may be unavoidable.

The chief scientist should also consult with the ship's captain and chief engineer to avoid, or at least minimize, overboard discharges while the ship is on station. Material from a ship's bilge or sewage treatment system can significantly change near-surface chemical and optical properties if discharged near the immediate site of a bio-optical profile or water sample.

In some coastal areas, where a relatively transparent water mass overlies a highly reflective bottom, $L_W(\lambda)$ includes light reflected from the sea floor. These cases require special treatment of bottom reflectance effects whether the local water mass regime is Case-1, Case-2, or a combination of both. Methods of measurement, experiment design, and sampling strategies to study bottom reflectance effects are beyond the scope of this revision to the ocean optics protocols. There is a significant current research effort focused in this area (Carder et al. 1992, Hamilton et al. 1992, and Lee et al. 1994), and it is expected that experience will evolve the basis for new protocols in this topic area to be included in the next revision of this document.

The bottom reflection of areas with a water depth exceeding 30 m normally does not contribute to the water leaving radiance, $L_W(\lambda)$. Areas with a depth shallower than 30 m will be flagged in the SeaWiFS level-2 data product. Pixels covering very turbid waters may, however, even be usable even in shallower areas. As a general rule, the water depth should be deeper than 2.5 attenuation lengths, $1/K(490)$, at all SeaWiFS algorithm development and validation stations. The prime exception to this rule is in developing local SeaWiFS algorithms where bottom reflectance contributions must be taken into account (Lee et al. 1994).

Variables to be measured at each validation station are summarized in Table 1, and methods for making each measurement are discussed in the previous subsections of Section 5. Methods of data analysis and reporting are discussed in Section 6.

5.8.1 Initialization and Validation

Data intended for direct comparisons between observed $L_u(\lambda)$ and SeaWiFS $L_W(\lambda)$ estimates should usually be acquired in areas where bio-optical variability is known to be very small. This will ordinarily dictate that such data be acquired from optically clear and persistently oligotrophic Case-1 water masses. Potentially suitable sites include the northeastern Pacific central gyre off Baja, California (to the southwest), and the central Sargasso Sea. When planning validation cruise locations and timing, seasonal and regional cloud cover statistics should also be considered in order to maximize the likelihood of simultaneous SeaWiFS and shipboard observations. A semi-oligotrophic site in the northeast Pacific, near Hawaii, is the prime candidate for placing a moored radiometer for continuous time-series radiometric comparisons with SeaWiFS $L_W(\lambda)$ estimates.

A series of radiometric comparison stations should be made over a wide range of latitude in both the Northern and Southern Hemispheres, to look for evidence of cyclic thermal sensitivity affecting SeaWiFS. The spacecraft and instrument will be heated by sunlight throughout the descending (daylight) data acquisition segment of each orbit and will be cooled by thermal radiation while in the Earth's shadow throughout the remainder of the orbit. This cycling is likely to induce transient thermal gradients in the instrument, as well as a time varying cycle in the temperatures of its detectors and other components; these thermal variations could affect the spectral bandpass or responsivity of one or more SeaWiFS channels. Unfortunately, a set of stations covering the full range of latitudes cannot all be sited in regions where mesoscale variability in ocean optical properties can be neglected. As when acquiring data for developing and validating Case-1 bio-optical algorithms (Section 5.8.2), a significant effort must be exerted to quantify spatial variability in normalized water-leaving radiance. When possible, airborne radiometer data, in combination with careful characterization of atmospheric aerosol and cloud conditions, should be employed to augment shipboard radiometry at the stations selected for this aspect of the validation. If aircraft support is not available, semi-synoptic shipboard transects covering a $20\times20\,\mathrm{km}^2$ grid should be used to characterize spatial bio-optical variability near a sampling station.

The minimum set of variables to be measured for radiometric validation are those from the *Product Verification* column of Table 1. Measurements used to calculate normalized water-leaving radiance for direct comparison to SeaWiFS radiances must be made under cloud-free conditions and within five minutes of the satellite overpass.

5.8.2 Case-1 Water Protocols

In open-ocean oligotrophic water, it is usually practical to assume that a station is in a Case-1 water mass, although some caution must be taken to detect coccolithophorid blooms and suspended coccoliths. In more turbid coastal transition regimes, however, the classification of the local water mass as Case-1 or Case-2 may be less obvious. In this environment, moreover, Case-1 and Case-2 water masses may both be present in the domain sampled by a ship. One example of this situation would be Case-1 water within an eddy-like intrusion from offshore into coastal areas normally occupied by Case-2 water masses. Another would be Case-2 waters in a major river plume intruding into an ambient Case-1 water mass regime.

In general, a water mass may be categorized as Case-1 if:

1) Gelbstoff absorption at 380 nm, $a_g(380)$, is less than $0.1\,\mathrm{m}^{-1}$ (Sections 5.2.4, 5.4.2, 6.8.1, and 6.8.2);
2) total SPM concentration is less than $0.5\,\mathrm{mg}\,\mathrm{l}^{-1}$ (dry weight) (Section 5.4.4);
3) measured $L_W(\lambda)$ values, used in the SeaWiFS Case-1 algorithm, predict measured fluorometric chlorophyll *a* concentration within 35%; and
4) measured $L_W(\lambda)$, used in the SeaWiFS algorithm, predicts measured remote sensing $K(490)$ within 20%.

The determination of criteria 1 and 2 above (Doerffer pers. comm.) will ordinarily require retrospective analysis. On the other hand, radiometric profiles and pigment samples can ordinarily be analyzed on board to allow determination of criteria 3 and 4 shortly after the samples are acquired.

SeaWiFS Case-1 algorithm development and validation requires measurements from Case-1 water masses spanning a wide range of optical properties and phytoplankton pigment concentrations. In optically transparent low-chlorophyll oligotrophic water masses, spatial variability is usually small and a station location and sampling strategy like that discussed in Section 5.8.1 is appropriate.

In high-chlorophyll mesotrophic Case-1 water masses with increased turbidity, mesoscale and smaller scale variability is often significant. In very productive Case-1 water masses, station placement and many other aspects of sampling schemes are similar to those appropriate for Case-2 water masses (Section 5.8.3). At algorithm development stations, where measurements need neither be coincident with, nor matched to, SeaWiFS observations, it will be necessary to characterize spatial and temporal variability only over the relatively short scales distinguishing the separate in-water radiometric, optical, and pigment measurements. Airborne ocean color, or lidar characterizations, of spatial variability in the vicinity of these stations will not usually

be essential, although such additional information may be very helpful.

At stations where data are acquired for algorithm validation, and where a match to concurrent SeaWiFS measurements is required, it will be necessary to determine the patterns of spatial variability over a domain extending approximately $20 \times 20\,km^2$ centered at the station, and to place the ship in a $2 \times 2\,km^2$ domain over which $K(490)$ and chlorophyll concentrations vary less than 35% about the mean. Within a few hours before and after a SeaWiFS overpass, in-water measurements should be made at several random locations to characterize variability within the $2 \times 2\,km^2$ validation comparison site. In some cases, it may be possible to determine spatial variability adequately from ship station data and along-track measurements alone. In regions of strong mesoscale variability, however, concurrent aircraft ocean color or lidar measurements should be used both as a guide for selecting the ship's location, and as a basis for spatially extrapolating the in-water measurements to match the much coarser resolution of the SeaWiFS measurements (Section 5.1.7). These topics are developed in more detail, with respect to Case-2 waters, in Section 5.8.3.

5.8.3 Case-2 Water Protocols

Although coastal and continental shelf areas comprise only 10% of the total ocean area, they provide roughly half of the oceanic new production and most of the sequesterable DOC (Walsh et al. 1981). These areas are typically higher in phytoplankton pigment concentration, and may include colored terrigenous constituents such as DOM and suspended sediments. In these *Case-2* waters, the global color ratio algorithms break down because two or more substances with different optical properties are present which do not co-vary with chlorophyll *a* concentration (Section 5.8 above). These might be waters with exceptional plankton blooms (such as red tides), areas discolored by dust transported by the wind from deserts into the sea, or coastal areas influenced by river discharge of mineral and organic suspended materials, and DOM, i.e., Gelbstoff, such as humic acids.

It is not always easy to decide to which case a water mass belongs. As a starting point, the water belongs to Case-2 if any of the four Case-1 criteria, set forth in Section 5.8.2, are not satisfied. For Case-2 waters defined by any one of these criteria, it remains a further problem to determine the specific bio-optical characteristics which distinguish it from Case-1. Case-2 sampling must usually include a more complete subset of the variables in Table 1, in addition to $a_g(\lambda)$ (Sections 5.2.4 and 5.4.2), SPM concentration (Section 5.4.3), chlorophyll *a* concentration, and radiometry. For example, it may be necessary to determine complete pigment composition and other optically important characteristics of exceptional phytoplankton blooms for such planktonic groups as coccolithophorids, diatoms, cyanobacteria, or microflagellates.

To achieve valid comparisons between the ship and satellite data, sharp horizontal gradients and sub-pixel patchiness must be avoided, and image navigation must have land anchor points near the study site. Suitable landmarks are usually available in near-shore coastal waters. The other conditions are difficult to meet in Case-2 water masses, where mesoscale and sub-mesoscale variability is typically very strong. Sub-pixel variations of no more than $\pm$ 35% of the mean pixel chlorophyll will be tolerated, but variability must be measured and taken into account statistically in the analysis (see below).

From the above generalities, it is clear that significant problems are encountered in near-shore coastal waters characterized by small scale patches and dynamic variability due to tidal currents. A particular problem occurs in the shallow areas which are influenced by strong tidal currents—areas that are normally well mixed during part of the tidal cycle. In the slack water tidal phase, however, a vertical gradient of the suspended matter concentration may form, which may cause problems in relating water-leaving radiance to the concentration of suspended matter. During calm periods with strong insolation, even water that is normally well mixed can become stratified. In these cases, the formation of very dense phytoplankton blooms, such as red tides, can be observed. Such blooms will occur in coastal seas when nutrient concentrations are elevated by the influx of river water. In these circumstances, it is especially critical to avoid disturbing the vertical stratification of the water column with the ship's propellers (Section 5.8 above).

5.8.4 Case-2 Sampling Strategy

One approach to sampling in this environment has been suggested by R. Doerffer (pers. comm.). In order to get a good statistical base, water samples are first taken in a random order within the area under research. The concentrations derived from the SeaWiFS data are then compared with the ground truth data by statistical parameters, such as the mean, median, standard deviation, and the shapes of histograms (frequency distribution). For this type of statistical comparison, only sections of SeaWiFS images which match the area covered by the ship should be analyzed. Water samples and satellite data should also be temporally concurrent within the same tidal phase in order to avoid biases due to temporal variability. In these regimes, analyses to validate algorithms cannot be based on SeaWiFS data directly, but must instead be based on water-leaving radiance spectra measured *in situ* (Sections 5.1.1–5.1.6) or from a ship (Section 5.1.8). This approach has the advantage that water samples and radiance spectra are taken nearly simultaneously.

Using either flow-through pumping systems or systems towed outside the ship's wake, fluorometry can be used to assess chlorophyll patchiness if frequent, i.e., every 10-15 minutes, chlorophyll fluorescence-yield calibration measurements are performed. Towed absorption, scattering,

reflectance, and beam transmission meters can also be used to characterize spatial variability. Within a few hours of the overpass, the ship should occupy several stations at random locations within a $2\times2\,km^2$ area central to the area selected for comparison with SeaWiFS data. Sampling stations placed across a tidal front during a SeaWiFS overpass may help to identify two different water masses even when the front has moved. Comparisons between *in situ* and SeaWiFS data in patchy coastal areas may be enhanced by using horizontal radiance profiles measured from an aircraft flying at low altitude (Section 5.1.7). Subsets of such airborne profiles allow direct comparisons with shipboard data. A corresponding profile may then be extracted from the SeaWiFS data for a direct comparison to the aircraft track line profiles. In Case-2 situations, such direct radiometric comparisons are valuable for validating and tuning local algorithms, but are not appropriate for SeaWiFS system validation per se.

To validate the SeaWiFS atmospheric correction, water-leaving radiances measured *in situ* from the ship should be compared with those derived from the SeaWiFS data. Sample matching problems aside, Case-2 waters are often characterized by strongly varying patchiness in optical properties, pigment concentrations, and remote sensing reflectance at spatial scales smaller than a SeaWiFS pixel. Because of the nonlinear relationship between $b_b(\lambda)/a(\lambda)$ and remote sensing reflectance, the pigment concentration derived from spatially averaged SeaWiFS $L_{WN}(\lambda)$ values will systematically underestimate the true spatial average concentration by as much as a factor of 2 when sub-pixel variability is significant. It is, therefore, essential to describe sub-pixel scale variability in Case-2 waters both statistically and in terms of organized structure. Such a description may be accomplished through rapid sampling at closely spaced ship stations in combination with airborne ocean color measurements—for this purpose, track line data from low altitudes and high-resolution imagery from high altitudes are both acceptable.

Absorption coefficients are large enough in all Case-2 waters to require instrument self-shadow corrections to $L_u(0^-,\lambda)$, even though the correction model (Gordon and Ding 1992) has been experimentally verified only for the case where $a(\lambda)r$ is less than 0.1 (Sections 5.1.6 and 6.1.7). In extreme Case-2 waters, large values of spectral absorption may confine the first optical attenuation depth to the top 1–2 m, where it is difficult to measure remote sensing reflectance *in situ*. Such short absorption scale lengths lead to instrument self-shading effects in $L_u(\lambda)$ which are correctable only for instruments with diameters no larger than approximately 1 cm (Gordon and Ding 1992). Radiometers with such a small shadow cross section are conceptually feasible, and a few prototype instruments exist which may be suitable, but they are not commercially available, and self-shadow sensitivities have not yet been experimentally verified for these extreme conditions. In these extreme cases, direct *in situ* measurements of $a(\lambda)$ and $c(\lambda)$ (Sections 5.2.4 and 6.8.1) and $\beta_b(\overline{\theta},\Delta\theta,\lambda,\Delta\lambda)$ (Section 5.2.5), together with above-water measurements of $L_W(\lambda)$ or $R_L(\lambda)$, may provide the only practical means of validating semi-analytic Case-2 algorithms. This topic is an important area for near-term research and development.

5.9 VICARIOUS CALIBRATIONS

An important obligation of any flight project is the production of a high quality, calibrated, Earth located (level-1) data set. Consequently, the production of a calibrated set of SeaWiFS radiances that have been verified through direct, or vicarious, calibration techniques was recommended by the original workshop participants.

One potentially useful technique follows the approach currently in use to verify the responsivity of the AVHRR Television and Infrared Observation Satellite (TIROS) satellite instruments. Twice a year, an aircraft instrument, which has been recently calibrated directly to laboratory-based NIST traceable standards, should be used to obtain simultaneous views of a particular ocean scene. The aircraft scene must be obtained from a high altitude aircraft, such as the NASA Earth Resources-2 (ER-2), and flown at an altitude above most of the terrestrial atmosphere. The existing data sets of the AVHRR-NASA Aircraft/Satellite Instrument Calibration (NASIC) Project demonstrate a capability to limit the uncorrected trend in the AVHRR data sets to under 2% over two years. This concept may allow an independent verification of the atmospheric radiative transfer models used to compute ocean biological quantities, when the aircraft data are used in conjunction with the surface truth campaign measurements of those same ocean biological quantities. The SeaWiFS absolute uncertainty requirements, however, are more stringent than those associated with the AVHRR, and a correspondingly more accurate airborne radiometer system (Sections 3.3 and 4.3) must be used (Section 2.3).

Chapter 6

Analytical Methods

INTRODUCTION

This chapter describes methods for processing, analyzing, and reporting SeaWiFS validation data sets acquired following the protocols of Chapter 5. Where a consensus from the community exists for a preferred method, it has been adopted and protocols are given accordingly, e.g., for phytoplankton pigments (Section 6.5). In other instances, different methods are in current use, and as yet, there is insufficient evidence to give protocols specifying a preferred approach, e.g., the different methods of K-analysis described in Section 6.1.4. Intercomparisons are in progress to evaluate this particular topic.

6.1 IN-WATER RADIOMETRY

Spectral surface irradiance, $E_s(\lambda)$; upwelling irradiance, $E_u(z,\lambda)$; downwelling irradiance, $E_d(z,\lambda)$; and upwelling radiance, $L_u(z,\lambda)$, measurements should all be recorded and archived at four levels.

a) level-0: raw instrument digital output;

b) level-1: instrument output in volts, or frequency (if appropriate), and depth;

c) level-2: calibrated irradiance and radiance, ancillary measurements in appropriate geophysical or biological units, and depth, with all variables corrected for dark or zero offsets;

d) level-3: Smoothed profiles of $K(z,\lambda)$ and associated $E_d(z,\lambda)$ or $L_u(z,\lambda)$ with irradiance or radiance normalized by measured surface irradiance; and

e) level-4: level-3 data normalized to clear-sky, a zenith sun at the mean Earth-sun distance, and spectrally adjusted to match the actual reference wavelengths and FWHM bandwidths.

The formats of these data sets will vary somewhat between individual instruments. It is anticipated that the SPO will promulgate suitable standard format specifications, or guidelines, to facilitate database management and interchanges of level-1, level-2, level-3, and level-4 data. These data files should each contain a header record identifying as a minimum:

1) date and time, i.e., GMT, of the station;

2) geographic location (latitude and longitude in decimal degrees to the nearest 0.001);

3) cloud cover and sky conditions;

4) identification of each variable, including units and wavelengths, for radiometric channels;

5) source of dark (zero-offset) data;

6) calibration date and file identification;

7) instrument identification;

8) method for determining K (level-3);

9) normalization algorithm (level-4);

10) Secchi depth;

11) depths of associated water samples, if any; and

12) depth offsets (to nearest cm) between the pressure transducer and all sensor probes, including L_u window, E_d and E_u collectors, and all ancillary probes on a package.

In addition to profile files, each data set should contain:

i) calibration files used to compute level-2 data;

ii) level-0 and level-1 dark files, and an average dark voltage file used for computing the corresponding level-2 files (in some cases a dark value may be extracted from the deep portion of a profile);

iii) files with data from comparisons with a portable irradiance and radiance reference standard made in the field and used to track the instrument's stability during a deployment; and

iv) anecdotal and environmental information about each profile, either in the header, or in an accompanying American Standard Code for Information Interchange (ASCII) text file.

In general, the data should be retained at full resolution as recorded, but with noise-contaminated records removed through level-2. If the data are binned prior to K-determination, as is sometimes done in the derivative method (Section 6.1.4), the binned representations should be recorded as a level-2a file, in addition to the full resolution level-2 file. Depth offsets between the sensor port (where depth is determined) and the sensor apertures [$E_d(\lambda)$ and $E_u(\lambda)$ collectors and $L_u(\lambda)$ window] must be

recorded as header information in level-2 data files, and applied to the data prior to K-analysis (see Section 6.1.4 below).

6.1.1 Instrument Calibration Analysis

Instrument data from pre- and post-deployment calibrations should be compared with:

1) each other;
2) the long-term history of an instrument's calibrations; and
3) the record of comparisons with a portable field irradiance and radiance standard, to be made frequently during a cruise.

Based on this analysis of the instrument's history, a calibration file will be generated and applied to transform the data from level-1 to level-2. This analysis, and the rationale for adopting a particular set of calibration coefficients, both for responsivity and wavelength, should be fully described in the documentation accompanying the data set, preferably in an ASCII file to be retained on line with each data set.

6.1.2 Raman Corrections

Marshall and Smith (1990), and the references cited therein, show transpectral Raman scattering contributes significantly to measured irradiance between 500–700 nm. At a particular wavelength, the Raman contribution is excited by ambient irradiance at a wavenumber shift of 3,400 cm^{-1}. For example, Raman scattering at a wavelength of 500 nm (20,000 cm^{-1}), is excited by light at wavelength 427 nm (23,400 cm^{-1}), and at 700 nm (14,286 cm^{-1}) by light at 565 nm (17,686 cm^{-1}). Marshall and Smith (1990) give a transverse Raman scattering cross section (at 90°) of 8.2×10^{-30} cm^{-2} $molecule^{-1}$ sr^{-1}, a value within the range of other published observations. By integration, they derive a total Raman scattering coefficient of:

$$b_r(488) \;=\; 2.6 \times 10^{-4}\,\mathrm{m}^{-1}. \qquad (23)$$

The wavelength dependence of the Raman scattering cross section is theoretically about the same as that for Rayleigh scattering

$$b_r(\lambda) \;\equiv\; b_r(488)\left(\frac{\lambda}{488}\right)^{-4}, \qquad (24)$$

although this has not yet been experimentally confirmed.

A method for applying Raman corrections to measured profiles of irradiance and radiance is suggested and applied to homogeneous clear-water profiles by Marshall and Smith (1990). Additional work is needed to develop a robust Raman scattering correction model for general application in more turbid and vertically stratified water masses. The relative magnitude, and thus importance, of the Raman signal at each wavelength in the upper three attenuation lengths should also be investigated more thoroughly than has been done to date.

6.1.3 Normalization by Surface Irradiance

The dominant errors in measured $K(z,\lambda)$ profiles result from changes in cloud cover. Cloud cover variability causes strong variations in incident surface irradiance, $E_s(\lambda,t)$, measured at time t, during the time required to complete a radiometric cast. In present usage, $E_s(\lambda,t)$ refers to incident spectral irradiance measured with a deck cell aboard a ship. Smith and Baker (1984 and 1986) discuss a method for propagating $E_s(\lambda)$ through the sea surface to estimate $E_d(0^-,\lambda)$, and they also present a model for adjusting $E_d(0^-,\lambda)$ to compensate for solar zenith angle.

An alternative, and conceptually better, scheme for estimating $E_d(0^-,\lambda)$ is to measure $E_d(z_r,\lambda)$ using a radiometer which has been floated away from the ship and held at a shallow depth, z_r, during a cast (Waters et al. 1990). In either case, the record of $E_s(\lambda,t)$ or $E_d(z_r,t)$ is recorded together with profiles of $E_d(z,\lambda,t)$, $E_u(z,\lambda)$, and $L_u(z,\lambda)$. Assuming that transmission of $E_s(\lambda,t)$ through the surface does not vary with time, then a simple and effective normalization of the profiles is obtained as

$$E'_d(z,\lambda) \;=\; \frac{E_d(z,\lambda)E_s(0^-,\lambda)}{E_s(\lambda,t)}, \qquad (25)$$

where $E_s(\lambda,t)$ is the deck cell irradiance measured at the time t when the radiometer was at depth z and $E_s(0^-,\lambda)$ is the measurement when the radiometer was at the surface.

Some previous investigators have used $E_s(\lambda,t)$ at a single reference wavelength, e.g., 550 nm, to normalize profiles, and have thus ignored the usually small spectral variations in incident irradiance. For SeaWiFS validation and algorithm development, however, the recommended protocol is to use multispectral $E_s(\lambda,t)$, or possibly near-surface $E_d(z_r,\lambda,t)$, to determine $E_d(z,\lambda,t)$ at each wavelength.

Because of spatial separation between the surface and underwater radiometers, cloud shadow variations are not measured, either identically or in phase, by the two instruments. The $E_s(\lambda,t)$ or $E_d(z_r,\lambda,t)$ profiles should, therefore, be smoothed to remove high frequency fluctuations while retaining variations with periods of 15 seconds or greater. The smoothed $E_s(0^-,\lambda)/E_s(\lambda,t)$ profiles should then be applied as a normalizing function to the irradiance and radiance profiles.

6.1.4 *K*-Analysis

Normalized and Raman corrected profiles of $E_d(z,\lambda)$, $E_u(z,\lambda)$, and $L_u(z,\lambda)$ (with z corrected for pressure transducer depth offset relative to each sensor) should be fit to the equations

$$E_d(z,\lambda) \;=\; E_d(0^-,\lambda)\,e^{-\int_0^z K_d(z',\lambda)dz'}, \qquad (26)$$

$$E_u(z,\lambda) \;=\; E_u(0^-,\lambda)\,e^{-\int_0^z K_u(z',\lambda)dz'}, \qquad (27)$$

and

$$L_u(z,\lambda) \;=\; L_u(0^-,\lambda)\, e^{-\int_0^z K_L(z',\lambda)dz'}, \qquad (28)$$

respectively. The vertical profiles of attenuation coefficients $K_d(z,\lambda)$, $K_u(z,\lambda)$, and $K_L(z,\lambda)$, together with the respective values of $E_d(0^-,\lambda)$, $E_u(0^-,\lambda)$, and $L_u(0^-,\lambda)$ at the surface, provide the needed specifications for the smoothed irradiance and radiance profiles.

If the natural logarithm of (26), (27), and (28) is taken, equations of the following form are obtained:

$$-\int_0^z K(z)dz \;=\; \ln\big(E(z)\big) \;-\; \ln\big(E(0^-)\big), \qquad (29)$$

so that

$$K(z) \;=\; -\left.\frac{d\,\ln\big(E(z)\big)}{dz}\right|_z. \qquad (30)$$

The traditional method of K-analysis, e.g., Smith and Baker (1984 and 1986), is to estimate $K(z)$ as the local slope of measured $\ln\big[E(z)\big]$ in an interval of a few meters centered at depth z_m, i.e., at depths near depth z_m,

$$\ln\big[E(z)\big] \;\cong\; \ln\big[\widehat{E}(z_m)\big] \;-\; (z-z_m)K(z_m). \qquad (31)$$

The unknowns $\ln\big[\widehat{E}(z_m)\big]$ and $K(z_m)$ are determined as the intercept and (negative) slope of a least-squares regression fit to measured $\ln\big[E(z)\big]$ data within the depth interval $z_m - \Delta z \le z < z_m + \Delta z$. The half-interval Δz is somewhat arbitrary. Smith and Baker (1984 and 1986) suggest a Δz of approximately 4 m, but for noisy profiles, a Δz as large as 10 m may be needed to smooth over incident irradiance fluctuations left as residuals by the deck cell normalization.

When this method is used, the shallowest possible values in the smoothed $\widehat{E}(z)$ and $K(z)$ profiles are at depth Δz m, and the deepest values are Δz m above the deepest measurements in the profile. If obvious ship shadow effects are present in the data, the shallowest valid smoothed data point will be at depth $z_s + \Delta z$, where z_s is the depth to which the data are regarded as contaminated and are excluded from the analysis.

It is often convenient, although not necessary, to preaverage radiometric data into, e.g., 1 m, bins prior to performing the least-squares analysis. If this is done, the data should be pre-filtered to remove any noise spikes and then averaged before it is log-transformed.

A corollary to having a large database is the need to facilitate its manipulation and analysis in order to make its application to various tasks feasible. In the proposed SeaWiFS effort, for example, radiometric measurements from many oceanographic stations will be examined. Each station will require one or more vertical profiles, from the surface to depths of up to 200 m, of downwelling irradiance, upwelling radiance, and upwelling irradiance, measured in at least 5–8 spectral bands. By using a multispectral radiometer (such as the MER class of instruments) during a profile, the data in all channels will be sampled contemporaneously and recorded digitally 2–10 times per meter. These are level-1 data and are stored in files for subsequent processing and analysis.

The level-2 through level-4 data give increasingly refined information in each successive processing level, which requires various amounts of intervention from the analyst. After appropriate editing to remove artifacts, such as the effects of ship shadow, vertical profiles of K are computed from the logarithmic decrement with depth of the radiometric profiles. Direct derivative method calculations of K profiles using computer techniques (see above) require the use of a depth interval so large, frequently 20 m, that information about the slope, and hence, about K near the top and bottom of the profile, is lost. Averaging over such a large interval causes the slopes in sharply defined layers, e.g., regions of high gradients, to be poorly represented. Attempts to reduce these effects by using a significantly smaller depth interval result in unacceptably noisy K profiles.

An improved approach, suggested by Petzold (1988), is to fit a series of analytic functions to the radiometric data using non-linear least-squares regression fitting techniques. The profiles are broken up into as many layers as required, and functions are fit to each layer, with the constraint that the functions and the derivatives of the functions be everywhere continuous and finite. It is found that the logarithm of the radiometric data versus depth can be fit by a series of hyperbolic tangents superimposed on straight lines using this technique. The data for a profile consisting of two layers can be matched by using the analytic expression together with the values of five parameters derived from the regression fitting procedure. In analyses of 2,100 profiles, the most complicated profiles encountered required 20 parameters—most required 5 or 10.

With the analytic form of the curve fitting the data, it is a simple matter to differentiate the function to determine the slope of the radiometric profile and obtain noise-free profiles of K. Using this technique, Petzold is able to store a very large database in a very compact form, storing only the parameters and the program for reconstructing the data. Additional analyses can be easily performed using the analytic representation of the data in lieu of the original large discrete data files.

The basic functional form of the expression used to fit the data is

$$Y \;=\; P_1 \;+\; P_2 B \;+\; P_3 \frac{A - \frac{1}{A}}{A + \frac{1}{A}}, \qquad (32)$$

where $B = P_4 - X$, $A = e^{B/P_5}$, P_1 through P_5 are coefficients to be determined in the analysis, X is the depth in meters, Y is the base 10 logarithm of the radiometric measurement, i.e., the downwelling irradiance (E_d), upwelling

irradiance (E_u) or upwelling radiance (L_u). The form of (32) is a hyperbolic tangent superimposed upon a straight line. It has a point of inflection at $X = P_4, Y = P_1$ and approaches the asymptote $Y = P_1 + P_2 B \pm P_3$ as X becomes larger or smaller than P_4.

The first derivative is

$$\frac{dY}{dX} = -P_2 - \frac{P_3}{P_5}\left(\frac{2}{A + \frac{1}{A}}\right)^2. \tag{33}$$

When $X = P_4$, $B = 0$, and $Y = P_1$, then

$$\frac{dY}{dX} = -P_2 - \frac{P_3}{P_5}. \tag{34}$$

It is also possible to define K as the slope of the plot of the natural logarithm of the measured radiometric variable against depth, or

$$K = 2.3026 \frac{dY}{dX}. \tag{35}$$

At the point of inflection ($X = P_4$ and $Y = P_1$),

$$K = 2.3026\left(P_2 + \frac{P_3}{P_5}\right). \tag{36}$$

In the limit $K \rightarrow 2.3026\, P_2$, and K will not exceed some finite value.

The method described above was applied to radiometric profile data from six cruises covering a wide variety of ocean regimes and latitudes from 24.0–77.4° N. Approximately 2,100 profiles were fitted, and typically, the standard deviation of the ratio between the function derived from the regression method and the original radiance and irradiance data was 6% or less. For a large fraction of the fitted profiles, the standard deviations were between 1–3%.

An alternative method of determining K-profiles was recently developed by Mueller (1991). Radiometric profiles are represented in terms of optical depth, τ, which from (26), (27), and (28) is

$$\begin{aligned}\tau(z,\lambda) &= \int_0^z K(z',\lambda)dz' \\ &= \ln\left[\frac{E(0^-,\lambda)}{E(z,\lambda)}\right].\end{aligned} \tag{37}$$

The K-profile is represented analytically by Hermitian cubic polynomials, $\gamma_{ij}(\xi)$, over finite depth elements. The argument ξ is a local coordinate such that $\xi = 0$ at the center of a finite depth element, $\xi = -1$ at the shallow end point (node) of the element and $\xi = 1$ at the deep node. [Hermitian cubic polynomials are defined in any text on finite element modeling, e.g., Pinder and Gray (1977).]

At depth z, $K(z,\lambda)$ is expressed as

$$\begin{aligned}K(z,\lambda) &= \overline{K}_0(\lambda)\gamma_{01}(\xi) + \partial_z\overline{K}_0(\lambda)\gamma_{11}(\xi) \\ &\quad + \overline{K}_1(\lambda)\gamma_{02}(\xi) + \partial_z\overline{K}_1(\lambda)\gamma_{12}(\xi),\end{aligned} \tag{38}$$

where $\overline{K}_0$ and $\overline{K}_1$ are values of K, and $\partial_z\overline{K}_0$ and $\partial_z\overline{K}_1$ are its vertical derivatives at the two nodes of the depth element containing z. With this representation of $K(z,\lambda)$, it is possible to write (37) for each measured depth z_m as the weighted sum

$$\tau(z_m,\lambda) = \sum_{n=0}^{N} h_{m,n}\overline{K}_n + h_{m,n+N}\partial_z\overline{K}_n \tag{39}$$

for the $n = 0, 1, \ldots, N$ nodes dividing the water column into N depth elements. The coefficients h_{ij} are obtained as analytic integrals over the Hermitian polynominals γ_{ij} for the finite elements above and including depth z; $h_{ij} = 0$ for elements below the one containing z. Since such an equation may be written for every measured optical depth, the profile may be represented in matrix form as

$$\vec{\tau} = \mathbb{H}\,\vec{\overline{K}}, \tag{40}$$

where $\vec{\tau}$ is the vector of measured optical depths, $\mathbb{H}$ is the matrix of coefficients h_{ij}, and $\vec{\overline{K}}$ is the vector of $\overline{K}_n$ and $\partial_z\overline{K}_n$ at the N nodes. The least-squares solution for the unknown vector $\vec{\overline{K}}$ is obtained as

$$\vec{\overline{K}} = \left[\mathbb{H}^T\mathbb{H}\right]^{-1}\mathbb{H}^T\vec{\tau}, \tag{41}$$

which with (38) yields the complete profile $K(z)$.

The surface boundary condition assumed by Mueller (1991) is that $K(z)$ is constant between the sea surface (node 0) and the first subsurface node (node 1). If obvious or suspected ship shadow effects are present in the upper profile, the depth of node 1 is set immediately below the affected area and the data in that top element are excluded from the fit; the solution to (41) at nodes 0 and 1 is, in this case, determined entirely by the data from depths below node 1.

The solution at the deepest node is not constrained and depends only on the observations in the depth element immediately above it. The one-sided solution to (41) is often unstable at this node. If two nodes are placed close together at the bottom of the cast, then the unstable solution is confined to only the bottom node, which may be discarded after (41) is solved.

In order to solve (41), the surface values of $E_d(0^-,\lambda)$, $E_u(0^-,\lambda)$, and $L_u(0^-,\lambda)$ must be independently determined or specified. At present, this is done iteratively by requiring the solution to closely approximate the mean value of measurements in the top 1–2 m of the profile. Data from this near-surface layer are usually not significantly affected by ship shadow, but they may be severely affected

by irradiance fluctuations associated with light focusing by surface waves. Additional research is needed to develop a more objective method of determining these surface values.

In the present implementation (Mueller 1991), placement of nodes is largely subjective, even when guided by structure in accompanying $c(660)$ and chlorophyll fluorescence profiles. Qualitatively, the integral solutions mimic the structure in the $c(660)$ and fluorescence profiles more faithfully than do the derivative solutions; they also do a better job of filtering irregularities that are apparently associated with large fluctuations in deck cell irradiance. Quantitative evaluation of sensitivity to exact node placement is in progress. Development of objective criteria for node placement will require further research.

6.1.5 Finite Bandwidth Correction

Siegel et al. (1986) and Marshall and Smith (1990) discuss the effects of finite spectral FWHM bandwidth, and the normalized response function, on determination of the attenuation coefficient, $K(\lambda)$, for a vertically homogeneous water column. Given a channel's nominal wavelength, λ', and normalized response function, $h(\lambda)$, the apparent attenuation coefficient measured in a homogeneous water column is approximately

$$K_s(z,\lambda') = \frac{\int_0^\infty K(\lambda)h(\lambda)e^{-K(\lambda)z}d\lambda}{\int_0^\infty h(\lambda)e^{-K(\lambda)z}d\lambda}. \qquad (42)$$

Marshall and Smith (1990) applied a correction for this effect to clear-water profiles of $E_d(z,589)$. In general, correction of $K_s(z,\lambda')$ for finite bandwidth effects associated with K for pure water is straightforward. Additional research will be needed to model, from the spectral irradiance data itself, additional bandwidth effects associated with attenuation by phytoplankton and other particles, and to correct $K_s(z,\lambda)$ accordingly.

6.1.6 Extrapolation to the Sea Surface

Because of surface waves, it is rarely possible to measure E_d, E_u, or L_u at depths that closely approximate $z \cong 0^-$. The shallowest reliable readings typically occur at depths ranging from 0.5–2 m. The data from this zone usually exhibit strong fluctuations associated with surface waves, and thus require some form of smoothing or averaging. It is almost always necessary to apply some means of extrapolating the data upward to the sea surface. Whatever method is used should reconcile extrapolated $E_d(0^-,\lambda)$ with deck measurements of $E_s(\lambda)$.

If $K(z)$ profiles are determined using the derivative method, the shallowest smoothed estimates will occur at depth $z_0 = \Delta z$, if there are no ship shadow effects. The usual procedure is to extrapolate values to $z = 0^-$ as

$$E_d(0^-,\lambda) = E_d(z_0,\lambda)e^{K_d(z_0,\lambda)z_0}, \qquad (43)$$

$$E_u(0^-,\lambda) = E_u(z_0,\lambda)e^{K_u(z_0,\lambda)z_0}, \qquad (44)$$

and

$$L_u(0^-,\lambda) = L_u(z_0,\lambda)e^{K_L(z_0,\lambda)z_0}. \qquad (45)$$

If ship shadow is present, z_0 may be 20 m or more, and the extrapolation becomes somewhat tenuous.

If $K(z)$ profiles are determined by means of the integral method, then $E_d(0^-,\lambda)$, $E_u(0^-,\lambda)$, and $L_u(0^-,\lambda)$ are automatically determined as part of the fitting procedure. The surface values thus obtained are not necessarily superior to those obtained by extrapolating the derivative method solutions, but they do have the advantage of representing an internally consistent fit to the entire profile beneath the surface boundary layer.

By either method, extrapolation of measured $E_d(z,\lambda)$, $E_u(z,\lambda)$, and $L_u(z,\lambda)$ to $z = 0^-$ becomes very difficult at $\lambda \geq 670$ nm. At these wavelengths, the rapid decrease in daylight over an extremely shallow first attenuation length may compete with an increase in flux with depth due to chlorophyll fluorescence. Additional research is needed to address measurement and estimation of $E_d(0^-,\lambda)$ and $L_u(0^-,\lambda)$ at these wavelengths, especially in chlorophyll-rich Case-2 waters.

6.1.7 Instrument Self-Shading Corrections

A provisional protocol is given here for radiometer self-shading corrections to $L_u(0^-,\lambda)$ and $E_u(0^-,\lambda)$ measurements (see also Section 5.1.6). The protocol is based on the model of Gordon and Ding (1992) and limited experimental confirmation by Zibordi and Ferrari (1994). Although additional research is necessary to extend and verify these correction algorithms, the results published to date show clearly that even a provisional correction will significantly improve $L_u(0^-,\lambda)$ and $E_u(0^-,\lambda)$ estimated from underwater measurements.

It is first necessary to estimate the spectral absorption coefficient $a(\lambda)$, preferably using measurements following the protocols of Sections 5.2.4, 5.4.2, 6.8.1, and 6.8.2. It is also possible to estimate $a(\lambda)$ using other approximations suggested by Gordon and Ding (1992), based either on measurements of phytoplankton pigment concentrations or of irradiance attenuation coefficients.

It will also be necessary to measure, or estimate, the direct solar, $E_{\rm sun}(\lambda)$, and skylight, $E_{\rm sky}(\lambda)$, components of incident spectral irradiance, $E_s(\lambda)$, where $E_s(\lambda) = E_{\rm sun}(\lambda) + E_{\rm sky}(\lambda)$. Zibordi and Ferrari (1994) describe one method of estimating the ratio $E_{\rm sky}(\lambda)/E_{\rm sun}(\lambda)$, and Gordon and Ding (1992) suggest other alternatives.

Following Zibordi and Ferrari (1994), the coefficients, κ', given in Table 2 of Gordon and Ding (1992), are fit to linear regression models as functions of the solar zenith angle θ_0 in the range $30° \leq \theta_0 \leq 70°$. The results given for $L_u(0^-,\lambda)$, with sun only, for a point sensor may be computed as

$$\kappa'_{\rm sun,0}\tan\theta_{0w} = 2.07 + 5.6\times10^{-3}\theta_0, \qquad (46)$$

and for a finite sensor occupying the full diameter of the instrument,

$$\kappa'_{\mathrm{sun},l} \tan\theta_{0w} = 1.59 + 6.3 \times 10^{-3}\theta_0, \quad (47)$$

where θ_0 and θ_{0w} are the solar zenith angles in air and water, respectively, measured in degrees. In practice, the diameter of the radiance sensor aperture is usually a small fraction of the instrument diameter. In the results reported by Zibordi and Ferrari (1994), the point sensor model always overestimated ϵ, and use of the finite sensor model (47) will always yield a lower estimate of ϵ. Pending new insights from future theoretical and experimental work, it is suggested to estimate

$$\kappa'_{\mathrm{sun}} \tan\theta_{0w} = (1-f)\kappa'_{\mathrm{sun},0} \tan\theta_0 + f\kappa'_{\mathrm{sun},l} \tan\theta_0, \quad (48)$$

where f is the ratio of sensor-to-instrument diameters. The coefficient, κ'_{sky}, for the self-shading effect on $L_u(0^-,\lambda)$ caused by incident diffuse skylight is similarly estimated as

$$\kappa'_{\mathrm{sky}} = 4.61 - 0.87f, \quad (49)$$

where the coefficients are derived from values given in Table 3 of Gordon and Ding (1992). Self-shading errors $\epsilon_{\mathrm{sun}}(\lambda)$ and $\epsilon_{\mathrm{sky}}(\lambda)$ for $E_{\mathrm{sun}}(\lambda)$ and $E_{\mathrm{sky}}(\lambda)$ components, respectively, are then computed as

$$\epsilon_{\mathrm{sun}}(\lambda) = 1 - e^{\kappa'_{\mathrm{sun}} a(\lambda) r}, \quad (50)$$

and

$$\epsilon_{\mathrm{sky}}(\lambda) = 1 - e^{\kappa'_{\mathrm{sky}} a(\lambda) r}, \quad (51)$$

where r is the instrument radius in meters, and the absorption coefficient $a(\lambda)$ is in units of m^{-1}.

The self-shading error in $L_u(0^-,\lambda)$ is then calculated as

$$\epsilon(\lambda) = \frac{\epsilon_{\mathrm{sun}}(\lambda) + \epsilon_{\mathrm{sky}}(\lambda)h}{1+h}, \quad (52)$$

where

$$h = \frac{E_{\mathrm{sky}}(\lambda)}{E_{\mathrm{sun}}(\lambda)}. \quad (53)$$

Finally, the corrected radiance $L_u(0^-,\lambda)$ is estimated as

$$L_u(0^-,\lambda) = \frac{L'_u(0^-,\lambda)}{1-\epsilon(\lambda)}, \quad (54)$$

where $L'_u(0^-,\lambda)$ is determined by analysis of the measured upwelled radiance profiles (Section 6.1.6).

Similarly, for $E_u(0^-,\lambda)$, the values given in Tables 2 and 3 of Gordon and Ding (1992) determine that for a point irradiance sensor,

$$\kappa'_{\mathrm{sun},0} = 3.41 - 1.55 \times 10^{-2}\theta_0. \quad (55)$$

For an irradiance collector with a diameter equal to that of the instrument,

$$\kappa'_{\mathrm{sun},l} = 2.76 - 1.21 \times 10^{-2}\theta_0, \quad (56)$$

so that

$$\kappa'_{\mathrm{sun}} = (1-f)\kappa'_{\mathrm{sun},0} + f\kappa'_{\mathrm{sun},l}, \quad (57)$$

where f is the ratio of the diameter of the irradiance collector to that of the instrument.

For the sky component, κ'_{sky} is defined as

$$\kappa'_{\mathrm{sky}} = 2.70 - 0.48f. \quad (58)$$

Values of κ'_{sun} and κ'_{sky} from (57) and (58) are then substituted in equations (50) and (51) to obtain $\epsilon_{\mathrm{sun}}(\lambda)$ and $\epsilon_{\mathrm{sky}}(\lambda)$, which are then used in (52) to solve for $\epsilon(\lambda)$. Finally, corrected upwelled spectral irradiance $E_u(0^-,\lambda)$ is estimated as

$$E_u(0^-,\lambda) = \frac{E'_u(0^-,\lambda)}{1-\epsilon(\lambda)}, \quad (59)$$

where $E'_u(0^-,\lambda)$ is determined from the upwelled spectral irradiance profile (Section 6.1.6).

It is recommended that this correction algorithm be applied to all $L_u(0^-,\lambda)$ and $E_u(0^-,\lambda)$ measurements used for SeaWiFS validation and algorithm development. Recognizing the provisional nature of the correction, however, the uncorrected measured values must also be reported. Moreover, the method and data used to estimate $a(\lambda)$, $E_{\mathrm{sun}}(\lambda)$, and $E_{\mathrm{sky}}(\lambda)$ must be documented and reported with all data sets corrected using this protocol.

6.1.8 Spectral Adjustments

New methods must be developed to reconcile in-water measurements $L_u(0^-,\lambda_0+\Delta\lambda_1)$ integrated over a sensor response function $h_1(\lambda)$ with SeaWiFS measurements of $L_t(\lambda_0+\Delta\lambda_2)$ integrated over a wider sensor response function $h_2(\lambda)$. The challenge is to account for differing radiometric sensitivities to fine-scale Fraunhofer structure in extraterrestrial solar spectral flux, $\overline{F}_0(\lambda)$, as modified by atmospheric spectral transmittance, $t(\lambda)$, and oceanic spectral reflectance, $R_L(\lambda)$. By assuming $\overline{F}_0(\lambda)$ is exactly known, and that over the wavelength range defined by $h_2(\lambda)$ and $h_1(\lambda)$, both $t(\lambda)$ and $R_L(\lambda)$ vary slowly with wavelength, it should be possible to adjust the $L_W(\lambda_0+\Delta\lambda_1)$ derived directly from the in-water instrument, to estimate the water-leaving radiance $L_W(\lambda_0+\Delta\lambda_2)$. This will be transmitted through the atmosphere and contribute to $L_t(\lambda_0+\Delta\lambda_2)$ measured by SeaWiFS. At the very least, this type of correction should be practical for a given atmosphere. Prelaunch radiative transfer model sensitivity studies and experimental verifications should be done to determine the magnitudes and uncertainties of such corrections for the various SeaWiFS bands.

6.1.9 Normalized Water-Leaving Radiance

To standardize the in-water SeaWiFS algorithms, it is necessary to normalize measured $L_W(\lambda)$ to those values

that would be measured were the sun at the zenith, at the mean Earth-sun distance, and with the effects of the atmosphere removed. Following Gordon (1988), normalized water-leaving radiance as measured by the satellite sensor may be defined as

$$L_{WN}(\lambda) = \frac{L_W}{t(\lambda,\theta_0)(1-\rho(\theta_0))\cos\theta_0}\left(\frac{r}{\bar{R}}\right)^2, \quad (60)$$

where θ_0 is the solar zenith angle, $\rho(\theta_0)$ is the air-water Fresnel reflectance for incident angle θ_0, $t(\lambda,\theta_0)$ is the atmospheric transmittance and $\bar{R}$ is the mean Earth-sun distance. The Earth-sun distance on the day of the measurement, r, is given by

$$r = \frac{\bar{R}}{1 + 0.0167\cos\left(\frac{D-3}{365}\right)}, \quad (61)$$

where D is the sequential day of the year.

The $(r/\bar{R})^2$ adjustment was not employed by Gordon and Clark (1981) or Gordon (1988) because it cancels in ratio algorithms, and the measurements they used were all taken within the span of a few months, so this source of variation was very small in their data. The range of variation in $(r/\bar{R})^2$ is approximately 6% over a full annual cycle. This adjustment should be made, nevertheless, for it becomes important in algorithms predicting absolute values of $L_W(\lambda)$, as in the clear-water radiance model of Gordon and Clark (1981), and in algorithms for either estimating or detecting anomalously high water reflectances in, for example, a coccolithophore bloom.

To obtain $L_W(\lambda)$ it is necessary to propagate $L_u(\lambda)$ upward through the sea surface as

$$L_W(0^+,\lambda) = L_u(0^-,\lambda)\frac{1-\rho(\lambda,\theta)}{n_w^2(\lambda)}, \quad (62)$$

where $\rho(\lambda,\theta$ and $n_w(\lambda)$ are the Fresnel reflectance and refractive index of sea water, respectively. Normalized water leaving radiance is then computed as

$$L_{WN}(\lambda) = L_W(\lambda)\frac{\overline{F}_0(\lambda)}{E_s(\lambda)}, \quad (63)$$

where $\overline{F}_0(\lambda)$ denotes the mean extraterrestrial solar irradiance (Neckel and Labs 1984).

6.2 ABOVE-WATER RADIANCE

When upwelled radiance above the water surface is measured from a ship (Section 5.1.8), the measured radiance, $L(\lambda,\theta,\phi)$, must be corrected for the reflected sky radiance, $L_{\rm sky}(\lambda,\theta,\phi)$. If $L_{\rm sky}(\lambda,\theta,\phi+\pi)$ is measured by directly viewing the sky, water-leaving radiance should be calculated as

$$L_W(\lambda) = L(\lambda,\theta,\phi) + \rho(\lambda,\theta)L_{\rm sky}(\lambda,\theta,\phi+\pi), \quad (64)$$

where $\rho(\lambda,\theta)$ is Fresnel reflectance of the water surface. If $L'_{\rm sky}(\lambda,\theta,\phi+\pi)$ is measured by viewing a horizontally oriented mirror of reflectance $\rho_m(\theta)$, then (64) must be modified to

$$L_W(\lambda) = L(\lambda,\theta,\phi) + \frac{\rho(\lambda,\theta)}{\rho_m(\lambda,\theta)}L'_{\rm sky}(\lambda,\theta,\phi+\pi). \quad (65)$$

The remote sensing reflectance, $R_L(0^+,\lambda)$, may be calculated from $L_W(\lambda)$ as

$$R_L(0^+,\lambda) = \frac{L_W(\lambda)}{E_s(\lambda)}, \quad (66)$$

where $E_s(\lambda)$ is incident spectral irradiance, preferably measured concurrently with a calibrated irradiance meter, or estimated with greater uncertainty by viewing a horizontally oriented gray reflectance plaque (Section 5.1.8). Normalized water-leaving radiance is similarly calculated using (63).

An alternative approach may be used to calculate reflectance from an uncalibrated radiometer as

$$R'_L(0^+,\lambda) = \frac{S_w(\lambda) - \rho(\lambda,\theta)S_{\rm sky}(\lambda)}{\pi S_G(\lambda)\rho_g(\lambda,\theta)}, \quad (67)$$

where $S_w(\lambda)$, $S_{\rm sky}(\lambda)$, and $S_G(\lambda)$ are the radiometer signals measured viewing the water, sky, and a reflectance plaque of approximately 10% reflectance (e.g., Spectralon), respectively; $\rho(\theta)$ is the Fresnel reflectance of the surface; and $\rho_g(\lambda)$ is the reflectance of the reference plaque. To remove residual surface reflectance due to wave facets, it is assumed that the residual signal at 750 nm is entirely due to surface reflection, so that the corrected reflectance is calculated as

$$R_L(\lambda) = R'_L(\lambda) - R'_L(0^+,750). \quad (68)$$

When using this technique, it is critical to measure all radiances well clear of the ship's superstructure and to hold the reference plaque horizontally.

It is more difficult to make verifiable corrections to $L(\lambda,\theta,\phi)$ when measured from low flying aircraft (Section 5.1.7). In this case, atmospheric transmittance and path radiance are not entirely negligible, and water-leaving radiance must be calculated as

$$L_W(\lambda,\theta,\phi) = t^{-1}\left[L(\lambda,\theta,\phi) - L^*(\lambda,\theta,\phi)\right] - \rho(\lambda,\theta)L_{\rm sky}(\lambda,\theta,\phi+\pi), \quad (69)$$

where $t(\lambda,\theta)$ is the atmospheric transmittance from the surface to the aircraft altitude, $L^*(\lambda,\theta,\phi)$ is the atmospheric path radiance at flight altitude, and $L_{\rm sky}(\lambda,\theta,\phi+\pi)$ is the sky radiance incident at the surface. At altitudes up to 300 m, $t(\lambda,\theta)$ is close to 1, and may usually be estimated with relatively low uncertainty. Unfortunately, there is no straightforward way to measure $L_{\rm sky}(\lambda,\theta,\phi+$

π) or $L^*(\lambda, \theta, \phi)$ from an aircraft. These variables must, therefore, normally be estimated using an atmospheric radiative transfer model. Verification of model estimates of $L_{\rm sky}(\lambda, \theta, \phi + \pi)$ and $L^*(\lambda, \theta, \phi)$ is difficult under ideal cloud-free sky conditions, and is wholly impractical under variable cloud cover.

Incident irradiance $E_d(z, \lambda)$ measured at flight altitude must also be propagated to the surface to compute $R_L(\lambda)$ and $L_{WN}(\lambda)$ from airborne measurements, i.e.,

$$R_L(\lambda) = \frac{L_W(\lambda)}{E_d(z, \lambda) t_d(z, \lambda)}, \quad (70)$$

and

$$L_{WN}(\lambda) = L_{WN}(\lambda) \frac{\overline{F}_0(\lambda)}{E_d(z, \lambda) t_d(z, \lambda)}, \quad (71)$$

where $t_d(z, \lambda)$ is the downward spectral irradiance transmittance from flight altitude z to the surface.

The authors defer any recommendation for specific protocols for applying atmospheric radiative transfer models to estimate $L_W(\lambda)$, $R_L(\lambda)$, and $L_{WN}(\lambda)$ with (69)–(71), respectively. It is incumbent on each investigator to report in detail the methods used to analyze (through measurements, models, or both) the necessary correction terms, and to include a detailed error analysis of the results which are obtained. Aircraft radiometric data sets that do not include this information should not be used for SeaWiFS algorithm development or validation.

6.3 MOORED RADIOMETRY

Methods are not highly developed for analyzing data from moored radiometers to calculate $L_{WN}(\lambda)$. The principles of this analysis are well understood, but the community has had little experience with moored measurements of $L_u(z, \lambda)$, determination of $K_L(z, \lambda)$, and extrapolation to $L_u(0^-, \lambda)$. The moored optical system being developed by D. Clark of the NOAA National Environmental Satellite Data Information Service (NESDIS) for SeaWiFS and MODIS is the first system to be specifically engineered to address this problem.

Smith et al. (1991) successfully acquired a nine-month time series of spectral $E_d(z, \lambda, t)$ and $L_u(z, \lambda, t)$ at three depths (32, 52, and 72 m). They placed an additional above-water radiometer on a surface float, but this unit failed and provided no data. Smith et al. (1991) analyzed the $K_d(441)$ time series using a broad-band irradiance measurement to estimate $E_d(0^-, 441)$ for the 0–32 m depth interval, and using measured $E_d(z, 441)$ over the 32–52 and 52–72 m depth intervals. They did not, however, estimate $K_L(\lambda)$ for $L_u(\lambda)$. They also developed and evaluated algorithms for estimating phytoplankton pigment concentrations from spectral reflectance and from naturally stimulated (by incident daylight) chlorophyll fluorescence at $L_u(683)$. Smith et al. (1991) demonstrated that continuous time series of $K_d(\lambda, t)$ and pigment concentration may be measured using this type of moored system.

Smith et al. (1991) and Dickey et al. (1991) together illustrate methods that can be used to specify protocols for oceanographic analyses of bio-optical time series measured using moored optical systems. Such protocols would be very valuable for planning and executing oceanographic studies using data from moored systems together with SeaWiFS time series data; they are not, however, directly relevant to SeaWiFS validation. It is anticipated that optical protocols for US and International JGOFS will be published by working groups convened by these programs.

6.4 AEROSOL OPTICAL DEPTH

If multiple measurements of the solar beam are obtained during stable atmospheric conditions, then the *Langley method* can be used to obtain the atmospheric transmittance. This method consists of plotting the natural logarithm of the voltage from the sun photometer versus the inverse of the cosine of the solar zenith angle. The slope of this straight line is the total optical depth of one atmosphere. If only a single measurement is obtained, the instrument calibration is applied to determine radiance, which can be combined with the extraterrestrial solar irradiance to calculate the atmospheric optical depth.

To obtain the aerosol optical depth, total optical depth must be used with computed optical depths due to molecular scattering (Rayleigh optical depth), and absorption by ozone and other important gases (NO_2 for some spectral bands). By subtracting the optical depths of these well-mixed gases from the total measurements, the aerosol optical depth can be determined.

6.5 SKY RADIANCE

Sky radiance distributions, $L_{\rm sky}$, measured with a calibrated radiance distribution camera, perhaps augmented by sun photometry or narrow FOV $L_{\rm sky}$ discrete measurements in the zenith-sun plane, will be used to estimate the aerosol phase function (Voss and Zibordi 1989). Development of detailed protocols and methods of analysis, including new inverse modeling techniques, for estimating aerosol optical depths and phase functions will require new research. The spectral mean cosine $\overline{\mu}_d(0^+, \lambda)$ for downwelling radiance at the sea surface will be calculated directly from radiance distribution camera data, when available. Under cloud-free conditions, $\overline{\mu}_d(0^+, \lambda)$ can also be estimated by measuring $E_{\rm sky}(\lambda) + E_{\rm sun}(\lambda)$ with an irradiance deck cell. The algorithm for these computations is given by Gordon (1989b).

When a spectral radiance distribution camera system is not available and skies are not cloud free, it may be possible to estimate $\overline{\mu}_d(0^+, \lambda)$ from some combination of deck cell unshaded $E_{\rm sky}(\lambda) + E_{\rm sun}(\lambda)$ and shaded $E_{\rm sky}(\lambda)$ measurements, all-sky photographs, and measurements of $L_{\rm sky}(\lambda, \theta_i, \phi_i)$ made at discrete angles with a hand-held radiometer. Additional research will be required to develop and test viable protocols for $\overline{\mu}_d(0^+, \lambda)$ estimation from these types of measurements.

6.6 PHYTOPLANKTON PIGMENTS

This section specifies methods of analysis for determining pigment concentrations by HPLC and fluorometry (following acetone extraction) from filtered water samples obtained at discrete depths, and for using *in situ* profiles of chlorophyll *a* fluorescence to interpolate pigment concentration over depth.

6.6.1 HPLC Pigment Concentration

The JGOFS protocols and standards for HPLC pigment concentration analysis (JGOFS 1991) will be the primary method of determining pigment concentrations for all SeaWiFS algorithm development and validation activities.

6.6.2 Fluorometric Determination

Protocols for fluorometric determination of the concentrations of chlorophyll and phaeopigments were developed initially by Yentsch and Menzel (1963) and Holm-Hansen et al. (1965), and are described in detail by Strickland and Parsons (1972). Although these measurements have been shown to contain errors as compared to HPLC determinations, e.g., Trees et al. (1985), the CZCS phytoplankton pigment concentration algorithms were based on them entirely. The SeaWiFS protocols for this analysis will be those given in Strickland and Parsons (1972) as updated by Smith et al. (1981).

6.6.3 *In Situ* Chlorophyll *a* Fluorescence

In situ fluorometers produce nearly continuous profiles of artificially stimulated chlorophyll *a* fluorescence. Level-1 fluorometer data (in volts) should be converted to level-2 simply by subtracting an offset, determined by shading the instrument on deck. For qualitative guidance in K-profile analysis, level-2 (or even level-1) fluorometer profiles are adequate.

To produce vertical profiles of pigment concentration, HPLC-derived pigment concentrations from water samples taken at discrete depths should be interpolated, with the aid of *in situ* fluorescence profiles, for SeaWiFS bio-optical algorithm development. These *fluorescence interpolated* profiles should then be used with $K_d(z,\lambda)$ profiles to compute optically weighted pigment concentration over the top attenuation length (Gordon and Clark 1980).

6.7 BEAM ATTENUATION

Raw beam transmissometer voltage profiles, $\widetilde{V}(z)$, are first corrected for any range-dependent bias of the A/D data acquisition system (Section 5.2.1). The corrected voltages, $\widehat{V}(z)$, are then further adjusted for instrument drift (occurring subsequent to the factory calibration) with the equation

$$V(z) \;=\; \Big(\widehat{V}(z) - V_{\text{dark}}\Big)\frac{V'_{\text{air}}}{V_{\text{air}}}, \qquad (72)$$

where V_{dark} is the instrument's current dark response with the light path blocked, and V'_{air} and V_{air} are, respectively, the current air calibration voltage (Section 5.2.1) and the air calibration voltage recorded when the instrument was calibrated at the factory. $V(z)$ is then converted to transmittance, $T(z,\lambda)$, over the transmissometer's path length, r, following the manufacturer's instructions for the particular instrument.

The beam attenuation coefficient $c(z,\lambda)$ is then computed as

$$c(z,\lambda) \;=\; -\frac{1}{r}\ln\big(T(z,\lambda)\big), \qquad (73)$$

which has units of m^{-1}. The apparent values of $c(z,\lambda)$ should be further corrected, again following the manufacturer's instructions, for the finite acceptance angle of the instrument's receiver; this is usually a small, but significant, correction. Finally, the beam attenuation coefficient due to particles is computed as

$$c_p(z,\lambda) \;=\; c(z,\lambda) \;-\; c_w(\lambda), \qquad (74)$$

where $c_w(\lambda)$ is the beam attenuation coefficient, i.e., the sum of absorption, $a_w(\lambda)$, and scattering, $b_w(\lambda)$, for pure water. Smith and Baker (1981) tabulate $a_w(\lambda)$ and $b_w(\lambda)$ over the spectral range of interest here.

6.8 SPECTRAL ABSORPTION

Protocols are given above in Section 5.2.4 for measuring absorption profiles *in situ* using reflective tube meters, and in Section 5.4.2 for laboratory spectrophotometric analyses of water samples captured at discrete depths.

Data from a reflective tube absorption and beam attenuation meter may be analyzed to obtain vertical profiles of $a(z,\lambda)$, $a_g(z,\lambda)$, and $c(z,\lambda)$, and by difference $b(z,\lambda) = c(z,\lambda) - a(z,\lambda)$ and $a_p(z,\lambda) = a(z,\lambda) - a_g(\lambda,t)$, using the protocols of Section 6.8.1. Optical density spectra for filtrate and filtered water samples (Section 5.4.2) may be analyzed to obtain independent measures of $a_g(z,\lambda)$, $a_p(z,\lambda)$, and $a_t(\lambda,t)$, and by difference $a_f(z,\lambda) = a_p(z,\lambda) - a_t(z,\lambda)$, using the protocols of Section 6.8.2. Methods for merging and comparing the two independent types of absorption measurements, and for interpreting the results in terms of remote sensing reflectance, are the subject of currently active research by several investigators. The next revision to this document may be expected to contain extensive modifications and extensions of these protocols.

6.8.1 Reflective Tube Measurements

At the time of this writing, there is only one commercially available reflective tube absorption and beam attenuation meter, the AC-9, manufactured by Western Environmental Technology, Inc., of Philomath, Oregon. The following data analysis protocol is, therefore, based on the characteristics of that instrument (Zaneveld and Moore pers. comm.).

The AC-9 output in each $a(\lambda)$ or $c(\lambda)$ channel consists of the digital responses of a reference detector and a water transmission detector, $C_r(\lambda)$ and $C_t(\lambda)$. During the instrument's factory calibration using optically pure water (Sections 4.4 and 5.2.4), the responses $C'(\lambda)$ and $C'_r(\lambda)$ are recorded and entered on the instrument's calibration sheet, along with the instrument temperature T' at which the calibration was performed. Calibration factors for each channel are then determined as

$$A(\lambda_a) = \frac{C'_r(\lambda_a)}{C'_t(\lambda_a)} e^{-a_w(\lambda_a)x}, \tag{75}$$

for absorption at wavelength λ_a, and

$$A(\lambda_c) = \frac{C'_r(\lambda_c)}{C'_t(\lambda_c)} e^{-c_w(\lambda_c)x}, \tag{76}$$

for beam attenuation at wavelength λ_c, where x is the optical pathlength in meters, and $a_w(\lambda_a)$ and $c_w(\lambda_c)$ are the absorption and beam attenuation coefficients of optically pure reference water, respectively (Smith and Baker 1981). The instrument's factory calibration also includes determination of a temperature coefficient $B_t(\lambda_n)$ for each channel.

In the subsequent discussion in this section, the subscript i designates initial values of the absorption beam attenuation coefficients derived directly from measurements. The subscript e denotes the corrected values of the same coefficients due to (extra) substances other than water.

When data are recorded in the field, apparent absorption coefficients $a_i(\lambda_a)$ due to substances other than pure water are calculated as

$$\begin{aligned} a_i(\lambda_a, T) = & -\ln\left[\frac{C_t(\lambda_a, T)}{C_r(\lambda_a, T)} T A(\lambda_a)\right] \\ & + (T' - T) B_t(\lambda_a) \\ & + \left[a_{\text{air}}(\lambda_a) - a'_{\text{air}}(\lambda_0)\right], \end{aligned} \tag{77}$$

where T' and T denote the instrument temperature, and $a'_{\text{air}}(\lambda_0)$ and $a_{\text{air}}(\lambda_0)$ are air calibration values at the times of the instrument factory calibration and field data recording, respectively (Section 5.2.4). A similar equation is applied to obtain apparent beam attenuation coefficients $c_i(\lambda_c)$ for substances other than water at each wavelength.

Apparent absorption coefficients $a_i(\lambda, T)$ must be corrected for the fraction of scattering that is undetected by the reflective tube and detector assembly (Section 5.2.4). An initial estimate of particle scattering at each wavelength $b_i(\lambda)$ is obtained as

$$b_i(\lambda) = c_i(\lambda) - a_i(\lambda, T), \tag{78}$$

recalling that attenuation by pure water already has been removed from $c_i(\lambda)$ and $a_i(\lambda, T)$ using the instrument's calibration coefficients. It is assumed that:

1) the uncertainty in $c_i(\lambda)$ due to forward scattered light, which is viewed by the detector (Section 6.7), is a wavelength-independent fraction k_c of total particle scattering $b_p(\lambda)$;
2) the fraction k of $b_p(\lambda)$ included in $a_i(\lambda)$ is also independent of wavelength; and
3) at a near-IR wavelength λ_r, absorption is entirely due to pure water, and the apparent absorption $a_i(\lambda_r, T)$ is completely due to undetected scattering $kb_p(\lambda_r)$ and temperature dependent variations in water absorption (Pegau and Zaneveld 1993) relative to absorption at T' (the calibration temperature).

From assumptions 1) and 2), it follows that

$$\frac{b_p(\lambda_1)}{b_p(\lambda_2)} = \frac{b_i(\lambda_1)}{b_i(\lambda_2)}. \tag{79}$$

From assumption 3), it follows that

$$k = \frac{a_i(\lambda_r, T) + S(\lambda_r)(T - T')}{b_i(\lambda_r)}, \tag{80}$$

where $S(\lambda_r)$ represents the coefficient of water temperature variation in $a_w(\lambda, T)$. At $\lambda_r = 712\,\text{nm}$, for example, $S(712 = 0.0035\,\text{m}^{-1}\,^{\circ}\text{C}^{-1}$, and $S(\lambda)$ is negligible at $\lambda < 700\,\text{nm}$ (Pegau and Zaneveld 1993). It is then useful to combine (79) and (80) to determine the absorption coefficient $a_e(\lambda)$ due to substances other than water (Zaneveld pers. comm.) as

$$\begin{aligned} a_e(\lambda) = & \; a_i(\lambda, T) \\ & - \frac{\left[a_i(\lambda_r, T) - S(\lambda_r)(T - T')\right] b_i(\lambda)}{b_i(\lambda_r)}. \end{aligned} \tag{81}$$

When equations (75) through (81) are applied to unfiltered total absorption measurements, it follows that

$$a_e(\lambda) = a_p(\lambda) + a_g(\lambda), \tag{82}$$

where $a_p(\lambda)$ and $a_g(\lambda)$ are respectively the particulate and Gelbstoff (dissolved substances) components of absorption. If a $0.2\,\mu\text{m}$ intake filter canister is used to exclude the particulate fraction from the water, then $a_e(\lambda)$ is due to $a_g(\lambda)$ alone. If profiles are made with two AC-9 meters (one filtered and one unfiltered), the total absorption coefficient may, therefore, be partitioned as

$$a(\lambda) = a_w(\lambda) + a_p(\lambda) + a_g(\lambda). \tag{83}$$

To further partition $a_p(\lambda)$ into $a_\phi(\lambda)$ (*phytoplankton pigments*) and $a_t(\lambda)$ (*tripton*) absorption coefficient components, it is necessary to obtain discrete water samples at several depths distributed over the profiles, and to apply

the filtration and spectrophotometry laboratory analyses described in Sections 5.4.2 and 6.8.2.

The fraction of total particle scattering, $k_c b_p(\lambda)$, included in the beam transmission measurement may be estimated from the detector acceptance angle and path length geometry of a particular instrument. Using this coefficient, the corrected non-water beam attenuation coefficient $c_e(\lambda)$ may be calculated as

$$c_e(\lambda) = c_i(\lambda) + k_c\left[c_e(\lambda) - a_e(\lambda)\right], \quad (84)$$

or

$$c_e(\lambda) = \frac{c_i(\lambda) - k_c a_e(\lambda)}{1 - k_c}. \quad (85)$$

Therefore, the corrected particle scattering coefficient may be estimated as

$$b_p(\lambda) = c_e(\lambda) - a_e(\lambda). \quad (86)$$

6.8.2 Analysis of Absorption Spectra

Spectral absorption coefficients $a_g(\lambda)$ (Gelbstoff), a_p (total particulates), and a_t (tripton) in units of m^{-1} are calculated from optical density spectra measured using the protocols of Section 5.4.2. For Gelbstoff,

$$a_g(\lambda) = \frac{2.303}{l}\left[\mathrm{OD}_g(\lambda) - \mathrm{OD}_r(\lambda)\right], \quad (87)$$

where l is the cuvette pathlength (0.1 m), and the other terms are introduced in Section 5.4.2.

An equation similar to (87) is used to calculate absorption coefficients $a_p(\lambda)$ and $a_t(\lambda)$, but in these cases, a correction must be applied to account for the effective increase in pathlength due to scattering in the GF/F filters (Mitchell and Kiefer 1984). The nominal absorption pathlength l_s of the filtered material in suspension is given by

$$l_s = \frac{V}{A}, \quad (88)$$

where V is the volume of water filtered and A is the clearance area of the filter. Scattering of light within the GF/F filter lengthens the absorption pathlength. This factor is termed the β factor by Mitchell and Kiefer (1988) after Butler (1962), which is not to be confused with the volume scattering coefficient $\beta(\theta)$ used elsewhere throughout this document. The absorption coefficient of filtered particles must, therefore, be corrected for pathlength amplification and the equivalent absorption in suspension is computed as

$$a_p(\lambda) = \frac{2.303A}{\beta V}\left[\mathrm{OD}_p(\lambda) - \mathrm{OD}_r(\lambda)\right]. \quad (89)$$

To correct for residual offsets in the filter spectrophotometric measurement, it is assumed that at 850 nm the true optical densities are zero. The apparent measured values of $\mathrm{OD}_p(850)$ and $\mathrm{OD}_r(850)$ are, therefore, subtracted from $\mathrm{OD}_p(\lambda)$ and $\mathrm{OD}_r(\lambda)$ prior to applying (89). Previously, some investigators have used apparent optical densities at 750 nm for this correction, but recent work has shown this wavelength to be inappropriate in some oceanic waters.

The prevalent current practice is to estimate β empirically through a function that may be expressed in the form

$$\beta^{-1} = C_1 + C_2\left[\mathrm{OD}_p(\lambda) - \mathrm{OD}_r(\lambda)\right], \quad (90)$$

where C_1 and C_2 are coefficients of a polynomial regression fit. For example, Mitchell (1990) gives $C_1 = 0.392$ and $C_2 = 0.665$, while Cleveland and Weidemann (1993) give $C_1 = 0.378$ and $C_2 = 0.523$.

Spectrophotometers that disperse white light into its spectrum using a monochromator prior to illuminating the sample are termed *pre-sample* monochromators, while instruments that pass the light through a monochromator after it has passed through the sample are termed *post-sample* monochromators. The value of the pathlength amplification factor has been found to be independent of post-sample optical geometry for a variety of standard laboratory instruments with pre-sample monochromators (Mitchell 1990, Stramski pers. comm., and Cleveland pers. comm.). Clark (pers. comm.) and Cleveland (pers. comm.) have found, however, that diode array spectrophotometers with a post-sample grating require the use of an integrating sphere attachment which may affect the β factor. Lee et al. (1994) use a diode array system, which collects and focuses the post-sample light and gives raw OD_p values similar to standard instruments with pre-sample monochromators (Cleveland pers. comm. and Carder pers. comm.).

Substituting (90) in (89) directly yields the spectral absorption coefficient for particles in suspension as

$$a_p(\lambda) = \frac{2.303A}{V}\Big[C_1\left[\mathrm{OD}_p(\lambda) - \mathrm{OD}_r(\lambda)\right] + C_2\left[\mathrm{OD}_p(\lambda) - \mathrm{OD}_r(\lambda)\right]^2\Big], \quad (91)$$

and for tripton

$$a_p(\lambda) = \frac{2.303A}{V}\Big[C_1\left[\mathrm{OD}_t(\lambda) - \mathrm{OD}_r(\lambda)\right] + C_2\left[\mathrm{OD}_t(\lambda) - \mathrm{OD}_r(\lambda)\right]^2\Big]. \quad (92)$$

Finally, the spectral absorption coefficient for *in vivo* phytoplankton pigments is computed as

$$a_\phi(\lambda) = a_p(\lambda) - a_t(\lambda). \quad (93)$$

The best overall performance of this algorithm will be achieved when filtered sample density yields $\mathrm{OD}_p(675)$ between 0.05 and 0.1. The volume of water filtered for particle absorption measurements should therefore be adjusted accordingly (Section 5.4.2).

For purposes of data reporting and archiving, the absorption coefficients $a_g(\lambda)$, $a_p(\lambda)$, and $a_t(\lambda)$ will be reported in m^{-1} as computed using equations (87), (91), and (92), respectively. Uncorrected optical density spectra for the blank filters and distilled water blank must be recorded and provided with absorption coefficients to allow reversal of the correction algorithms. The values of $OD_p(850)$ and $OD_r(850)$, which have been subtracted to remove residual instrument offset, must also be reported with each absorption spectrum. The pathlength amplification factor, together with a description of the method and date of its determination, must also be reported with all particle absorption coefficients based on filter spectrophotometry.

Roesler and Perry (pers. comm.) have proposed a theoretically derived expression for β, with a formulation different from (90). At this writing, however, this approach has not gained widespread acceptance in the community. Further review of this protocol is warranted for possible future revision. Sosik and Mitchell (1994) have proposed a spectrofluorescence excitation method to make direct estimates of absorption by the photosynthetically active pigments $[a_{ps}(\lambda)]$. They found $a_{ps}(\lambda) \leq a_\phi(\lambda)$, where the difference is attributable to photo-protective pigments in the phytoplankton. Carder and some of his associates (pers. comm.) recommend the determination of $a_\phi^M(666)$ in the methanol extract using a spectrophotometric method at 666 nm with 850 nm zero. This method sets an upper limit to $a_\phi(675)$ for the unpackaged state, and allows an alternate estimate of chlorophyll *a*.

6.9 CTD PROFILE ANALYSES

Each CTD profile should be prefiltered to remove any depth reversal segments resulting from violent ship or hydrowire motions. This will remove many instances of *salinity spiking*, an artifact which occurs when water temperature changes at a rate faster than the conductivity probe can follow. The CTD data should then be processed to profiles of potential temperature (°C), salinity (Practical Salinity Units [PSU] based on the Practical Salinity Scale of 1978, PSS78), and density ($kg\,m^{-3}$) using the algorithms which have been endorsed by the United Nations Educational, Scientific, and Cultural Organization (UNESCO)/SCOR/International Council of Exploration of the Seas (ICES)/IAPSO Joint Panel on Oceanographic Tables and Standards, and also by SCOR Working Group 51 (Fofonoff and Millard 1983).

At this stage, each set of CTD profiles should be carefully examined to detect any significant static instability artifacts resulting from salinity spiking. After any such major artifacts are removed by editing, the data should be further smoothed by averaging temperature and conductivity data into 2 m depth bins, and the final profiles of salinity, density, and other derived parameters should be recomputed using the smoothed CTD profile.

For any hydrographic station, descriptive hydrographic analyses should include T-S profile characterizations of water masses. Features in the density profile which appear to be related to physical mixing and stability should be compared with features in the corresponding bio-optical profiles. CTD profiles from horizontal transects (i.e., two-dimensional grids) should be used in the computation of two-dimensional sections, or three-dimensional gridded arrays, for such variables as geostrophic currents, temperature, salinity, and the density anomaly σ_t. These analysis products, together with corresponding two- or three-dimensional representations of bio-optical variability, can be used to estimate the relative importance of advection and isopycnal mixing in redistributing or modifying upper ocean optical properties during a cruise.

Acknowledgments

These protocols originated from discussions and draft material contributed by the workshop participants in April 1991. The authors thank all of them for their help. The participants' names and affiliations (as of the time the workshop was held in April 1991) are given in Table 7.

Table 7. Workshop Participants.

Name	Affiliation
Workshop Co-chairs	
Roswell Austin	SDSU/CHORS
James Mueller	SDSU/CHORS
Workshop Participants	
Robert Arnone	NOARL/Stennis Space Center
Rocky Booth	BSI
Kendall Carder	Univ. of South Florida
Dennis Clark	NOAA/NESDIS
Donald Collins	Jet Propulsion Laboratory
Wayne Esaias	NASA/GSFC
Howard Gordon	Univ. of Miami
Bruce Guenther	NASA/GSFC
Ronald Holyer	NOARL/Stennis Space Center
Robert Kirk	NASA/GSFC
Charles McClain	NASA/GSFC
James McLean	NASA/GSFC
B. Gregory Mitchell	NASA Headquarters
Donald Montgomery	Ofc. Oceanogr. of the Navy
Raymond Smith	Univ. of Calif. Santa Barbara
Charles Trees	SDSU/CHORS
Kenneth Voss	Univ. of Miami
Alan Weidemann	NOARL/Stennis Space Center
Ronald Zaneveld	Oregon State University
Administrative Support	
Meta Frost	Westover Consultants

Over the past two years, many of the above scientists, and others from the SeaWiFS Science Team and oceanographic community at large, have participated in the ongoing evolution of these ocean optics protocols, culminating in the present revision. Several people deserve special recognition and thanks for their time and effort. Robert Bidigare (Univ. of Hawaii) drafted the improved protocols for pigment analyses. Ronald Zaneveld contributed draft versions of new protocols for calibrating and using instruments for *in situ* spectral absorption and beam attenuation profiles, and for backscattering measurements. Expanded protocols for spectrophotometric determination of absorption by particles and dissolved matter were contributed through the combined efforts of Charles Trees, B. Gregory Mitchell, Joan Cleveland (SDSU/CHORS), Charles Yentsch (Bigelow Marine Laboratory), Colin Roesler (Univ. of Connecticut), Kendall Carder, and David Phinney (Bigelow Marine Laboratory). New protocols for Case-2 waters and above-water radiometry are based on material contributed by Kendall Carder, Roland Doerffer (GKSS Forschungszenstrum, Germany), Curtiss Davis (Naval Research Laboratory), and Robert Arnone. Thanks are due to all of these people, and other colleagues who continue to participate in the critical review, discussion, and improvement of this body of protocols.

Glossary

A/D Analog-to-Digital
ALSCAT ALPHA and Scattering Meter (Note: the symbol α corresponds to $c(\lambda)$, the beam attenuation coefficient, in present usage.)
AOL Airborne Oceanographic Lidar
ARGOS Not an acronym: the name given to the data collection and location system on NOAA Operational Satellites
ASCII American Standard Code for Information Interchange
AVHRR Advanced Very High Resolution Radiometer
AVIRIS Advanced Visible and Infrared Imaging Spectrometer

BSI Biospherical Instruments, Inc.
CDOM Colored Dissolved Organic Material
CHN Carbon, Hydrogen, and Nitrogen
CTD Conductivity, Temperature, and Depth
CW Continuous Wave
CZCS Coastal Zone Color Scanner

DIW Distilled Water
DOC Dissolved Organic Carbon
DOM Dissolved Organic Matter

ER-2 Earth Resources-2, a research aircraft

FEL Not an acronym; a type of standard lamp for irradiance and radiance calibration
FOV Field-of-View
FWHM Full-Width at Half-Maximum

GAC Global Area Coverage
GASM General Angle Scattering Meter
GF/F Not an acronym; a specific type of glass fiber filter manufactured by Whatman
GMT Greenwich Mean Time
GOES Geostationary Operational Environmental Satellite
GPS Global Positioning System
GSFC Goddard Space Flight Center

HPLC High Performance Liquid Chromatography

IAPSO International Association for the Physical Sciences of the Ocean
ICES International Council on Exploration of the Seas
IFOV Instantaneous field-of-view
IOP Inherent Optical Properties
IR Infrared

JGOFS Joint Global Ocean Flux Study

MARS Multispectral Airborne Radiometer System
MER Marine Environmental Radiometer
MERIS Marine Environment Research Imaging Spectroradiometer (French)
MODIS Moderate Resolution Imaging Spectrometer

NAS National Academy of Science
NASA National Aeronautics and Space Administration
NASIC NASA Aircraft/Satellite Instrument Calibration
NESDIS National Environmental Satellite Data Information Service
NIST National Institute of Standards and Technology
NOAA National Oceanic and Atmospheric Administration
NOARL Naval Oceanographic and Atmospheric Research Laboratory

OCTS Ocean Color and Temperature Sensor (Japanese)
OFFI Optical Free-Fall Instrument
OMP-8 Not an acronym; a type of marine anti-biofouling compound
OSFI Optical Surface Floating Instrument

PAR Photosynthetically Available Radiation
POC Particulate Organic Carbon
POLDER Polarization and Directionality of the Earth Reflectance (French)
PON Particulate Organic Nitrogen
PSU Practical Salinity Units
PTFE Polytetrafluoroethylene, commonly known by the trade name Teflon®

QED Quantum Efficient Device

ROSIS Remote Ocean Sensing Imaging Spectrometer, also known as the Reflecting Optics System Imaging Spectrometer (German)
ROV Remotely Operated Vehicle
ROW Reverse Osmosis Water

SCOR Scientific Committee on Oceanographic Research
SeaWiFS Sea-viewing Wide Field-of-view Sensor
SIRREX SeaWiFS Intercalibration Round-Robin Experiment
SNR Signal-to-Noise Ratio
SPM Suspended Particulate Material
SPO SeaWiFS Project Office
SPSWG SeaWiFS Prelaunch Science Working Group
SST Sea Surface Temperature

T-S Temperature-Salinity
TIROS Television Infrared Observation Satellite
TSM Total Suspended Material

UNESCO United Nations Educational, Scientific, and Cultural Organizations
UV Ultraviolet
UVB Ultraviolet-B

WMO World Meteorological Organization

Symbols

A Fitting coefficient for $P_4 - X$, or clearance area of a filter, depending on usage.
$A(\lambda_a)$ AC-9 instrument calibration factor for absorption.
$A(\lambda_c)$ AC-9 instrument calibration factor for beam attenuation.
$a(\lambda)$ Total absorption coefficient.
$a(z,\lambda)$ Spectral absorption coefficient.
$a_e(\lambda)$ Absorption coefficient due to substances other than water.
$a_f(z,\lambda)$ $a_p(\lambda) - a_t(z,\lambda)$.
$a_g(\lambda)$ Gelbstoff spectral absorption coefficient.
$a_i(\lambda_a, T)$ Initial estimate of the apparent absorption coefficient; used for determining the apparent absorption coefficient for substances other than water.
$a_\phi^M(\lambda)$ Phytoplankton pigment spectral absorption coefficient determined in methanol extract.
$a_p(\lambda)$ Particulate spectral absorption coefficient.
$a_{ps}(\lambda)$ Photosynthetically active pigment spectral absorption coefficient.
$a_t(\lambda)$ Tripton spectral absorption coefficient.
$a_w(\lambda)$ Absorption coefficient for pure water.
$a_\phi(\lambda)$ Phytoplankton pigment spectral absorption coefficient.

B Fitting coefficient for e^{B/P_5}.
$b(z,\lambda)$ Total scattering coefficient.
$b(z,\lambda_0,\theta)$ Volume scattering coefficient.
$b_b(z,\lambda)$ Spectral backscattering coefficient.
$b_i(\lambda)$ Initial estimate of the particle scattering coefficient; used for determining the apparent particle scattering coefficient for substances other than water.
$b_p(\lambda)$ Total particle scattering.
$b_r(\lambda)$ Total Raman scattering coefficient.
$b_w(\lambda)$ Scattering coefficient for pure water.

$c(z,\lambda)$ Spectral beam attenuation coefficient.
$c(z,660)$ Red beam attenuation (at 660 nm).
$c_e(\lambda)$ Corrected non-water beam attenuation coefficient.
$c_i(\lambda)$ Initial estimate of the beam attenuation coefficient; used for determining the apparent beam attenuation coefficient for substances other than water.
$c_p(\lambda)$ Beam attenuation coefficient due to particles.
$c_w(\lambda)$ Beam attenuation coefficient for pure water equal to $a_w(\lambda) + b_w(\lambda)$.
C_1 Polynomial regression factor.
C_2 Additional polynomial regression factor.
$C'(\lambda)$ AC-9 factory calibration coefficient.
$C'_r(\lambda)$ Additional AC-9 factory calibration coefficient.
$C_r(\lambda)$ Digital response of reference detector.
$C_t(\lambda)$ Digital response of water transmission detector.

D Sequential day of the year.
d Distance of lamp source from collector surface.

$E(\lambda)$ Irradiance.
$\hat{E}(z,m$ Smoothed estimate of irradiance obtained by least-squares regression fit in the center of a depth interval.
$E_a(\lambda)$ Irradiance in air.
E_{cal} Calibration source irradiance.
$E_d(0^-,\lambda)$ Incident spectral irradiance.
$E'_d(z,\lambda)$ Normalized downwelled spectral irradiance
$E_d(z,\lambda)$ Downwelled spectral irradiance
$E_s(\lambda)$ Surface irradiance.
$E_{\text{sky}}(\lambda)$ Spectral sky irradiance.
$E_{\text{sun}}(\lambda)$ Spectral sun irradiance.
$E_u(z,\lambda)$ Upwelled spectral irradiance.
$E_w(z,\lambda)$ Irradiance in water.

$\overline{F}_0(\lambda)$ Mean extraterrestrial solar flux.
$F_i(\lambda)$ Immersion correction factor.
$F_v(\lambda)$ Field-of-view coefficient.
f Ratio of sensor-to-instrument diameters.
$f(T)$ Offset voltage correction from the linear function characterizing temperature response.

$G(z,\lambda)$ Solid angle dependence with water depth.
$g(T)$ Coefficient of a linear function characterizing temperature response.

$\mathbb{H}$ Matrix of coefficients h_{ij}.
h_{ij} Analytic integral coefficients over the Hermitian polynomials γ_{ij}.
$h(\lambda)$ Normalized response function.

$\vec{\overline{K}}$ Vector of $\overline{K}_n$.
$K(\lambda)$ Generic irradiance attenuation coefficient.
$K(z,\lambda)$ Diffuse attenuation coefficient.
$K_d(z,\lambda)$ Vertical attenuation coefficient for downwelled irradiance.

$K_L(z,\lambda)$ Attenuation coefficient upwelled radiance.
$\overline{K}_n$ K at node depth z_n determined, with its vertical derivative by least-squares fit to radiometric profiles. (See equations 37–41 and surrounding text.)
$K_s(z,\lambda')$ Apparent attenuation coefficient measured in a homogenous water column.
$K_u(z,\lambda)$ Vertical attenuation coefficient for upwelled irradiance.
k Fractional factor of total particle scattering.
k' $y/\tan\theta_{0w}$.
k_c Wavelength independent fraction.

l Cuvette pathlength.
l_s Nominal absorption pathlength.
$L(z,\theta,\phi)$ Submerged upwelled radiance distribution.
$L^*(\lambda,\theta,\phi)$ Atmospheric path radiance at flight altitude.
$L_{\rm cal}$ Calibration source radiance.
$L_{\rm sky}(\lambda,\theta,\phi)$ Spectral sky radiance distribution.
L_t Radiance at top of atmosphere.
$L_u(z,\lambda)$ Upwelled spectral radiance.
$\hat{L}_u(\lambda)$ True upwelled spectral radiance.
$\tilde{L}_u(\lambda)$ Measured upwelled spectral radiance.
$L_W(\lambda)$ Water-leaving radiance.
$L_{WN}(\lambda)$ Normalized water-leaving radiance.
$L_1(\lambda)$ Apparent radiance response to a linearly polarized source.
$L_2(\lambda)$ Orthogonal apparent radiance response to a linearly polarized source.

n Starting index in measurement for angular measurements, or node index for the integral K analysis.
$n_g(\lambda)$ Index of refraction of Plexiglas.
$n_w(\lambda)$ Index of refraction of water.
N Ending index in measurement sequence for angular measurements.

$\mathrm{OD}_b(\lambda)$ Baseline optical density spectrum.
$\mathrm{OD}_g(\lambda)$ Optical density of soluble material (Gelbstoff).
$\mathrm{OD}_p(\lambda)$ Optical density spectra of filtered particles.
$\mathrm{OD}_r(\lambda)$ Optical density reference for filter or distilled water.
$\mathrm{OD}_t(\lambda)$ Optical density of non-pigmented particulates (tripton).

$P(\lambda)$ Polarization sensitivity.
P_i Fitting coefficient for $i = 1$ to 5.

$Q(\lambda)$ $L_u(0^-,\lambda)$ to $E_u(0^-,\lambda)$ relation factor (equal to π for a Lambertian surface).

$\overline{R}$ Mean Earth-sun distance.
R'_L Reflectance from an uncalibrated radiometer.
$R_L(z,\lambda)$ Spectral reflectance.
r Radius, or Earth-sun distance depending on usage.

$S(\lambda_r)$ A coefficient of water temperature variation in $a_w(\lambda,T)$.
$S_G(\lambda)$ Radiometer signal (uncalibrated) measured viewing a reflectance plaque.
S_{sky} Radiometer signal (uncalibrated) measured viewing the sky.
$S_W(\lambda)$ Radiometer signal (uncalibrated) measured viewing the water.

T' Instrument temperature during calibration.
$T_g(\lambda)$ Transmittance through a glass window.
$T_s(\lambda)$ Transmittance through the surface.
$T_w(\lambda)$ Transmittance through a water path.
$t_d(z,\lambda)$ Downward spectral irradiance transmittance from flight altitude z to the surface.

V Volume of water filtered.
$\hat{V}$ True voltage.
$\tilde{V}$ Measured voltage.
$V(z)$ Transmissometer voltage.
$V'_{\rm air}$ Current transmissometer air calibration voltage.
$V(\theta)$ Normalized measured value for a cosine collector.
$\overline{V}(\theta_i)$ Mean normalized measured value of instrument response.
$V_{\rm air}$ Factory transmissometer air calibration voltage.
$V_{\rm dark}$ Transmissometer dark response.

W_θ Weighting function.

X Depth in meters.

y Empirical factor.
Y Base 10 logarithm of the radiometric measurement E_d, E_u, or L_u.

z Vertical coordinate.
z' Corrected depth for pressure transducer depth offset relative to a sensor.
z_m Centered depth.
z_r Shallow depth.
z_s Exclusion depth due to data contamination.

β Filter absorption correction factor for scattering within the filter.
$\beta(z,\theta,\lambda)$ Spectral volume scattering function.
$\overline{\beta}_b$ The measured integral of the volume scattering function in the backward direction. The symbol in the text—$\overline{\beta}_b(\overline{\theta},\Delta\theta,\lambda,\Delta\lambda)$—is for the measurement in the backward direction over the angle θ at a given wavelength λ.

$\gamma_{ij}(\xi)$ Hermitian cubic polynomial.

Δz Half-interval depth increment.
$\Delta\theta$ Angular increment.
δ Cosine response asymmetry.

ϵ Cosine collector response error.
$\epsilon_{\rm sun}$ Self-shading error for $E_{\rm sun}$.
$\epsilon_{\rm sky}$ Self-shading error for $E_{\rm sky}$.
$\varepsilon(\lambda)$ $1 - e^{-k'a(\lambda)r}$.

θ Centroid angle of the scattering measurement.
θ_a In-air measurement angle.
θ_i Any nominal angle.
θ_N Angular terminus.
θ_n Angular origin.
θ_t Tilt angle.
θ_w In-water measurement angle.
θ_{0w} Refracted solar zenith angle.
θ_1 Lower integration limit.
θ_2 Upper integration limit.

κ' Self-shading coefficients.

λ' Channel of nominal wavelength.
λ_0 Center wavelength.
λ_n Any nominal wavelength.
λ_r Near-IR wavelength.

$\overline{\mu}_d(z,\lambda)$ Spectral mean cosine for downwelling radiance at depth z.

$\xi(\lambda)$ Minimum ship-shadow avoidance distance.

$\rho(\lambda)$ Bidirectional reflectance.
$\rho_g(\lambda)$ Gray card or plaque reflectance.

σ_t Density anomaly.

$\vec{\tau}$ Vector of measured optical depths.
$\tau(z,\lambda)$ Spectral optical depth.
$\tau_s(\lambda)$ Spectral solar atmospheric transmission.

ϕ Azimuth angle.

REFERENCES

Austin, R.W., 1976: Air-water radiance calibration factor. *Tech. Memo. ML-76-004t,* Vis. Lab., Scripps Inst. of Oceanogr., La Jolla, California, 8 pp.

——, and G. Halikas, 1976: The index of refraction of seawater. *SIO Ref. 76-1,* Vis. Lab., Scripps Inst. of Oceanogr., La Jolla, California, 64 pp.

——, and T.J. Petzold, 1981: The determination of diffuse attenuation coefficient of sea water using the Coastal Zone Color Scanner. *Oceanography from Space,* J.F.R. Gower, Ed., Plenum Press, 239–256.

Baker, K.S., and R.C. Smith, 1990: Irradiance transmittance through the air/water interface. *Ocean Optics X,* R.W. Spinrad, Ed., SPIE, **1,302,** 556–565.

Balch, W.M., P.M. Holligan, S.G. Ackleson, and K.J. Voss, 1991: Biological and optical properties of mesoscale coccolithophore blooms in the Gulf of Maine. *Limnol. Oceanogr.,* **36,** 629–643.

Bidigare, R.R., 1991: Analysis of algal chlorophylls and carotenoids. In: *Marine Particles: Analysis and Characterization,* D.C. Hurd and D.W. Spencer, Eds., Am. Geophys. Union, Washington, DC, 119–123.

——, L. Campbell, M.E. Ondrusek, R. Letelier, D. Vaulot and D.M. Karl, 1995: Phytoplankton community structure at station ALOHA (22° 45' N, 158° W) during fall 1991. *Deep Sea Res.,* (submitted).

——, and M.E. Ondrusek, 1995: Influence of the 1992 El Ninō on phytoplankton pigment distributions in the equatorial Pacific Ocean. *Deep-Sea Res.,* (submitted).

Booth, C.R.B., and R.C. Smith, 1988: Moorable spectroradiometer in the Biowatt Experiment. *Ocean Optics IX,* SPIE, **925,** 176–188.

Boyd, R.A., 1951: The development of prismatic glass block and the daylight laboratory. *Eng. Res. Bull. No. 32,* Eng. Res. Inst., University of Michigan, Ann Arbor, Michigan, 88 pp.

Bricaud, A., A. Morel, and L. Prieur, 1981: Absorption by dissolved organic matter of the sea (yellow substance) in the UV and visible domains. *Limnol. Oceanogr.,* **26,** 43–53.

Brown, O.B., and R.H. Evans, 1985: Calibration of Advanced Very High Resolution Radiometer infrared observations. *J. Geophys. Res.,* **90,** 11,667–11,677.

Butler, W.L., 1962: Absorption of light by turbid materials. *J. Opt. Soc. Amer.,* **52,** 292–299.

Carder, K.L., and R.G. Steward, 1985: A remote-sensing reflectance model of red-tide dinoflagellate off West Florida. *Limnol. Oceanogr.,* **30,** 286–298.

——, G.R. Harvey, R.G. Steward, and P.B. Ortner, 1989: Marine humic and fulvic acids: their effects on remote sensing of ocean chlorophyll. *Limnol. Oceanogr.,* **34,** 68–81.

——, P. Reinersman, R. Chen, F. Muller-Karger, and C.O. Davis, 1993: AVIRIS calibration and application in coastal oceanic environments. *Remote Sens. Environ.,* **44,** 205–216.

Chavez, F.P., K.R. Buck, R.R. Bidigare, D.M. Karl, D. Hebel, M. Latasa, L. Campbell and J. Newton, 1995: On the chlorophyll *a* retention properties of glass-fiber GF/F filters. *Limnol. Oceanogr.,* (in press).

Clark, D.K., 1981: Phytoplankton algorithms for the Nimbus-7 CZCS. *Oceanography from Space,* J.F.R. Gower, Ed., Plenum Press, 227–238.

Cleveland, J.S., and A.D. Weidemann, 1993: Quantifying absorption by aquatic particles: A multiple scattering correction for glass-fiber filters. *Limnol. Oceanogr.,* **38,** 1,321–1,327.

Cox, C., and W. Munk, 1954: Measurements of the roughness of the sea surface from photographs of the sun's glitter. *J. Opt. Soc. Am.,* **44,** 838–850.

Dickey, T., J. Marra, T. Granata, C. Langdon, M. Hamilton, J. Wiggert, D. Siegel, and A. Bratkovich, 1991: Concurrent high-resolution bio-optical and physical time series observations in the Sargasso Sea during the spring of 1987. *J. Geophys. Res.,* **96,** 8,643–8,663.

Esaias, W., G. Feldman, C.R. McClain, and J. Elrod, 1986: Satellite observations of oceanic primary productivity. *EOS, Trans. AGU,* **67,** 835–837.

Evans, R.H., and H.R. Gordon, 1994: Coastal zone color scanner "system calibration": A retrospective examination. *J. Geophys. Res.,* **99,** 7,293–7,307.

Feldman, G., N. Kuring, C. Ng, W. Esaias, C. McClain, J. Elrod, N. Maynard, D. Endres, R. Evans, J. Brown, S. Walsh, M. Carle, and G. Podesta, 1989: Ocean Color: Availability of the global data set. *EOS, Trans. AGU,* **70,** 634.

Fofonoff, N.P., and R.C. Millard, Jr., 1983: Algorithms for computation of fundamental properties of seawater. *UNESCO Tech. Papers in Marine Science,* **44,** UNESCO, 53 pp.

Frohlich, C., 1979: WMO/PMOD Sun photometer: Instructions for manufacture. *World Meteor. Org.,* Geneva, Switzerland, 3 pp., (plus tables and drawings).

Goericke, R., and D.J. Repeta, 1993: Chlorophylls *a* and *b* and divinyl chlorophylls *a* and *b* in the open subtropical North Atlantic Ocean. *Mar. Ecol. Prog. Ser.,* **10,** 307–313.

Gordon, H.R., 1981: Reduction of error introduced in the processing of coastal zone color scanner-type imagery resulting from sensor calibration and solar irradiance uncertainty. *Appl. Opt.*, **20,** 207–210.

——, 1985: Ship perturbations of irradiance measurements at sea, 1: Monte Carlo simulations. *Appl. Opt.*, **24,** 4,172–4,182.

——, 1987: Calibration requirements and methodology for remote sensors viewing the ocean in the visible. *Remote Sens. Environ.*, **22,** 103–126.

——, 1988: Ocean color remote sensing systems: radiometric requirements. *Recent Advances in Sensors, Radiometry, and Data Processing for Remote Sensing,* P.N. Slater, Ed., SPIE, **924,** 151–167.

——, 1989a: Dependence of the diffuse reflectance of natural waters on the sun angle. *Limnol. Oceanogr.*, **34**, 1,484–1,489.

——, 1989b: Can the Lambert-Beer law be applied to the diffuse attenuation coefficient of ocean water? *Limnol. Oceanogr.*, **34,** 1,389–1,409.

——, 1991: Absorption and scattering estimates from irradiance measurements: Monte Carlo simulations. *Limnol. Oceanogr.*, **36,** 769–777.

——, and D.K. Clark, 1980: Remote sensing optical properties of a stratified ocean: an improved interpretation. *Appl. Optics,* **19,** 3,428–3,430.

——, and ——, 1981: Clear water radiances for atmospheric correction of Coastal Zone Color Scanner imagery. *Appl. Opt.*, **20,** 4,175–4,180.

——, J.W. Brown, O.B. Brown, R.H. Evans, and D.K. Clark, 1983: Nimbus-7 CZCS: Reduction of its radiometric sensitivity with time. *Appl. Opt.*, **24,** 3,929–3,931.

——, and K. Ding, 1992: Self shading of in-water optical instruments. *Limnol. Oceanogr.*, **37**, 491–500.

Groom, S.B., and P.M. Holligan, 1987: Remote sensing of coccolithophorid blooms. *Adv. Space Res.*, **7,** 73–78.

Hamilton, M.K., C.O. Davis, W.J. Rhea, S.H. Pilorz, and K.L. Carder, 1993: Estimating chlorophyll content and bathymetry of Lake Tahoe using AVIRIS data. *Remote Sens. Environ.*, **44,** 217–230.

Helliwell, W.S., G.N. Sullivan, B. Macdonald, and K.J. Voss, 1990: Ship shadowing: model and data comparison. *Ocean Optics X,* R.W. Spinrad, Ed., SPIE, **1,302,** 55–71.

Holm-Hansen, O., C.J. Lorenzen, R.W. Holmes, and J.D.H. Strickland, 1965: Fluorometric determination of chlorophyll. *J. du Cons. Intl. pour l'Expl. de la Mer.*, **30,** 3–15.

Hovis, W.A., J.S. Knoll, and G.R. Smith, 1985: Aircraft measurements for calibration of an orbiting spacecraft sensor. *Appl. Opt.*, **24,** 407–410.

James, H.R., and E.A. Birge, 1938: A laboratory study of the absorption of light by lake waters. *Trans. Wis. Acad. Sci.*, **31,** 1–154.

Joint Global Ocean Flux Study, 1991: JGOFS Core Measurements Protocols. *JGOFS Report No. 6,* Scientific Committee on Oceanic Research, 40 pp.

Kishino, M., N. Okami, and S. Ichimura, 1985: Estimation of the spectral absorption coefficients of phytoplankton in the sea. *Bull. Mar. Sci.*, **37,** 634–642.

Kohler, R., R. Pello, and J. Bonhoure, 1990: Temperature dependent nonlinearity effects of a QED-200 detector in the visible. *Appl. Opt.*, **29,** 4,212–4,215.

Latasa, M., R.R. Bidigare, M.C. Kennicutt II, and M.E. Ondrusek, 1995: HPLC analysis of algal pigments: A comparison among laboratories. *Mar. Chem.*, (submitted).

Lee, Z., K.L. Carder, S.K. Hawes, R.G. Steward, T.G. Peacock, and C.O. Davis, 1994: A model for the interpretation of hyperspectral remote-sensing reflectance. *Appl. Opt.*, **33,** 5,721–5,732.

Letelier, R.M., R.R. Bidigare, D.V. Hebel, M.E. Ondrusek, C.D. Winn, and D.M. Karl, 1993: Temporal variability of phytoplankton community structure at the U.S.-JGOFS time-series Station ALOHA (22° 45' N, 158° W) based on HPLC pigment analysis. *Limnol. Oceanogr.*, **38,** 1,420–1,437.

Maffione, R.A., D.R. Dana, and R.C. Honey, 1991: Instrument for underwater measurement of optical backscatter. In: *Underwater Imaging, Photography, and Visibility,* R.W. Spinrad, Ed., SPIE, **1,537,** 173–184.

Marshall, B.R., and R.C. Smith, 1990: Raman scattering and in-water optical properties. *Appl. Opt.*, **29,** 71–84.

McLean, J.T., and B.W. Guenther, 1989: Radiance calibration of spherical integrators. *Optical Radiation Measurements II,* SPIE, **1,109,** 114–121.

Michaelsen, J., X. Zhang, and R.C. Smith, 1988: Variability of pigment biomass in the California Current system as determined by satellite imagery. *J. Geophys. Res.*, **93,** 10,883–10,896.

Mitchell, B.G., 1990: Algorithms for determining the absorption coefficient for aquatic particulates using the quantitative filter technique. *Ocean Optics X,* R.W. Spinrad, Ed., SPIE, **1,302,** 137–148.

——, and D.A. Kiefer, 1984: Determination of absorption and fluorescence excitation spectra for phytoplankton. *Marine Phytoplankton and Productivity,* O. Holm-Hansen, L. Bolis, and R. Gilles, Eds., Springer-Verlag, 157–169.

——, and ——, 1988: Chlorophyll-*a* specific absorption and fluorescence excitation spectra for light-limited phytoplankton. *Deep-Sea Res.*, **35,** 639–663.

Morel, A., and L. Prieur, 1977: Analysis of variations in ocean color. *Limnol. Oceanogr.*, **22,** 709–722.

——, and R.C. Smith, 1982: Terminology and units in optical oceanography. *Mar. Geod.*, **5,** 335–349.

——, and B. Gentili, 1993: Diffuse reflectance of oceanic waters. II. Bidirectional aspects. *Appl. Opt.*, **32,** 6,864–6,879.

Mueller, J.L., 1985: Nimbus-7 CZCS: confirmation of its radiometric sensitivity decay rate through 1982. *Appl. Opt.*, **24,** 1,043–1,047.

——, 1991: Integral method for irradiance profile analysis. *CHORS Tech. Memo. 007-91,* San Diego State University, San Diego, California, 10 pp.

——, 1993: The First SeaWiFS Intercalibration Round-Robin Experiment, SIRREX-1, July 1992. *NASA Tech. Memo. 104566, Vol. 14,* S.B. Hooker and E.R. Firestone, Eds., NASA Goddard Space Flight Center, Greenbelt, Maryland, 60 pp.

——, and R.W. Austin, 1992: Ocean Optics Protocols. *NASA Tech. Memo. 104566, Vol. 5,* S.B. Hooker and E.R. Firestone, Eds., NASA Goddard Space Flight Center, Greenbelt, Maryland, 43 pp.

——, B.C. Johnson, C.L. Cromer, J.W. Cooper, J.T. McLean, S.B. Hooker, and T.L. Westphal, 1994: The Second SeaWiFS Intercalibration Round-Robin Experiment, SIREX-2, June 1993. *NASA Tech. Memo. 104566, Vol. 16,* S.B. Hooker and E.R. Firestone, Eds., NASA Goddard Space Flight Center, Greenbelt, Maryland, 121 pp.

Muller-Karger, F.E., C.R. McClain, R.N. Sambrotto, and G.C. Ray, 1990: A comparison of ship and Coastal Zone Color Scanner mapped distribution of phytoplankton in the southeastern Bering Sea. *J. Geophys. Res.*, **95,** 11,483–11,499.

National Academy of Sciences, 1984: *Global Ocean Flux Study, Proceedings of a Workshop.* National Academy Press, 360 pp.

Neckel, H., and D. Labs, 1984: The solar radiation between 3,300 and 12,500 Å. *Solar Phys.*, **90,** 205–258.

Palmer, J.M., 1988: Use of self-calibrated detectors in radiometric instruments. *Recent advances in sensors, radiometry, and data processing for remote sensing,* P.N. Slater, Ed., SPIE, **924,** 224–231.

Pegau, W.S., and J.R.V. Zaneveld, 1993: Temperature dependent absorption of water in the red and near infrared portions of the spectrum. *Limnol. Oceanogr.*, **38,** 188–192.

——, J.S. Cleveland, W. Doss, C.D. Kennedy, R.A. Maffione, J.L. Mueller, R. Stone, C.C. Trees, A.D. Weidemann, W.H. Wells, and J.R.V. Zaneveld, 1995: A comparison of methods for the measurement of the absorption coefficient in natural waters. *J. Geophys. Res.*, (submitted).

Petzold, T.J., 1972: Volume Scattering Functions for Selected Ocean Waters. *SIO Ref. No. 72-78,* Scripps Institution of Oceanography, La Jolla, California, 79 pp.

——, 1988: A method for obtaining analytical curve fits to underwater radiometric measurements. *Tech. Memo. Oc Op/TJP-88-06t,* Scripps Inst. of Oceanogr., La Jolla, California, 20 pp.

——, and R.W. Austin, 1988: Characterization of MER-1032. *Tech. Memo. EV-001-88t,* Vis. Lab., Scripps Institution of Oceanography, La Jolla, California, 56 pp.

Pinder, G.F., and W.G. Gray, 1977: *Finite Element Simulation in Surface and Subsurface Hydrology,* Academic Press, 295 pp.

Shaw, G.E., 1976: Error analysis of multiwavelength sun photometry. *Pure Appl. Geophys.*, **114,** 1–14.

Siegel, D.A., C.R. Booth, and T.D. Dickey, 1986: Effects of sensor characteristics on the inferred vertical structure of the diffuse attentuation coefficient spectrum. *Ocean Optics VIII,* M.A. Blizard, Ed., *SPIE,* **637,** 115–124.

Smart, J.H., 1992: Empirical relationships between optical properties in the ocean. In: *Ocean Optics XI,* SPIE, **1,750,** 276–298.

Smith, R.C., and K.S. Baker, 1981: Optical properties of the clearest natural waters (200–800 nm). *Appl. Opt.*, **20,** 177–184.

——, ——, and P. Dustan, 1981: Fluorometric techniques for the measurement of oceanic chlorophyll in the support of remote sensing. *SIO Ref. 81-17,* Scripps Inst. of Oceanogr., La Jolla, California, 14 pp.

——, and ——, 1984: Analysis of ocean optical data, *Ocean Optics VII,* M. Blizard, Ed., SPIE, **478,** 119–126.

——, and ——, 1986: Analysis of ocean optical data. *Ocean Optics VIII,* P.N. Slater, Ed., SPIE, **637,** 95–107.

——, R. Bidigare, B. Prézelin, K. Baker, and J. Brooks, 1987: Optical Characterization of Primary Productivity Across a Coastal Front. *Mar. Biol.*, **96,** 575–591.

——, K.J. Waters, and K.S. Baker, 1991: Optical variability and pigment biomass in the Sargasso Sea as determined using deep-sea optical mooring data. *J. Geophys. Res.*, **96,** 8,665–8,686.

Sosik, H.M., and B.G. Mitchell, 1995: Light absorption by phytoplankton, photosynthetic pigments, and detritus in the California Current System. *Deep-Sea Res.*, (in press).

Stramski, D., 1990: Artifacts in measuring absorption spectra of phytoplankton collected on a filter. *Limnol. Oceanogr.*, **35,** 1,804–1,809.

Strickland, J.D.H., and T.R. Parsons, 1972: *A Practical Handbook of Sea Water Analysis,* Fisheries Research Board of Canada, 310 pp.

Trees, C.C., M.C. Kennicutt II, and J.M. Brooks, 1985: Errors associated with the standard fluorometric determination of chlorophylls and phaeopigments. *Mar. Chem.*, **17,** 1–12.

Tyler, J.E., and R.C. Smith, 1979: *Measurements of Spectral Irradiance Underwater,* Gordon and Breach, New York, 103 pp.

Viollier, M., 1982: Radiance calibration of the Coastal Zone Color Scanner: a proposed adjustment. *Appl. Opt.*, **21,** 1,142–1,145.

Voss, K.J., J.W. Nolten, and G.D. Edwards, 1986: Ship shadow effects on apparent optical properties. *Ocean Optics VIII,* M. Blizard, Ed., SPIE, **637,** 186–190.

——, K.J. and G. Zibordi, 1989: Radiometric and geometric calibration of a spectral electro-optic "fisheye" camera radiance distribution system. *J. Atmos. Ocean. Technol.*, **6,** 652–662.

Walker, J.H., R.D. Saunders, J.K. Jackson, and D.A. McSparron, 1987: Spectral Irradiance Calibrations. *NBS Special Publication 250–20,* U.S. Dept. of Commerce, National Bureau of Standards, Washington, DC, 37 pp. plus appendices.

——, C.L. Cromer, and J.T. McLean, 1991: Technique for improving the calibration of large-area sphere sources. *Ocean Optics,* B.W. Guenther, Ed., SPIE, **1,493,** 224–230.

Walsh, J.J., G.T. Rowe, R.L. Iverson, and C.P. McRoy, 1981: Biological export of shelf carbon is a sink of the global CO_2 cycle. *Nature,* **291,** 196–201.

Waters, K.J., R.C. Smith, and M.R. Lewis, 1990: Avoiding ship induced light field perturbation in the determination of oceanic optical properties. *Oceanogr.,* **3,** 18–21.

Weinreb, M.P., G. Hamilton, S. Brown, and R.J. Koczor, 1990: Nonlinear corrections in calibration of Advanced Very High Resolution Radiometer infrared channels. *J. Geophys. Res.,* **95,** 7,381–7,388.

Wright, S.W., S.W. Jeffrey, R.F.C. Mantoura, C.A. Llewellyn, T. Bjornland, D. Repeta, and N. Welschmeyer, 1991: Improved HPLC method for the analysis of chlorophylls and carotenoids from marine phytoplankton. *Mar. Ecol. Prog. Ser.,* **77,** 183–196.

Wyman, M., 1992: An *in vivo* method for the estimation of phycoerythrin concentrations in marine cyanobacteria. *Limnol. Oceanogr.,* **37,** 1,300–1,306.

Yentsch, C.S., and D.W. Menzel, 1963: A method for the determination of phytoplankton, chlorophyll, and phaeophytin by fluorescence. *Deep-Sea Res.,* **10,** 221–231.

Zaneveld, J.R.V., J.C. Kitchen, A. Bricaud, and C. Moore, 1992: Analysis in *in situ* spectral absorption meter data. *Ocean Optics XI,* G.D. Gilbert, Ed., SPIE, **1750,** 187–200.

——, 1995: A theoretical deviation of the dependence of the remotely sensed reflectance on the IOP. *J. Geophys. Res.,* (in press).

Zibordi, G., and G.M. Ferrari, 1995: Instrument self-shading in underwater optical measurements: experimental data. *Appl. Opt.,* (submitted).

The SeaWiFS Technical Report Series

Vol. 1

Hooker, S.B., W.E. Esaias, G.C. Feldman, W.W. Gregg, and C.R. McClain, 1992: An Overview of SeaWiFS and Ocean Color. *NASA Tech. Memo. 104566, Vol. 1,* S.B. Hooker and E.R. Firestone, Eds., NASA Goddard Space Flight Center, Greenbelt, Maryland, 24 pp., plus color plates.

Vol. 2

Gregg, W.W., 1992: Analysis of Orbit Selection for SeaWiFS: Ascending vs. Descending Node. *NASA Tech. Memo. 104566, Vol. 2,* S.B. Hooker and E.R. Firestone, Eds., NASA Goddard Space Flight Center, Greenbelt, Maryland, 16 pp.

Vol. 3

McClain, C.R., W.E. Esaias, W. Barnes, B. Guenther, D. Endres, S. Hooker, G. Mitchell, and R. Barnes, 1992: Calibration and Validation Plan for SeaWiFS. *NASA Tech. Memo. 104566, Vol. 3,* S.B. Hooker and E.R. Firestone, Eds., NASA Goddard Space Flight Center, Greenbelt, Maryland, 41 pp.

Vol. 4

McClain, C.R., E. Yeh, and G. Fu, 1992: An Analysis of GAC Sampling Algorithms: A Case Study. *NASA Tech. Memo. 104566, Vol. 4,* S.B. Hooker and E.R. Firestone, Eds., NASA Goddard Space Flight Center, Greenbelt, Maryland, 22 pp., plus color plates.

Vol. 5

Mueller, J.L., and R.W. Austin, 1992: Ocean Optics Protocols for SeaWiFS Validation. *NASA Tech. Memo. 104566, Vol. 5,* S.B. Hooker and E.R. Firestone, Eds., NASA Goddard Space Flight Center, Greenbelt, Maryland, 43 pp.

Vol. 6

Firestone, E.R., and S.B. Hooker, 1992: SeaWiFS Technical Report Series Summary Index: Volumes 1–5. *NASA Tech. Memo. 104566, Vol. 6,* S.B. Hooker and E.R. Firestone, Eds., NASA Goddard Space Flight Center, Greenbelt, Maryland, 9 pp.

Vol. 7

Darzi, M., 1992: Cloud Screening for Polar Orbiting Visible and IR Satellite Sensors. *NASA Tech. Memo. 104566, Vol. 7,* S.B. Hooker and E.R. Firestone, Eds., NASA Goddard Space Flight Center, Greenbelt, Maryland, 7 pp.

Vol. 8

Hooker, S.B., W.E. Esaias, and L.A. Rexrode, 1993: Proceedings of the First SeaWiFS Science Team Meeting. *NASA Tech. Memo. 104566, Vol. 8,* S.B. Hooker and E.R. Firestone, Eds., NASA Goddard Space Flight Center, Greenbelt, Maryland, 61 pp.

Vol. 9

Gregg, W.W., F.C. Chen, A.L. Mezaache, J.D. Chen, J.A. Whiting, 1993: The Simulated SeaWiFS Data Set, Version 1. *NASA Tech. Memo. 104566, Vol. 9,* S.B. Hooker, E.R. Firestone, and A.W. Indest, Eds., NASA Goddard Space Flight Center, Greenbelt, Maryland, 17 pp.

Vol. 10

Woodward, R.H., R.A. Barnes, C.R. McClain, W.E. Esaias, W.L. Barnes, and A.T. Mecherikunnel, 1993: Modeling of the SeaWiFS Solar and Lunar Observations. *NASA Tech. Memo. 104566, Vol. 10,* S.B. Hooker and E.R. Firestone, Eds., NASA Goddard Space Flight Center, Greenbelt, Maryland, 26 pp.

Vol. 11

Patt, F.S., C.M. Hoisington, W.W. Gregg, and P.L. Coronado, 1993: Analysis of Selected Orbit Propagation Models for the SeaWiFS Mission. *NASA Tech. Memo. 104566, Vol. 11,* S.B. Hooker, E.R. Firestone, and A.W. Indest, Eds., NASA Goddard Space Flight Center, Greenbelt, Maryland, 16 pp.

Vol. 12

Firestone, E.R., and S.B. Hooker, 1993: SeaWiFS Technical Report Series Summary Index: Volumes 1–11. *NASA Tech. Memo. 104566, Vol. 12,* S.B. Hooker and E.R. Firestone, Eds., NASA Goddard Space Flight Center, Greenbelt, Maryland, 28 pp.

Vol. 13

McClain, C.R., K.R. Arrigo, J. Comiso, R. Fraser, M. Darzi, J.K. Firestone, B. Schieber, E-n. Yeh, and C.W. Sullivan, 1994: Case Studies for SeaWiFS Calibration and Validation, Part 1. *NASA Tech. Memo. 104566, Vol. 13,* S.B. Hooker and E.R. Firestone, Eds., NASA Goddard Space Flight Center, Greenbelt, Maryland, 52 pp., plus color plates.

Vol. 14

Mueller, J.L., 1993: The First SeaWiFS Intercalibration Round-Robin Experiment, SIRREX-1, July 1992. *NASA Tech. Memo. 104566, Vol. 14,* S.B. Hooker and E.R. Firestone, Eds., NASA Goddard Space Flight Center, Greenbelt, Maryland, 60 pp.

Vol. 15

Gregg, W.W., F.S. Patt, and R.H. Woodward, 1994: The Simulated SeaWiFS Data Set, Version 2. *NASA Tech. Memo. 104566, Vol. 15,* S.B. Hooker and E.R. Firestone, Eds., NASA Goddard Space Flight Center, Greenbelt, Maryland, 42 pp., plus color plates.

Vol. 16

Mueller, J.L., B.C. Johnson, C.L. Cromer, J.W. Cooper, J.T. McLean, S.B. Hooker, and T.L. Westphal, 1994: The Second SeaWiFS Intercalibration Round-Robin Experiment, SIRREX-2, June 1993. *NASA Tech. Memo. 104566, Vol. 16,* S.B. Hooker and E.R. Firestone, Eds., NASA Goddard Space Flight Center, Greenbelt, Maryland, 121 pp.

Vol. 17

Abbott, M.R., O.B. Brown, H.R. Gordon, K.L. Carder, R.E. Evans, F.E. Muller-Karger, and W.E. Esaias, 1994: Ocean Color in the 21st Century: A Strategy for a 20-Year Time Series. *NASA Tech. Memo. 104566, Vol. 17,* S.B. Hooker and E.R. Firestone, Eds., NASA Goddard Space Flight Center, Greenbelt, Maryland, 20 pp.

Vol. 18

Firestone, E.R., and S.B. Hooker, 1994: SeaWiFS Technical Report Series Summary Index: Volumes 1–17. *NASA Tech. Memo. 104566, Vol. 18,* S.B. Hooker and E.R. Firestone, Eds., NASA Goddard Space Flight Center, Greenbelt, Maryland, 47 pp.

Vol. 19

McClain, C.R., R.S. Fraser, J.T. McLean, M. Darzi, J.K. Firestone, F.S. Patt, B.D. Schieber, R.H. Woodward, E-n. Yeh, S. Mattoo, S.F. Biggar, P.N. Slater, K.J. Thome, A.W. Holmes, R.A. Barnes, and K.J. Voss, 1994: Case Studies for SeaWiFS Calibration and Validation, Part 2. *NASA Tech. Memo. 104566, Vol. 19,* S.B. Hooker, E.R. Firestone, and J.G. Acker, Eds., NASA Goddard Space Flight Center, Greenbelt, Maryland, 73 pp.

Vol. 20

Hooker, S.B., C.R. McClain, J.K. Firestone, T.L. Westphal, E-n. Yeh, and Y. Ge, 1994: The SeaWiFS Bio-Optical Archive and Storage System (SeaBASS), Part 1. *NASA Tech. Memo. 104566, Vol. 20,* S.B. Hooker and E.R. Firestone, Eds., NASA Goddard Space Flight Center, Greenbelt, Maryland, 40 pp.

Vol. 21

Acker, J.G., 1994: The Heritage of SeaWiFS: A Retrospective on the CZCS NIMBUS Experiment Team (NET) Program. *NASA Tech. Memo. 104566, Vol. 21,* S.B. Hooker and E.R. Firestone, Eds., NASA Goddard Space Flight Center, Greenbelt, Maryland, 43 pp.

Vol. 22

Barnes, R.A., W.L. Barnes, W.E. Esaias, and C.R. McClain, 1994: Prelaunch Acceptance Report for the SeaWiFS Radiometer. *NASA Tech. Memo. 104566, Vol. 22,* S.B. Hooker, E.R. Firestone, and J.G. Acker, Eds., NASA Goddard Space Flight Center, Greenbelt, Maryland, 32 pp.

Vol. 23

Barnes, R.A., A.W. Holmes, W.L. Barnes, W.E. Esaias, C.R. McClain, and T. Svitek, 1994: SeaWiFS Prelaunch Radiometric Calibration and Spectral Characterization. *NASA Tech. Memo. 104566, Vol. 23,* S.B. Hooker, E.R. Firestone, and J.G. Acker, Eds., NASA Goddard Space Flight Center, Greenbelt, Maryland, 55 pp.

Vol. 24

Firestone, E.R., and S.B. Hooker, 1995: SeaWiFS Technical Report Series Summary Index: Volumes 1–23. *NASA Tech. Memo. 104566, Vol. 24,* S.B. Hooker and E.R. Firestone, Eds., NASA Goddard Space Flight Center, Greenbelt, Maryland, (in production).

Vol. 25

Mueller, J.L., and R.W. Austin, 1995: Ocean Optics Protocols for SeaWiFS Validation, Revision 1. *NASA Tech. Memo. 104566, Vol. 25,* S.B. Hooker and E.R. Firestone, Eds., NASA Goddard Space Flight Center, Greenbelt, Maryland, 67 pp.

REPORT DOCUMENTATION PAGE

Form Approved
OMB No. 0704-0188

1. AGENCY USE ONLY *(Leave blank)*

2. REPORT DATE
February 1995

3. REPORT TYPE AND DATES COVERED
Technical Memorandum

4. TITLE AND SUBTITLE
SeaWiFS Technical Report Series
Volume 25—Ocean Optics Protocols for SeaWiFS Validation, Revision 1

5. FUNDING NUMBERS
Code 970.2

6. AUTHOR(S)
James L. Mueller and Roswell W. Austin

Series Editors: Stanford B. Hooker and Elaine R. Firestone
Technical Editor: James G. Acker

7. PERFORMING ORGANIZATION NAME(S) AND ADDRESS(ES)
Laboratory for Hydrospheric Processes
Goddard Space Flight Center
Greenbelt, Maryland 20771

8. PERFORMING ORGANIZATION REPORT NUMBER
95B00043

9. SPONSORING/MONITORING AGENCY NAME(S) AND ADDRESS(ES)
NASA Aeronautics and Space Administration
Washington, D.C. 20546-0001

10. SPONSORING/MONITORING AGENCY REPORT NUMBER
TM-104566, Vol. 25

11. SUPPLEMENTARY NOTES
James L. Mueller and Roswell W. Austin: San Diego State University, San Diego, California; Elaine R. Firestone: General Sciences Corporation, Laurel, Maryland; and James G. Acker: Hughes STX, Lanham, Maryland

12a. DISTRIBUTION/AVAILABILITY STATEMENT
Unclassified-Unlimited
Subject Category 48
Report is available from NASA Center for AeroSpace Information (CASI), 800 Elkridge Landing Road, Linthicum Heights, MD 21090; (301) 621-0390.

12b. DISTRIBUTION CODE

13. ABSTRACT *(Maximum 200 words)*

This report presents protocols for measuring optical properties, and other environmental variables, to validate the radiometric performance of the Sea-viewing Wide Field-of-view Sensor (SeaWiFS), and to develop and validate bio-optical algorithms for use with SeaWiFS data. The protocols are intended to establish foundations for a measurement strategy to verify the challenging SeaWiFS uncertainty goals of 5% in water-leaving radiances and 35% in chlorophyll *a* concentration. The protocols first specify the variables which must be measured, and briefly review the rationale for measuring each variable. Subsequent chapters cover detailed protocols for instrument performance specifications, characterizing and calibrating instruments, methods of making measurements in the field, and methods of data analysis. These protocols were developed at a workshop sponsored by the SeaWiFS Project Ofice (SPO) and held at the Naval Postgraduate School in Monterey, California (9–12 April 1991). This report began as the proceedings of the workshop, as interpreted and expanded by the authors and reviewed by workshop participants and other members of the bio-optical research community. The protocols are an evolving prescription to allow the research community to approach the unprecedented measurement uncertainties implied by the SeaWiFS goals; research and development are needed to improve the state-of-the-art in specific areas. These protocols should be periodically revised to reflect technical advances during the SeaWiFS Project cycle. The present edition (Revision 1) incorporates new protocols in several areas, including expanded protocol descriptions for Case-2 waters and other improvements, as contributed by several members of the SeaWiFS Science Team.

14. SUBJECT TERMS
SeaWiFS, Oceanography, Ocean Optics, Bio-optics, Protocols, Standards, Data Requirements, Specification, Sensor Characterization, Measurement Protocols, Analytical Methods

15. NUMBER OF PAGES
67

16. PRICE CODE

17. SECURITY CLASSIFICATION OF REPORT	18. SECURITY CLASSIFICATION OF THIS PAGE	19. SECURITY CLASSIFICATION OF ABSTRACT	20. LIMITATION OF ABSTRACT
Unclassified	Unclassified	Unclassified	Unlimited